

## **Numerical modelling of the Balatonaliga slope (Hungary)**

**Márton Zsolt Wagner**

Thesis to obtain the Master of Science Degree in

### **Civil engineering**

Supervisor: Prof. Rui Pedro Carrilho Gomes

### **Jury**

Chairperson: Prof. Orlando José Barreiros D'Almeida Pereira

Supervisor: Prof. Rui Pedro Carrilho Gomes

Member of the Committee: Prof. Peter John Bourne-Webb

**July 2022**



## **Declaration**

I hereby declare that this document is an original work of my own authorship and that it fulfils all the requirements of the Code of Conduct and Good Practices of the Universidade de Lisboa.



# Abstract

In this dissertation the slope stability analysis of a high bank under persistent and seismic design situation is studied. This involves determining the soil parameters, building the model in Plaxis, and then fitting the parameters using an iterative procedure. Later, analysis of the safety factors calculated using horizontal ground acceleration. Additionally, reinforcement measures are proposed.

First of all, it was necessary to determine the soil parameters from laboratory tests and field tests on site. Based on the investigations and geological conditions, the study area was divided into three geotechnical zones and parameters were defined for each one.

Subsequently, the model was built in Plaxis 2D and two geotechnical zones were defined by modelling the parameters before the occurred landslides to select the appropriate parameter. Then, using the previous parameters, a third geotechnical zone was defined.

Finally, it was assessed how much horizontal and vertical ground acceleration the high bank can withstand with the defined soil parameters, geotechnical zones, and geometry. Three different reinforcement measures were studied to increase the factor of safety of the slope for seismic situation. Two of these are cutting, with a ratio of 1:2 and 1:3, and the third is soil nailing.

**keywords:** high bank, slope, earthquake, pseudo-static analysis, numerical modelling, Plaxis, reinforcement measures



# Resumo

Esta dissertação estuda a análise da estabilidade do talude sob uma situação de projecto persistente e sísmica. Isto implica determinar os parâmetros do solo, construir o modelo em Plaxis, e depois afinar os parâmetros usando um procedimento iterativo. A seguir realizou-se a análise dos factores de segurança calculados utilizando a aceleração horizontal do solo. Além disso, foram propostas medidas de reforço.

Primeiramente, foi necessário determinar os parâmetros do solo, a partir de ensaios laboratoriais no local e ensaios de campo. Com base nas prospeção e condições geológicas, a área de estudo foi dividida em três zonas geotécnicas e foram definidos parâmetros para cada uma delas.

Posteriormente, o modelo foi construído em Plaxis 2D e duas zonas geotécnicas foram definidas através da modelação dos parâmetros antes dos deslizamentos de terra ocorridos para seleccionar o parâmetro apropriado. Logo, utilizando os parâmetros anteriores, foi definida uma terceira zona geotécnica.

Finalmente, foi avaliada a aceleração horizontal e vertical do solo que a margem alta pode suportar com os parâmetros definidos de solo, zonas geotécnicas e geometria. Foram estudadas três medidas de reforço diferentes para aumentar o fator de segurança do declive para a situação sísmica. Duas delas são a redução da inclinação do talude, com uma relação de 1:2 e 1:3, e a terceira é o recurso a pregagens.

**palavras-chave:** encosta, terramoto, análise pseudo-estática, modelação numérica, Plaxis, medidas de reforço





# Acknowledgements

I would like to thank my supervisor, Prof. Rui Carrillo Gomes from Instituto Superior Técnico. During the semester I had consultations with him week-by-week at IST.

During my last year I had received the Erasmus+ scholarship to study in Instituto Superior Técnico. Where, I meet new students and new teachers, whom influenced my attitude and point of view towards studying, examination and what is knowledge. It was a smashing experience to study for a whole year in Lisbon after completing almost all my studies in the Technical University of Budapest.

Finally, I would like to express my gratitude to my family for supporting me all the way through my studies.



# **TABLE OF CONTENTS**

<b>TABLE OF CONTENTS</b>	<b>XI</b>
<b>LIST OF FIGURES</b>	<b>XV</b>
<b>LIST OF TABLES</b>	<b>XIX</b>
<b>LIST OF SYMBOLS</b>	<b>XXI</b>
<b>CHAPTER 1 - INTRODUCTION</b>	<b>1</b>
1.1 MOTIVATION	1
1.2 SCOPE OF THE DISSERTATION	1
1.3 OUTLINE OF THE DOCUMENT	1
<b>CHAPTER 2 - SEISMIC ACTION</b>	<b>2</b>
2.1 EARTHQUAKE SOURCES	2
2.1.1 EARTHQUAKE WAVE TYPES	2
2.3 EARTHQUAKE VULNERABILITY	4
2.4 SEISMICITY IN HUNGARY	5
2.4.1 PAST EARTHQUAKES	5
2.4.2 DESIGN SEISMIC ACTION DEFINED IN NATIONAL ANNEX TO EUROCODE 8	6
2.4.3 SEISMIC DESIGN ACTION	7
<b>CHAPTER 3 – CASE STUDY</b>	<b>8</b>
3.1 GEOLOGICAL SETTING	8
3.1.1 THE GEOGRAPHICAL LOCATION OF THE STUDY AREA	8
3.1.2 HIGH BANKS OF BALATON	9
3.1.2.1 PRESENTATION OF HIGH BANK AREAS	10
3.1.3. HIGH BANK OF BALATONALIGA	11
3.1.3.1 PARTITION OF THE HIGH BANK	13
3.1.3.2. GROUND AND STRATIFIED WATERS	14
3.1.3.3 PAST SURFACE MOVEMENTS	16
3.1.4 SITE DESCRIPTION	18
3.1.5 FORMATIONS OF THE AREA	21
3.1.5.1 QUATERNARY PERIOD FORMATIONS	21
3.1.5.2 OLDER GEOLOGICAL FORMATIONS	22

3.1.5.2.1 MIOCENE _____	22
3.1.5.2.2 PANNONIAN ELEVATION _____	22
3.1.5.3 DEEP GEOLOGICAL PROPERTIES _____	22
3.1.5.4 QUARTZ PHILLITE _____	24
3.1.5.5. ORDOCIVIAN AGE _____	24
3.1.6. THE TECTONIC CONDITIONS OF THE AREA _____	24
3.2 GEOTECHNICAL DATA AND ZONATION _____	26
3.2.1 BOREHOLES AND CPTS _____	26
3.2.1.1 GROUND- AND STRATIFY WATERS _____	27
3.2.2 SOIL CLASSIFICATION _____	27
3.2.3 LABORATORY TESTS _____	29
3.2.3.1. SIEVE ANALYSIS _____	29
3.2.3.2. ATTERBERG LIMITS _____	30
3.2.3.3. TRIAXIAL ANALYSIS _____	32
3.2.3.4. UNDRAINED DIRECT SHEAR TEST _____	33
3.2.3.5. MATERIAL DENSITY AND PHASE COMPOSITION STUDIES _____	34
3.2.4 FIELD TESTS _____	36
3.2.4.1 CPT SOUNDING _____	36
3.2.5 SOIL PARAMETERS _____	37
3.2.5.1 ESTIMATION OF ANGLE OF SHEARING STRENGTH _____	37
3.2.5.2 ESTIMATION OF E50 VALUES _____	39
3.2.5.3 ESTIMATION OF UNDRAINED SHEAR STRENGTH _____	40
3.2.6 DEFORMATION CURVES _____	42
<b>CHAPTER 4 – BASIS FOR ANALYSIS AND STATIC STABILITY ANALYSIS _____</b>	<b>45</b>
4.1 MODEL STRUCTURE _____	45
4.1.1 GEOMETRY _____	45
4.1.2 MESH _____	46
4.1.3 GROUNDWATER AND SEEPAGE CONDITIONS _____	46
4.1.3 STAGED CONDITIONS _____	48
4.2 MODELLING _____	49
4.2.1 PHASES _____	49
4.2.2. INTERFACE ELEMENTS _____	51
4.2.3 BOUNDARY CONDITIONS _____	52
4.3 BACK ANALYSIS UNDER STATIC LOADING _____	53

4.3.1 SENSITIVITY STUDY ON GZ1 AND GZ2 PARAMETERS	53
4.3.2 SENSITIVITY STUDY ON GZ3 PARAMETERS	57
4.3.4 SUMMARY OF THE SOIL PARAMTERS	58
<b>CHAPTER 5 – SLOPE SEISMIC STABILITY ANALYSIS</b>	<b>59</b>
5.1 SENSITIVITY ANALYSIS	59
5.2 RECOMMENDATIONS FOR SLOPE STABILITY IMPROVEMENT	61
5.2.1 CUTTING	61
5.2.1.1. 1:2 SLOPE RATIO CUTTING	61
5.2.1.2. 1:3 SLOPE RATIO CUTTING	63
5.2.2 NAILS	64
5.2.2.1 GEO5 PRE-ITARATION	64
<b>CHAPTER 6 - CONCLUSIONS AND FURTHER DEVELOPMENT</b>	<b>69</b>
6.1 CONCLUSIONS	69
6.2 FURTHER DEVELOPMENT	70
<b>BIBLIOGRAPHY</b>	<b>71</b>



# **LIST OF FIGURES**

Figure 1 Epicentre and hypocentre [3] .....	2
Figure 2 Longitudinal (primary) waves .....	3
Figure 3 Shear (secondary) waves.....	3
Figure 4 Rayleigh wave .....	3
Figure 5 LOVE wave .....	4
Figure 6 Global earthquake hazard map [5].....	4
Figure 7 Seismicity of the north-eastern part of Lake Balaton, Hungary. The Berhida earthquake in 1985 (M = 4.8), red circle – study area [6, p. 6].....	5
Figure 8 Seismic zone map of Hungary (study area with red dot) [10] .....	7
Figure 9 Elastic response spectra for each soil class as defined in EN 1998 [9].....	7
Figure 10 Position of Balatonaliga in Hungary [12] .....	8
Figure 11 Lake Balaton. The study area (Balatonaliga) located at the most north-eastern point of Lake Balaton (marker) [12].....	8
Figure 12 High banks of Lake Balaton [14, p. 14].....	9
Figure 13 Pannonian sea on the territory of present-day Hungary and surrounding area [15].....	10
Figure 14 Morphological and geological sketch of the Balatonakarattya high bank deposits on 19 April 1908 [18].....	11
Figure 15 „Túrzó” islands in the Balatonaliga area [19] .....	11
Figure 16 Military survey maps, First Military survey (1782-1785) upper left corner, Second Military survey (1819-1869) upper right corner, Third Military survey (1869 – 1887) bottom centre [20].....	12
Figure 17 Postcard from Balatonaliga dating from the early 1900s - since then, the landscape of the high bank has changed, with predominantly damaged vegetation in these areas [17] .....	12
Figure 18 The schematic geological structure of the high banks of Lake Balaton and the typical cross-section of the high bank highlands [18] .....	13
Figure 19 Typical hydrogeological cross-section of the High Bank (horizontal and vertical scales are differ) [16].....	15
Figure 20 surface springs in the debris slope in the northern part of the area (site visit photo) .....	16
Figure 21 The sandy loess wall of the high bank (site visit photo).....	17
Figure 22 Block detachments on the wall in 2021, near the study area (site visit photo) .....	17
Figure 23 Topographic map of the study area. The red box shows the specific area .....	19
Figure 24 aerial photographs of the study area (left 1966, right 1992) [23] .....	19
Figure 25 vegetation on sloped debris [17] .....	20

Figure 26 Deformation on the edge of the high bank (photo taken at the top of the high bank) [17]....	20
Figure 27 Quarter period formations at the study area (red rectangle) [25].....	21
Figure 28 Deep geological map of the north-eastern part of Lake Balaton [30] .....	22
Figure 29 Deep boreholes around the study area.....	23
Figure 30 Left: quartzfillite on the surface, right: quartzfillite built cellar row in Balatonfőkajár (site photo) .....	23
Figure 31 Eras and periods of the Phanerozoic [47].....	24
Figure 32 Component units and location of the Mid-Hungarian Zone [34] .....	24
Figure 33 Balatonfő and Balaton seismic lines, tectonic fault line, and earthquake epicentres [37] [36] .....	25
Figure 34 Boreholes and CPT explorations on the study area .....	26
Figure 35 Geological setting of the 101F, 102F,103F, 1F and 2F boreholes and K-46, B-2 are deep boreholes .....	28
Figure 36 Sieve analysis result regarding the Geotechnical Zone 1 .....	29
Figure 37 Sieve analysis result regarding the Geotechnical Zone 2.....	29
Figure 38 Sieve analysis result regarding the Geotechnical Zone 3.....	30
Figure 39 Atterberg limit results regarding the Geotechnical Zone 1 .....	30
Figure 40 Atterberg limit results regarding the Geotechnical Zone 2.....	31
Figure 41 Atterberg limit results regarding the Geotechnical Zone 3.....	31
Figure 42 Angle of shearing resistance from drained triaxial analysis .....	32
Figure 43 Apparent cohesion from drained triaxial analysis .....	32
Figure 44 Angle of shearing resistance from undrained direct shear test.....	33
Figure 45 Undrained shear strength from undrained direct shear test .....	33
Figure 46 Dry unit weight from material density analysis .....	34
Figure 47 Unit weight from material density analysis .....	34
Figure 48 Void ratio from material density analysis.....	35
Figure 49 Saturation ratio .....	35
Figure 50 Silty soil CPT data on Robertson diagram [39] .....	36
Figure 51 E50 values of GZ1.....	37
Figure 52 E50 values of GZ2.....	38
Figure 53 E50 values of GZ3.....	38
Figure 54 Triaxial analysis of the 101F borehole sample at a depth of 31,2m .....	39
Figure 55 E50 values regarding Geotechnical zone 1 .....	40
Figure 56 E50 values regarding Geotechnical zone 2 .....	40
Figure 57 Undrained shear strength of GZ1.....	41



Figure 58 Undrained shear strength of GZ2.....	41
Figure 59 Deformation curves regarding sandy soils .....	42
Figure 60 Deformation curves regarding silty soils .....	43
Figure 61 Deformation curves regarding medium plasticity clay soils .....	43
Figure 62 Deformation curves regarding high plasticity clay soils .....	44
Figure 63 Model geometry.....	45
Figure 64 Model geometry of the slope debris .....	45
Figure 65 Mesh of the cross-section .....	46
Figure 66 Water flow conditions in the model .....	46
Figure 67 Observed (dark blue) and applied (light blue) aquifers .....	47
Figure 68 Modelling of stratified waters in Plaxis .....	47
Figure 69 Adjustment of layered water in Plaxis .....	48
Figure 70 Staged construction menu of the model without aquifers .....	48
Figure 71 Calculation phases in Plaxis .....	49
Figure 72 Initial stress field of the model at gravitational loading.....	49
Figure 73 Steps over Factor of safety curve of an iteration analysis .....	50
Figure 74 Shape of moving slip surface in Factor of Safety analysis, Drained case .....	50
Figure 75 Setting pseudo static parameters in Plaxis .....	51
Figure 76 The model with interface elements and the GZ3 turned off .....	51
Figure 77 Setting of interface elements.....	51
Figure 78 Boundary conditions.....	52
Figure 79 E50 and phi' values of GZ1 over FS .....	54
Figure 80 Cohesion values of GZ1 over FS .....	54
Figure 81 E50 and phi' values of GZ2 over FS .....	55
Figure 82 Cohesion and undrained shear strength values of GZ2 over FS.....	55
Figure 83 The model with the activated GZ3 .....	57
Figure 84 E50 and phi' iteration values of GZ3 .....	57
Figure 85 Cohesion and Su iteration value of GZ3 .....	57
Figure 86 Formation of a slip surface under 0,05*g horizontal ground acceleration.....	59
Figure 87 Effect of horizontal and vertical ground accelerations on factor of safety.....	60
Figure 88 Effect of horizontal and vertical ground accelerations over factor of safety with aquifers ....	60
Figure 89 Cutting with 1:2 slope ratio .....	61
Figure 90 Horizontal acceleration values over factor of safety regarding 1:2 cut .....	61
Figure 91 Cutting with 1:2 slope ratio with aquifers.....	62

Figure 92 Horizontal acceleration values over factor of safety regarding 1:2 cut with aquifers .....	62
Figure 93 Cutting with 1:3 slope ratio .....	63
Figure 94 Horizontal acceleration values over factor of safety regarding 1:3 cut .....	63
Figure 95 Cutting of slope debris at a ratio of 1:3 .....	63
Figure 96 Tension crack at the level of an aquifer .....	64
Figure 97 Optimised slip surface without nails .....	64
Figure 98 Soil nail properties.....	65
Figure 99 Location of soil nails used in Geo5 .....	65
Figure 100 The applied horizontal and vertical soil acceleration values on the slope .....	65
Figure 101 Partial factors used for permanent design situation in Geo 5 .....	66
Figure 102 Partial factors used for seismic design situation in Geo 5 .....	66
Figure 103 The optimised slip surface in Geo 5 model.....	66
Figure 104 Bishop method .....	66
Figure 105 Reinforcement with nails .....	67
Figure 106 Applied parameters for soil nails in Plaxis .....	67
Figure 107 Horizontal acceleration values over factor of safety regarding nailing.....	68
Figure 108 Nail reinforcement with aquifers (green bands – aquifers) .....	68
Figure 109 Horizontal acceleration values over factor of safety regarding nailing with aquifers .....	68

## **LIST OF TABLES**

Table 1 Soil type characterisation according to EUROCODE 8 [9].....	6
Table 2 Soil factor value by soil and earthquake impact type [9] .....	6
Table 3 Borehole and field tests at the study area .....	26
Table 4 Ground and stratified waters .....	27
Table 5 CPT test categorisation .....	36
Table 6 separating layers by CPT results .....	36
Table 7 Properties of the modelled aquifers.....	47
Table 8 $R_{inter}$ parameters for Geotechnical zones .....	52
Table 9 Combinations studied .....	53
Table 10 The possible range of the parameters for GZ1 and GZ2 .....	53
Table 11 Iterated parameters for GZ1 and GZ2.....	56
Table 12 Applied soil parameters.....	58
Table 13 calculated variations .....	59
Table 14 Applied horizontal and vertical ground acceleration.....	59



# **LIST OF SYMBOLS**

## **CAPITAL LETTERS**

ML	Richter scale
Mb	field wave magnitude
MS	surface wave magnitude
MW	moment magnitude
Vs	velocity of wave propagation
NSPT	standard penetration test with N values
S	soil type
CPT	Cone penetration test
GZ	Geotechnical zone
E50	Secant young modulus
CD	consolidated – drained triaxial analysis
UU	unconsolidated - undrained triaxial analysis
Sr	Saturation
MPa	Mega pascal
Fr	Friction ratio
PI	Plastic index
M	Constrain modulus
Ic	Consistency index
Nkt	Cone factor
FS	Factor of safety
PS	Pseudo static force

## SMALL LETTERS

mBf	meters above Baltic Sea level
su	undrained shear strength
cu	undrained shear strength
$a_g^R$	ground acceleration on rock
$a_g$	ground acceleration at given soil
g	gravity
m	meter
s	second
v	velocity
qt	corrected cone resistance
qc	cone resistance
$\phi'$	angle of shearing resistance
kPa	kilo pascal
u <sub>2</sub>	pore pressure
a	area (CPT test)
q	deviator stress
c	cohesion

## GREEK INDEXES

$\lambda$	linear deformation
$\mu$	shear modulus
$\rho$	density
$\varphi$	inner friction angle
$\varphi'$	angle of shearing resistance
$\gamma$	natural unit weight
$\gamma_d$	dry unit weight
$\sigma$	stress
$\sigma_{v0}$	overburden stress
$\sigma_1$	Axial stress
$\sigma_3$	Confining pressure / radial stress
$\sigma_c$	confining pressure
$u$	Poisson ratio
$\alpha_M$	constrained modulus cone factor





# **CHAPTER 1 - INTRODUCTION**

## **1.1 MOTIVATION**

I chose this field and topic because I was working in this area as part of a project assignment in a university course. At that time, the task was like investigate the resistance of the high bank, but the soil parameters were given in advance. As part of the assignment, the task was to test 10 cross sections with the given soil parameters and geometry. After that, however, I became interested in the steps to be taken to complete such a project. I was also interested in the complexity of the high bank and the procedures to deal with such a problem. This is why I decided to use this area for my Master's thesis.

The high bank sliding events in the area are well documented and the drilling and CPT study in the area provide sufficient data for modelling, so there is enough information available.

Weaving all the above together to look at a specific case, a real situation, how an earthquake can be modelled for a high bank and what reinforcement options can be used to improve stability.

## **1.2 SCOPE OF THE DISSERTATION**

The objective of the dissertation is to consolidate and expand the knowledge on slope stability, including the revision of geology, laboratory, and field tests in order to create a synthesis of knowledge.

Plaxis program was used to perform a sensitivity study, to characterize slope stability for the persistent and seismic situations and assessing reinforcement methods.

## **1.3 OUTLINE OF THE DOCUMENT**

Chapter 2 describes the formation of earthquakes, including the types of earthquake waves, and the classification of earthquakes according to the Richter, the European Macro seismic scale, and the modified Mercalli scale. This was followed by a description of earthquake vulnerability. Then, the earthquakes near the study site were presented, and the maximum possible earthquake magnitude was explained. Later, the ground acceleration parameter for the site was defined.

Chapter 3.1 describes the geology of the study area. The formation and development of the high bank. Morphology of the area, representation of the Quaternary formations, description of the soil type that built up the high bank. Description of the bedrock and its age from deep boreholes. This is followed by a description of the tectonic conditions of the site.

Chapter 3.2 includes the geotechnical data, such as the borehole and CPT field test, and soil classification and its analysis. Then a detailed description of the laboratory and field tests. Three geotechnical zones are defined based on the laboratory results and geology. Detailed description of the correlation calculations for E50, angle of shearing resistance, and undrained shear strength, and determination of soil parameter range.

Chapter 4 is devoted to numerical modelling, where the model was built in Plaxis 2D. The parameters of the GZ1 and GZ2 layers were refined by iterative calculations. Afterwards, the parameters of GZ3 were determined.

In Chapter 5 the horizontal soil acceleration value that the high bank can withstand with the current geometry was checked. The value was found to be considerably lower than expected, so in the next step, proposals were made to reinforce the high bank.

The first type is to cut the high bank with the usual 1:2 and 1:3 ratio. The second method proposed is reinforcement by soil nailing.

Chapter 6 includes the conclusions and further developments.

## **CHAPTER 2 - SEISMIC ACTION**

Almost all earthquakes of natural origin are triggered by tectonic movements, and the theory of plate tectonics, which describes the origin of these movements, began to emerge in the second half of the last century, thanks to significant developments in four main scientific fields such as radiometric dating, paleomagnetic research oceanology and seismology. [1]

The largest documented earthquake in Europe was the Lisbon earthquake of 1755, with an estimated magnitude of 8.5 on the Richter scale. The epicentre of the earthquake was about 200 km W-SW of SW Cape of St. Vincent of Portugal, but the greatest devastation was in Lisbon. This earthquake highlights the importance of understanding and knowing what earthquakes are, as they can cause enormous damage [2].

### **2.1 EARTHQUAKE SOURCES**

Earthquakes that occur in tectonic plates are triggered by deformations resulting from the forces acting on the solid, elastic rocks that make up the earth's crust.

The elasticity of a solid body can be seen when an external force tries to change its shape or size. In this case, stresses occur inside the body to prevent changes in shape and size. However, when this external force is removed, the stresses cause the body to regain its original shape and volume. The stresses cause the body to deform, and the energy is stored in this form. However, the rock body can only withstand this force to a certain extent, and once a certain limit is exceeded, the material no longer behaves in a plastic way, but is fractured and the accumulated energy is converted partly into heat and partly into kinetic energy. The resulting motion is called an earthquake, and the resulting elastic waves that propagate in a sphere from the hypocentre are called earthquake waves. The resulting motion eliminates the deformation and creates a new state of rest.

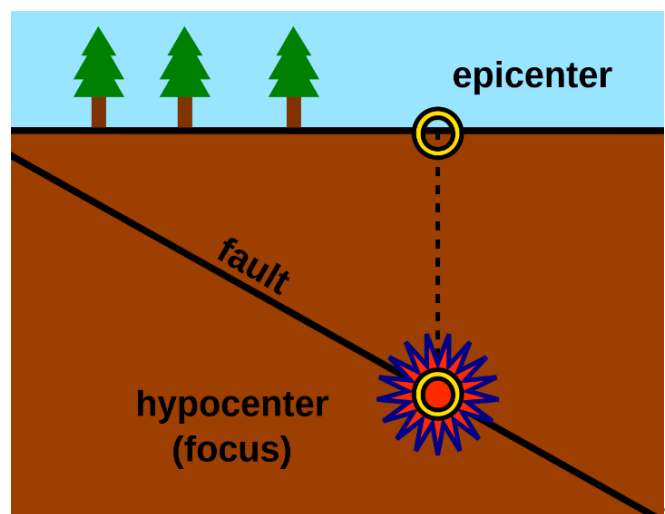


*Figure 1 Epicentre and hypocentre [3]*

Earthquakes can be characterised by the location of the origin (hypocentre), and the location at the surface (epicentre) as Figure 1 shows, and by scaling depending on the magnitude of the earthquake (Richter and Mercalli scales) [1] [3].

#### **2.1.1 EARTHQUAKE WAVE TYPES**

One way of classifying earthquake waves is by their longitudinal or transverse motion in a solid-elastic medium. They can also be grouped as surface or subsurface waves.

##### *Longitudinal wave*

Particles vibrate in the direction of wave propagation, which means they have a pressure effect. The materials are also cubed to obtain the following deformation for a longitudinal wave:

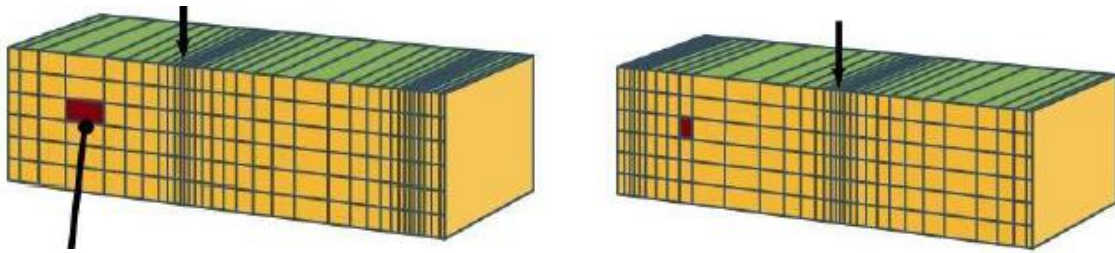


*Figure 2 Longitudinal (primary) waves*

A transverse wave, the oscillatory motion is perpendicular to the direction of propagation of the wave, it has a shearing behaviour, it propagates only in a solid medium.

*Shear wave*

In the case of shear waves (transversal waves), the displacement is perpendicular to the wave propagation:

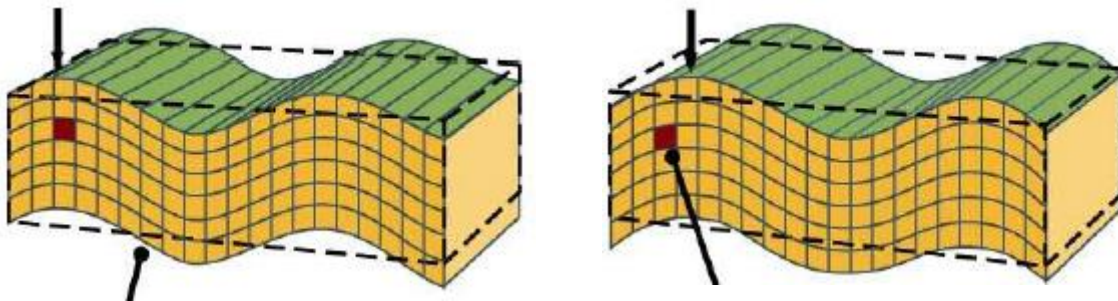


*Figure 3 Shear (secondary) waves*

The propagation speed of P and S waves is different. The propagation velocity of the longitudinal wave is influenced by the shear modulus and the coefficient of linear deformation ( $\lambda$ ). However, the propagation velocity of shear waves is a function of shear modulus ( $\mu$ ) and density ( $\rho$ ).

The propagation speed of primaries is higher than that of shear waves, which is why longitudinal waves are called primaries, because they are the first to reach the detecting stations. Shear waves are roughly  $\sim\sqrt{3}$  times the primary wave.

*Rayleigh*

One type of surface wave is the Rayleigh wave, which ripples across the surface, formed by the interference of P and S waves. Its propagation speed is about 90% that of a shear wave.

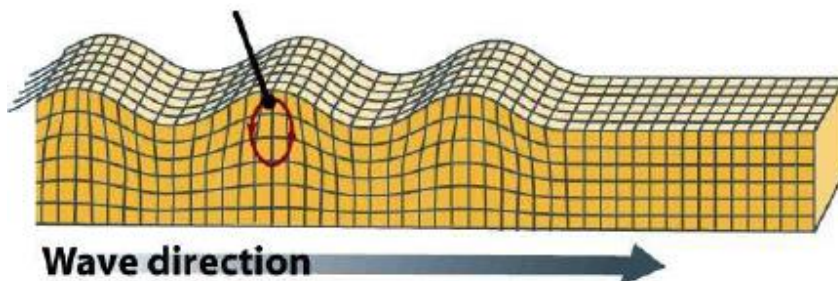


*Figure 4 Rayleigh wave*

*Love waves*

Love waves are also surface waves, which are observed in the case of significantly different surface roughness.

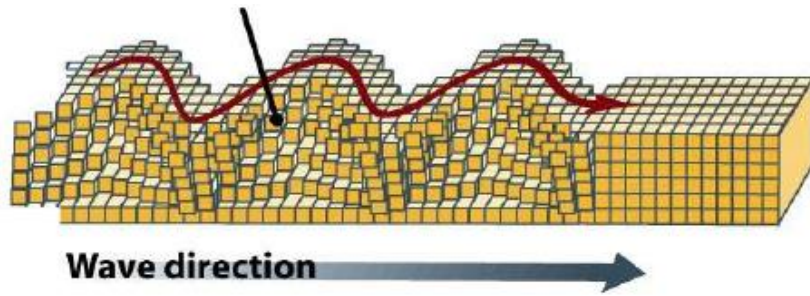


Figure 5 LOVE wave

Earthquake waves have a velocity of 100-600 m/s in soils and rocks typically above 800m/s [4] [1]

Earthquake records are stored in data centres, such as PEER (Pacific Earthquake Engineering Research Centre), from where some earthquake records can be downloaded. [1]

### 2.3 EARTHQUAKE VULNERABILITY

The earthquake data sets collected in previous decades allow us to determine, on an earthquake risk probability basis, the magnitude of an earthquake event that could occur in an area with a large return period. This procedure can be used to reduce earthquake damage by sizing structures for earthquakes.

Two methods are possible for determining these, using the amount of vibration generated by an earthquake event in the surface and near-surface layers. The deterministic method is recommended for seismically active areas, while the probabilistic method is recommended for less seismically active areas.

In European practice, the maximum earthquake magnitude likely to occur in the hot zone is defined for the 475-year return interval. The magnitude of the maximum ground motion expected in the area can be determined from the source parameters and is usually expressed in terms of bedrock, as the soil stratification of the surface can be complex. The earthquake hazard map of Hungary, with the maximum ground acceleration value for a return period of 475 years, is shown in Figure 8

A similar vulnerability map can be defined for the entire Earth, as shown in Figure 6.

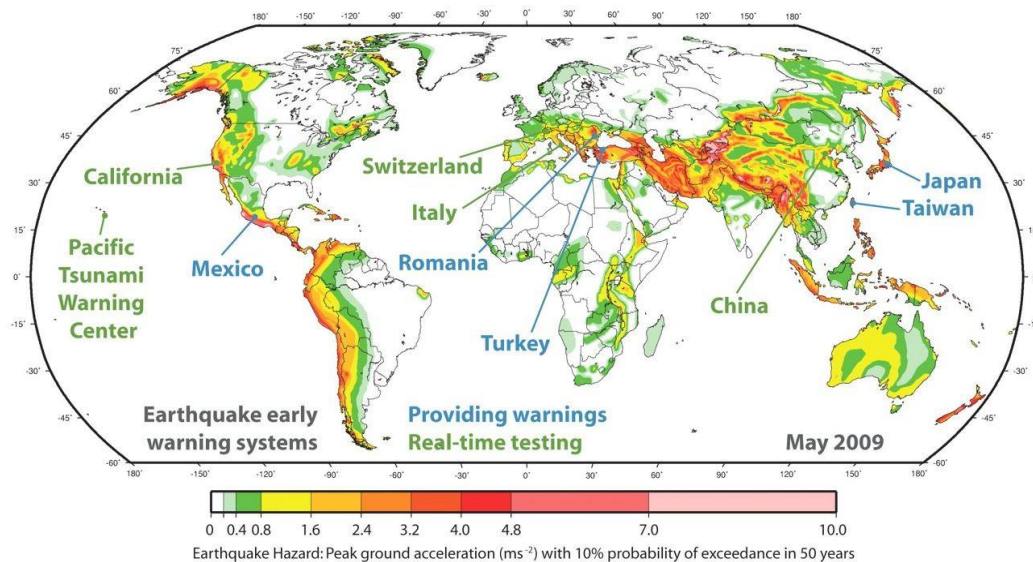


Figure 6 Global earthquake hazard map [5]

The ground acceleration given is the maximum horizontal ground acceleration expected to occur in earthquakes. The damage caused by earthquakes in each area is usually determined by three factors:

the magnitude of the earthquake, the distance from the focal point, and the geological and soil conditions of the area under investigation.

Soil type affects the extent of damage. Young, loose sandy and clayey sediments close to the surface cause much more damage than areas where harder, older rocks are found at the surface. The manmade backfill further increases the impact of the damage. Changes in subsoil conditions can cause the extent of damage to vary significantly in areas spaced even tens of meters apart. Therefore, when determining the earthquake hazard, it is not sufficient to take into account the acceleration value calculated for the bedrock, but it must be modified by a factor depending on the ground conditions.

In engineering terms, a bedrock is considered to be the soil type for which the above-mentioned earthquake hazard is defined, in which the propagation velocity of transverse waves exceeds 750-800 m/s. [1]

## 2.4 SEISMICITY IN HUNGARY

### 2.4.1 PAST EARTHQUAKES

Hungary is located far from major fault lines, and its seismology is likely to have an earthquake event of  $ML=6.0$  at most, but a magnitude 4.5-5 earthquake can occur every 10 years. The largest recorded earthquake in the country was the Komárom earthquake of 1763, which had a Richter magnitude of 6.3.

The shore of Lake Balaton (Chapter 3) has experienced 2 small earthquakes in the last 40 years, both in the Berhida area. The settlement is located ~14km to the north-east of the study area. In 1985, Berhida recorded a  $ML=4.9$ , magnitude VII on the Mercalli scale. Then in 2009 an earthquake with  $ML=2.8$  occurred. (Figure 7)

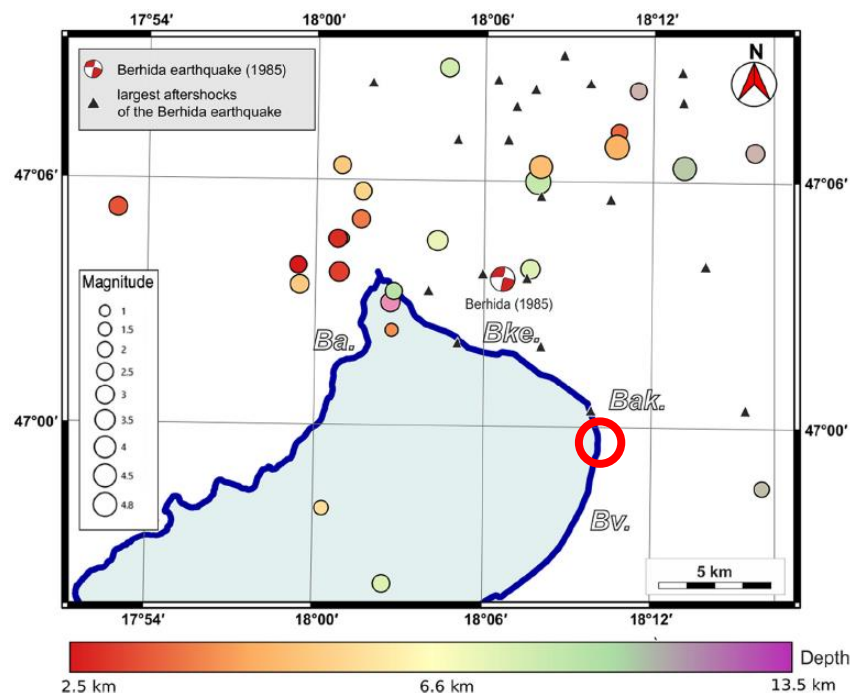


**Figure 7 Seismicity of the north-eastern part of Lake Balaton, Hungary. The Berhida earthquake in 1985 ( $M = 4.8$ ), red circle – study area [6, p. 6]**

From an earthquake point of view, it is important to mention that the study area is located close to the geological fault lines of the Lake Balaton Line and the Balatonfő Line. Based on the investigations, it was found that the rock environment is currently active, and earthquakes may occur near the fault lines. This is described in more detail in the Chapter 3. [7] [8]

## 2.4.2 DESIGN SEISMIC ACTION DEFINED IN NATIONAL ANNEX TO EUROCODE 8

In engineering practice, determining the earthquake hazard of an area means obtaining the horizontal acceleration value ( $a_g$ ) for the area. According to the Hungarian national annex of Eurocode 8, to determine the horizontal and vertical acceleration values for a given area, the horizontal soil acceleration value on rock ( $a_g^R$ , Figure 8), soil type factor (Table 1), importance factor, and in some cases the topographic amplification factor are needed.

**Table 1 Soil type characterisation according to EUROCODE 8 [9]**

Ground type	Description of stratigraphic profile	$V_{s,30}$ (m/s)	NSPT	$c_u$ (kPa)
A	rock or other rock-like geological formation	> 800	-	-
B	very dense sand, gravel, or very stiff clay	360 –800	> 50	>250
C	deep deposits of dense or medium-dense sand, gravel, or stiff clay	180 --360	15 – 50	70 - 250
D	loose-to-medium cohesionless soil or soft-to-firm cohesive soil	<180	< 15	< 70
E	surface alluvium layer with $v_s$ of type C or D and thickness varying between about 5 and 20 m, underlain by stiffer material with $V_s > 800$ ms <sup>-1</sup>	Type C or D		
S1	deposits consisting or containing a layer with at least 10m of soft clays/silts with a high plasticity index ( $IP > 40$ ) and high-water content	<100 indicative	-	10 - 20
S2	deposits of liquefiable soils of sensitive clays or any other soil type not included in types A-E or S1			

The undrained shear strength values are higher than 250 kPa, based on laboratory results (Chapter 3.2), taking values between 300 - 450 kPa. However, the CPT sounding result does not classify the soil as "very dense sand, gravel, or very stiff clay" category B, as the maximum achieved resistance is ~12 MPa, which does not consider the soil to be very dense. Therefore, to be on the safe side, the soil in the study area was classified as soil type C.

**Table 2 Soil factor value by soil and earthquake impact type [9]**

Ground Type	Soil factor	
	Type	Type
	I	II
A	1	1
B	1.2	1.35
C	1.15	1.5
D	1.35	1.8
E	1.4	1.6



Table 2 shows the modifying factors for the importance factors I and II as a function of soil type. The two types have different shapes, one or the other is used based on the amplitude of the quakes in a given area. According to the Hungarian national annex of Eurocode 8, for typical earthquake values  $M_s \leq 5.5$ , the type II values should be considered as soil factor (S) which is 1,5 for type C soils.

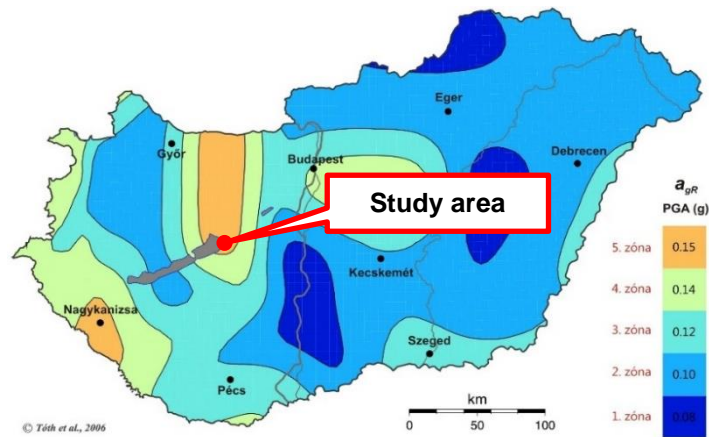


Figure 8 Seismic zone map of Hungary (study area with red dot) [10]

According to Figure 8 the  $a_{gR}$  value at the study area is 0,15g.

### 2.4.3 SEISMIC DESIGN ACTION

There are residential houses ~30 meters from the edge of the top of the high bank, that is why a value of 1.0 has been taken as the importance factor ( $\gamma_I$ ). According to the Eurocode 8, topographic amplification factor ( $S_T$ ) should use if the angle of the slope is higher than  $15^\circ$  coefficient variation of 1,2 should be taken into account. To calculate the pseudo static acceleration according to the Eurocode 8 recommendation, the above values must be multiplied by 0.5. Equation 1.

Multiplying the coefficients gives the horizontal soil acceleration value for the area (Equation 1)

**Equation 1 Calculation of the ground acceleration according to the soil type, and acceleration on rock specific to the study area [11]**

$$a_g = 0,5 * a_{gR} * \gamma_I * S * S_T = 0,5 * 0,15g * 1 * 1,5 * 1,2 = 0,135 * g = 1,324m/s^2$$

The flexible response spectrum defined for each subclass is shown in the Figure 9:

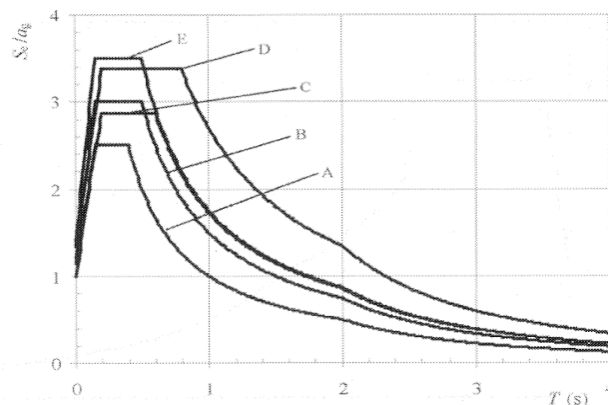


Figure 9 Elastic response spectra for each soil class as defined in EN 1998 [9]

In the design of general engineering structures for earthquakes, the response spectrum for the subsoil class determined by the soil properties and the multiplication of the bedrock horizontal acceleration value for the area by the soil factor are considered.

## **CHAPTER 3 – CASE STUDY**

### **3.1 GEOLOGICAL SETTING**

#### *3.1.1 THE GEOGRAPHICAL LOCATION OF THE STUDY AREA*

The topic of the dissertation is the study of a high bank in Hungary under persistent and seismic situations. The high bank is located at Lake Balaton, in the village of Balatonaliga. Figure 10 and Figure 11 shows the location of Balatonaliga in Hungary. This lake is the largest in Central Europe and a popular holiday destination for locals and visitors from the surrounding countries.

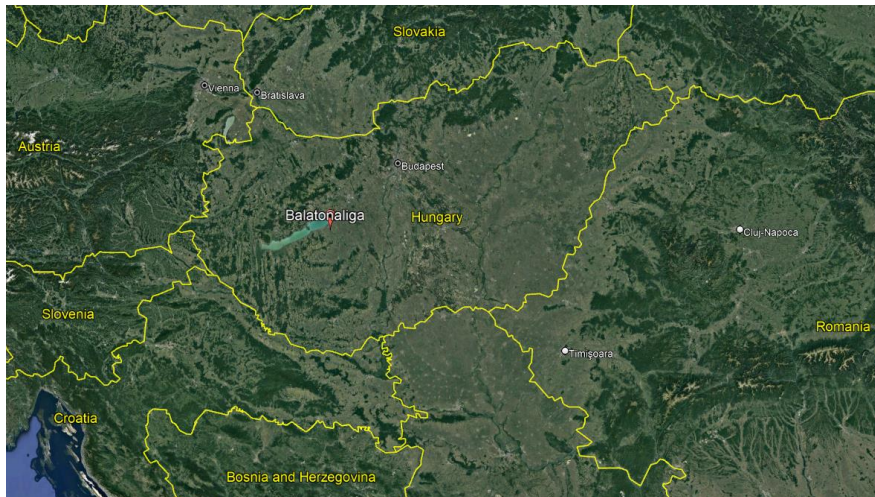


***Figure 10 Position of Balatonaliga in Hungary [12]***



***Figure 11 Lake Balaton. The study area (Balatonaliga) located at the most north-eastern point of Lake Balaton (marker) [12]***

In the following subchapters, the origin of Lake Balaton is described, the formation, characteristics, and structure of the high banks of Lake Balaton. Later, it will be described in more detail the Balatonaliga high bank and the slides that occurred there in the past decades.

According to the Cadastre of the Small Landscapes of Hungary the high bank areas are part of the Somogy coastal plain, which is located in the eastern - south-eastern part of lake Balaton, in the central part of Hungary. [13]

The topography of the small area is represented by the hilly sloping plains in the foothills of the Somogy meridional ridges, which are in the south-eastern part of the southern shore of Lake Balaton, 2-4 km from Balatonaliga. Gently sloping, low relief (120-160 m above sea level). [13]



The intermediate meridional valleys running out to the lake are funnel-like bays, the berms are the recharge sites. Specific formations of the meridional spines extending to the lake, which frame the waterfront as high, steep walls underlain by lake abrasion. The slopes of some of the volcanic witness hills towards the lake are similar. Between the low and high steep walls and the water's edge lies the actual shoreline. Today it is largely levelled, filled, almost entirely built-up 'holiday strip'. [13]

Geologically, the basement of the area is formed by the shallow Opaleozoic metamorphic rocks, mainly late Miocene rocks. There are volcanic rocks in the area, which are about 3.5 million years old. The sloping downslope plain, which occupies the greater part of the area, was formed by the Prebalaton alluvial cone material deposited on the subducted Pannonian sand and clay sediments. The clay, sand and tuff layers of the monadnock hills are accessible on the surface. In the alluvial coastal strip, interspersed with swell, coarse and medium-grained sand is mixed with gravel. [13]

Hydrographically, the eastern edge of Lake Balaton covers the southern edge from Fonyód to Balatonkenese, the eastern and southern edges of the eastern and southern estuaries of some watercourses. The depth of the groundwater in the study area is around 4 m below the surface, while in the south-south-western part of Lake Balaton it is around 2 m. In general, it tends to rise as it approaches Lake Balaton, and its volume is low as it seeps below the surface into the lake. Chemically, the calcium-magnesium-hydrogen carbonate character is typical, but sodium is also present in places. The artesian wells are generally less than 100 m deep, with water yields ranging from moderate to medium. [13]

The study area is located at the hydrogeological interface of two major hydrogeological landscape units, the Balaton basin, and the Kűngösi Pannonian plate, and it also has unique characteristics of the high banks. Due to this transitional situation, exploration have shown that both groundwater and stratified water occur in the study area. In one of the boreholes drilled in the high bank, aquifers have been found, which are recharged by rainwater in places where the aquifers are located on or near the surface. The movement and flow of the aquifer water is presumably towards Lake Balaton. [13]

### 3.1.2 HIGH BANKS OF BALATON

At Lake Balaton there are several high bank ranges in the middle of the coast, stretching along the eastern and southern shores between Balatonűzfű and Fonyód cities as Figure 12 shows. The high bank in study is marked with a red circle.

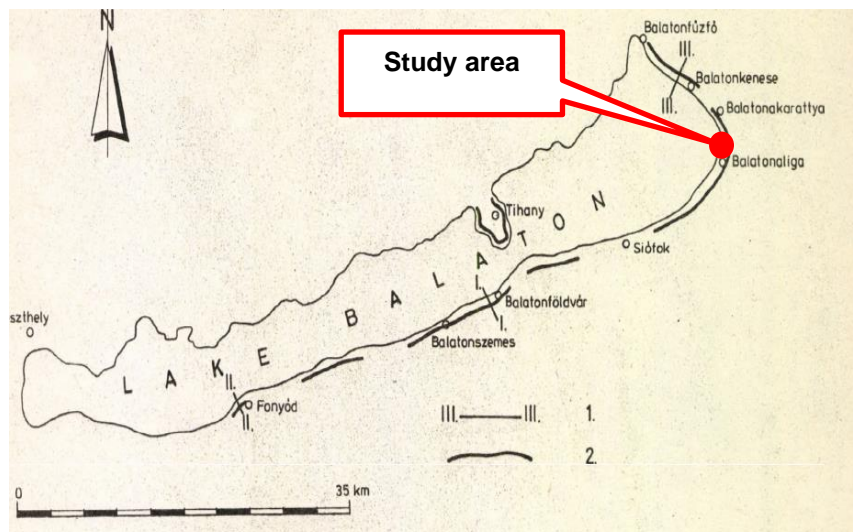


**Figure 12 High banks of Lake Balaton [14, p. 14]**

The formation of Lake Balaton and its surroundings took place in the Eocene Epoch (~35 - 23 million years ago) with the convergence of the continents. Mountain formation processes were triggered by continental drift, during which the Paratethys Sea detached approximately 11 million years ago. As the continents moved closer together, the Carpathian Mountain range began to rise, thus separating the

Pannonian Sea from the Paratethys. At this time, the Pannonian Sea was saltwater, but was diluted by the freshwater rivers that flowed into it subsequently. (Figure 13)



*Figure 13 Pannonian sea on the territory of present-day Hungary and surrounding area [15]*

The upper and lower Pannonian sediments of the high banks were deposited at this time, and the open lake areas between the deltas were then gradually filled, later saturated, and finally formed into muddy bays. The slight fluctuations in the lake water level meant that this cycle could be repeated many times. The accumulation of 4-8 m thick sediment deposits because of cyclical deposition can be observed, for example, on the whitecoast in Tihany or on Csittény Hill in Balatonakarattya. [16]

### 3.1.2.1 PRESENTATION OF HIGH BANK AREAS

The Balatonaliga high bank is part of the high bank line at the eastern tip of Lake Balaton, which runs from Balatonfűzfő with small interruptions to Balatonvilágos. Its formation is associated with the phased subsidence of the upper Pleistocene basin and the erosion activity of the lake.

The sediments that build up the high banks are most visible in the Fonyód area. On the coastline, the cross-layered sediments of the rivers that filled Lake Pannon and the shell fragments that have been moulded into them are clearly visible. Today's near-vertical shoreline used to be gently sloping and extended all the way to Lake Balaton, which was then at a higher level.

The high banks of Lake Balaton are largely built up by layers of shallow marine sand, silty sand, and clay of Upper Pannonian age. These formations are overlain by 4-5 m thick Pleistocene silt, sand, and sandy gravel. This sedimentary sequence, however, was intruded by basalt tuff associated with the basaltic volcanism of southern Balaton, which now occurs only in a small area on the surface.

At the Balatonkenese high bank the stratification is fine, the predominant clay layers are densely divided by sand veins and small sand layers, which slope towards Lake Balaton. Behind the high banks from Balatonfűzfő to Balatonaliga, there are extensive plateaus, the layers of which also slope towards Lake Balaton. The strata are tilted towards S-SE, and not towards Lake Balaton.

The hydrogeological section of Balatonkenese is quite different from the other high bank at Lake Balaton. Here the groundwater descends along a depression curve to the level of Lake Balaton, soaking the debris slope. [17]

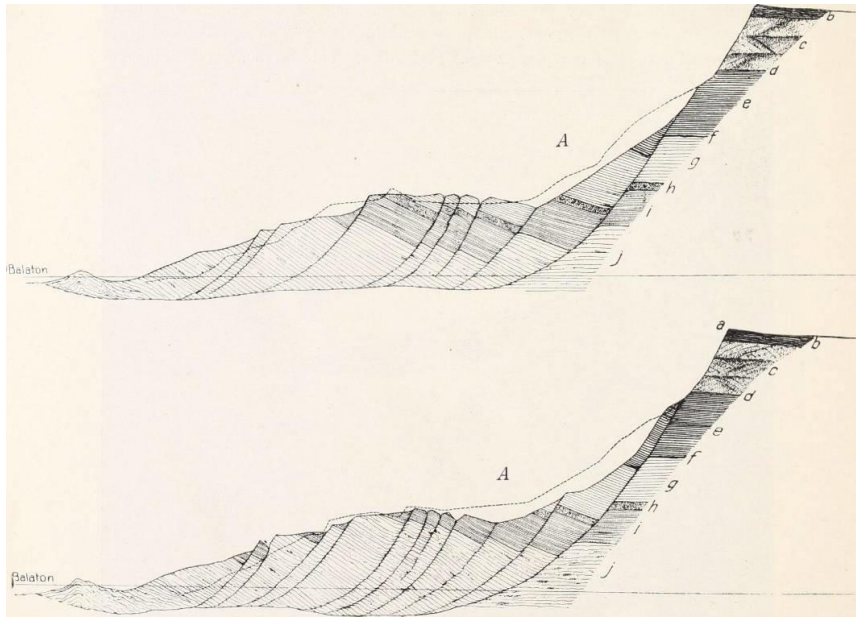


**Figure 14 Morphological and geological sketch of the Balatonakarattya high bank deposits on 19 April 1908 [18]**

### 3.1.3. HIGH BANK OF BALATONALIGA

In the area of invest, the earliest recorded earth movements were landslides of various sizes, some of which formed on the bed of the Balaton, and then on the bed of the river. On the map of 1769, islands were mapped in the vicinity of the area in a longitudinal direction to the shore, so-called 'túrzó islands' (emerging island), as shown in Figure 15, which were slip surface cutting into the Balaton bed, causing the bottom to rise and thus small islands to form in the lake. However, by the mid-1800s, when the surveys for the planned railway line began, the islands had disappeared and had been eroded. [17]

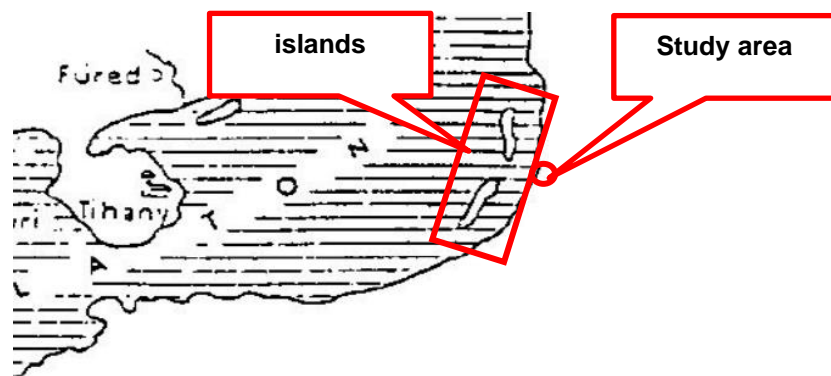


**Figure 15 „Túrzó” islands in the Balatonaliga area [19]**

There were three military geodetic surveys in Hungary between 1782 and 1887, the earliest detailed maps of the area are the First, Second and Third Military Survey Maps. In the northern part of the figures below, an erosion gully can be clearly seen, which is already visible on the 18th century map, and the sloping terrain towards the gully can be clearly seen on all three surveys. (Figure 16)



**Figure 16 Military survey maps,  
First Military survey (1782-1785) upper left corner,  
Second Military survey (1819-1869) upper right corner,  
Third Military survey (1869 – 1887) bottom centre [20]**

The resolution of the First Military Survey was not yet detailed enough, but the Second and Third Military Surveys clearly show the stepped slope northwest of the railway line, with significant gullies in the present terrain. During the 1960s, 1970s and 1980s, movement and damage was observed in the southern part of the area.

Several previous boreholes drilled in the former Club Aliga area show that the aquifers that build up the high section of the high bank are structured by lignite-clay layers and are replaced by clay layers at deeper levels. Water seeping downwards is trapped above the aquifers and seeps out according to the slope of the upper layer. At Balatonaliga, this means a south-westerly slope of 2-5°, so that the water flows towards Lake Balaton and appears as small springs at different heights on the hillside. [17]

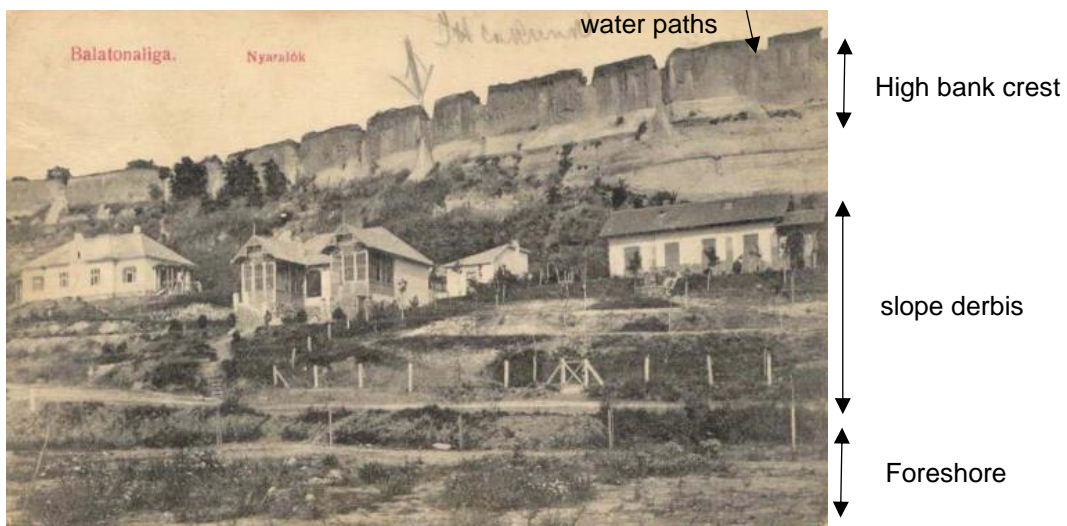


**Figure 17 Postcard from Balatonaliga dating from the early 1900s - since then, the landscape of the high bank has changed, with predominantly damaged vegetation in these areas [17]**

The postcard above (Figure 17) shows the foreshore, the slope derbis, and the high bank crest, as well as the path of the water as it broke down the high bank crest.



### 3.1.3.1 PARTITION OF THE HIGH BANK

The Upper Pannonian assemblage is known in detail to a depth of 50 m from drilling along the periphery of the high bank and can be divided into two well-defined parts based on the results and investigations: Figure 18

#### Lower aggregate section:

Characterized by the rapid alternation of differently developed layers and their consequent smaller thickness, the assemblage section is composed of alternating layers of clay, silt, sand and "sandy silt".

#### Upper aggregate section:

The alluvium typically starts with sand, "sandy silt" layers, which in places accumulated to a thickness of more than 10 m. The formation of these sandy layers is probably related to the transport of sediment by rivers from the nearby mainland and has been deposited. The accumulation above the granular layers indicates the gradual deepening of the lake. Dark marshy layers appear, followed by heavily calcareous, hard deposits indicating drying out, which in places give way to limestone.

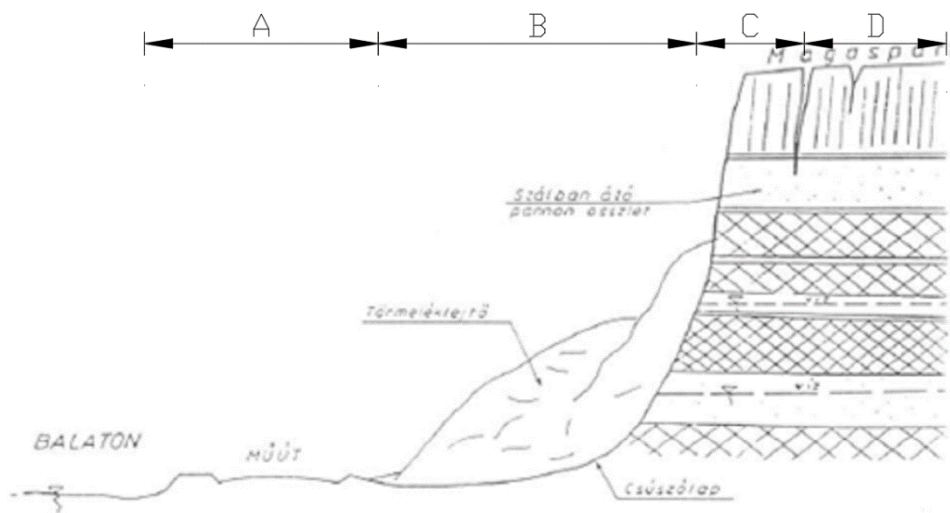


**Figure 18 The schematic geological structure of the high banks of Lake Balaton and the typical cross-section of the high bank highlands [18]**

As the layers accumulated, the sedimentation of the area was also brought to a long end by the disappearance of the upper Pannonian assemblage. Morphologically, the high bank can be divided into four distinct areas:

#### A) Fore shore

Height ~105-106mBf. The foreground is located between Lake Balaton and the foot of the high bank. It was formed by filling and landscaping, partly away from Lake Balaton, with a width of ~100-200m depending on the landscaping.

#### B) Debris slope

The average elevation of the ground level here is ~107-139mBf with a steep slope. It extends between the edge of the high bank and the foreshore. It is formed by the collapse, sliding and creep movements of high banks. It is usually characterised by dense vegetation.

#### C) Wall of the high bank.

A vertical or near-vertical wall 15-20 m above the debris slope, where the rocks that built it up can be observed in their original settlement. In the central part of the area, the steep coastline has been transformed by past movements and erosion into a rubble slope with a 45-60° angle of inclination.

#### D) Coastline and the area behind:

The top part of the bank, where it breaks or starts to break away, is the shore. Behind the shore edge is a barely indented, almost flat, gently sloping area rising gently in an east-southeast direction, with a morphological boundary extending for several kilometres. The area between Lake Balaton and the shore wall is morphologically part of the Balaton basin, while the prominent area behind the shore wall is an integral part of the so-called Balatonkenese - Kungösi Pannonian plate.

Of particular importance in the geological history of the area is the depression of the tectonic lines along the Upper Pleistocene, which led to the formation of the present-day unified Lake Balaton in several stages. According to the investigations, the lake accumulated sandy, calcareous, sometimes organic sediments in the foreshore of the high bank, 3-5 m thick, which are mainly derived from the erosion of the Upper Pannonian sediments. The process of lake sedimentation in the area ceased with the levelling of the lake shore.

The debris slope between the wall of the high bank and the forebay is predominantly composed of mixed material from upper Pannonian strata, formed by the sliding and collapse of the wall of the high bank.

The Balaton-Land part of the Balaton High bank is composed of Neogene Upper Pannonian and Quaternary loess and sedimentary layers of Lake Balaton. In the Upper Pannonian period, the Balatonvilágos highland section was part of a fresh water sea, in which clayey, silty, sandy, 'sandy-silt' formations accumulated. Some geological literature classifies the strata that built up the high banks as part of the Tihany Formation, which was formed by the filling of the Pannonian basin. The total thickness of the layers of this formation is defined as 80 m. In the section of the high bank wall, the uppermost sedimentary layers of the Pannonian sedimentary complexes occur, indicating the gradual deepening and complete drying out of the lake in this section. [17]

#### 3.1.3.2. GROUND AND STRATIFIED WATERS

Groundwater is found in a partially artificially created almost flat area between the debris pile and Lake Balaton. The groundwater is stored in silty, sandy sediments and moves towards the lake where it is drained. The outflow of stratified waters along the shoreline plays a key role in recharging the groundwater, as studies show that the main water receptors are sediments deposited or accumulated by Lake Balaton on the upper Pannonian assemblage. Consequently, the groundwater in the area in front of the high bank is nothing more than the groundwater from the outflow of the upper sand layers of the Upper Pannonian assemblage.

From the documented typical aquifer section, shown in the Figure 19, it can be seen that in addition to the uppermost seeps, several aquifers are also completed at high banks and their water is transferred to the sediments that build up the debris slope, thus degrading their soil physics. The lowest aquifers, in turn, are partially naturally drained by springs at the foot of the high bank and artificially drained by seeps in some sections. Where there is no seepage, the water continues to flow towards Lake Balaton. It can be seen on Figure 20

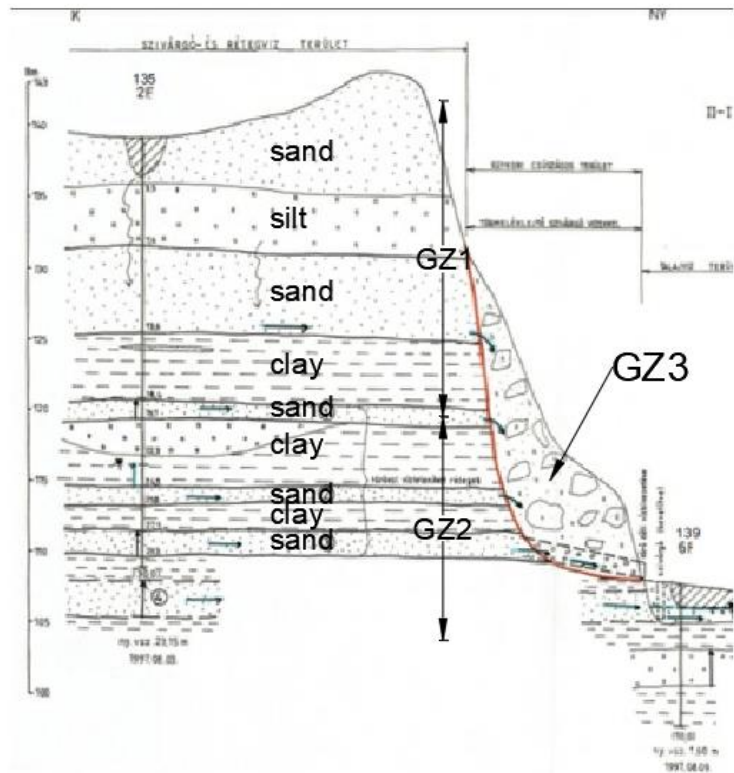


**Figure 19 Typical hydrogeological cross-section of the High Bank (horizontal and vertical scales are differ) [16]**

The debris slope is not a separate unit from a hydrological point of view. Its role is mainly to capture the outflow from the high banks. Partly it transports them towards the erosion base and partly it creates springs, thus facilitating their natural drainage. In line with this mediating role, their rock and soil physical properties are largely determined by the amount of aquifer water coming from the high banks but are also significantly influenced by surface water coming from the high banks and flowing onto the debris slope.

The drilling has uncovered stratified water in the high bank boreholes. In the lower and middle parts of the Upper Pannonian layer, a thicker ~10-12m of granular, sandy clayey silt and sandy silt were encountered in both boreholes. The lower zone of this layer is one of the most significant aquifers in the area, where water flows at the boundary of the more granular and underlying less permeable layers. Towards the bottom of the layer, the water content increases, the shear strength parameters decrease, and the bottom tens of centimeters of the layer are in a fully softened state. In the excavations, this occurred around the 127.3-127.7 mBf levels. Then the water flowing here exits the wall of the high bank and enters the slope debris and soaks it.

During the site visit, such a spring was observed, which exited the wall of the high bank and soaked the rubble plateau behind the building and continued its way towards Lake Balaton. It can see on Figure 20.



*Figure 20 surface springs in the debris slope in the northern part of the area (site visit photo)*

In the northern part of the area, wetter zones are found between 115-120 mBf and around 113 mBf, while there were also unconnected water levels in the current 101F and 102F boreholes. The aquifers are not found throughout the entire area but show a limited distribution because they are embedded in some direction. Recharge of the aquifers encountered in upland boreholes is provided by rainwater in places where the aquifers are located at or near the surface.

The high bank drillings have also been observed in deeper granular layers with stratified water. These are ~1.5-3.5m water pressure relative to the aquifer. [17]

### 3.1.3.3 PAST SURFACE MOVEMENTS

The surface movements closely associated with the high banks of Lake Balaton are part of a natural process of surface evolution linked to the dynamic, constantly changing activity of the high banks, both building and degrading. Therefore, the movements of the high banks of Lake Balaton are a complex process, influenced by natural forces, which can also be affected by human intervention, both positively and negatively. Inappropriate interventions can cause movements, but if the laws and processes that cause the movements are recognised and acted upon by correct technical interventions, stability can be ensured or increased. Surface movements on high banks can typically be divided into two major groups.

- Blocky collapse of the high bank
- Swelling, creep-like movements of debris accumulating at the toe of the high bank



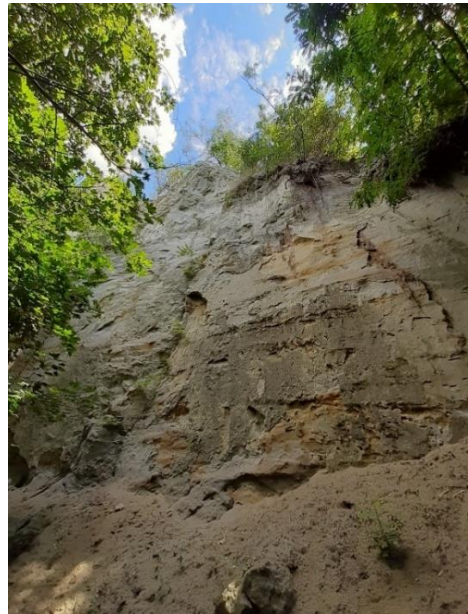


*Figure 21 The sandy loess wall of the high bank (site visit photo)*

The typical reason for the movement of the debris slope is that the naturally formed debris slope prevents the escape of the water layer, which is forced to swell back and degrades the shear strength of the aquifer and the underlying bound layers.

The other types of movement that are typical of high coasts (collapse, clogging, scouring and scouring) are caused by the loss of cohesion of the upper layers of the high coast due to natural precipitation falling and infiltrating, and excess water infiltration from human activities. Although in their natural state these soils remain in a near-vertical or vertical wall, the above causes the formation of additional infiltration cracks in these water-sensitive layers. Winter precipitation, frost and melting also contribute to the widening of cracks and the reduction of the internal resistance of the soil mass. Such a recurring process causes the separation of small and large blocks, resulting in collapse and detachment. Thus, the high bank gradually recedes and the remaining wall after the break-off remains nearly vertical. (Figure 22)



*Figure 22 Block detachments on the wall in 2021, near the study area (site visit photo)*

Until the last decades, large-scale shoreline failures occurred on the high banks, which were particularly accelerated during the construction and operation of the railway in the eastern basin of Lake Balaton, where eight large-scale shoreline failures occurred between 1875 and 1946 along the high bank line to

the north-east of the study area. During the same period, no significant movements occurred on the southern shore of Lake Balaton, and there was no repetition of previous large-scale shore collapses. It can be concluded that the natural conditions of the high banks are not identical, and that the stability of the high banks has not been affected in the same way by large-scale human intervention.

Many of the properties around the high bank have been subjected to undercutting and large-scale deforestation, which has resulted in frequent surface movements, especially after the wet winter-spring periods, affecting small areas but causing significant building damage.

Previous studies report that several close to the surface ground motions have been dated on the high banks for ~150 years, some of which are listed below in chronological order:

During the construction of the railway between 1857 and 1861, water leakage was noted in several places in the notch, causing problems

Several times in 1936, 1938 and 1940, after periods of rainfall, damage and movements were detected in the railway track's slope at 10 m from the edge of the high bank at Balatonaliga, after which a drainage shaft seepage and drainage pipes have been built.

In 1950, the first slide was observed on the southern part of the Balatonaliga high bank ~350m south of the study area. Here, too, dewatering trenches were built for stabilisation, and a leakage network for dewatering the trenches was constructed at the same time as the gully was being levelled.

Between 1958-60, a damaged watering system caused further slides in the same area. The pipeline was removed, and the gully was repaired. The footing drain behind the buildings was rebuilt and new leaks were installed.

During the 1960s, 1970s and 1980s, several bank failures were observed from ~800m south of the planning area: slow creep with building damage, bank peeling, soil erosion, tree uprooting, movement and damage, several of which were due to inadequate drainage.

Also in the 90s, several collapses were observed in the area around the former technical warehouse ~750m south, with 300-1200m<sup>3</sup> of slides and collapses. In 1994, ~800m<sup>3</sup> of soil collapsed, toppling 20 trees with 15-20 cm in diameter. The water level in two wells near the study area then rose to the top of the wells.

On 15 April 1997, 50m<sup>3</sup>, on 10 May 250m<sup>3</sup> and on 6 June another 60m<sup>3</sup> of soil collapsed behind the former wine cellar ~500m from the study area, causing significant damage.

On 29 July 2000, after a rainfall ~150mm to the north, the upper 8-12m of a 30m long section of the bank collapsed.

Decades of excavation and subsequent conservation measures have resulted in the disappearance of large-scale erosion events. However, in 2021 - Figure 22 - and 2022, there were major erosion events. These are likely to have occurred again due to inadequate drainage.

Based on these past movements and the fact that the collapse of the bank is still occurring today, it can be concluded that the high bank section under study is considered to be geotechnically hazardous.

Based on the map of hazardous areas in Hungary and the reports described, there is still active poaching activity on the coastline. [21] [22] [17]

The above-mentioned high bank slip data do not support that an earthquake could have caused a slip event. However, they may have indirectly impacted the high bank, causing a small displacement from which, thus contributing to a later slip event.

### *3.1.4 SITE DESCRIPTION*

The area in question is in the Balatonaliga part of the Balatonvilágos municipality, in the resort zone - Club Aliga. It is a holiday strip with an approximate north-south orientation and a length of about 1600 m. In the last century, several villa buildings and hotels were built on the side of the high bank. Most of the buildings are in the coastal strip, at the foot of the debris slope and on the plateaus left over from previous earth movements. Most of them have now been abandoned and have deteriorated considerably.



The Club Aliga site is divided into three parts: the northern part, which is about 500 m long and 150-200 m wide (north of the port), the central part, which widens to 350-500 m (at the port), and the southern part, which is 300 m wide and narrows to 50 m towards the site boundary. The area is bounded to the south-south-east by a railway line which runs along the top of the high bank. Figure 23



**Figure 23** Topographic map of the study area. The red box shows the specific area

The study area is located on the northern section of Club Aliga, as shown in Figure 23 with the dashed red line in the red box. The high bank is located where the level lines are very dense, in the middle of the red box.

Morphologically, the investigated high bank section is organically linked to the high bank line in the north-eastern part of Lake Balaton, which extends from Balatonfűzfő with minor interruptions to Balatonvilágos, as described in 313 subchapter.



**Figure 24** aerial photographs of the study area (left 1966, right 1992) [23]

In the Balatonaliga area there is a boat harbour, behind it is the erosion gully, which divides the area into 2 parts, north and south. The presence of this is attested by military surveys. There is no active erosion activity in this erosion gully. Rather, it is concentrated in the tributaries branching off from the main valley laterally and at its ends. In this main erosion ditch, an access road leads down from the plateau above to the foreland. A smaller, but also significant, erosion ditch is located to the south of the main ditch. The erosion gully has resulted in sedimentation activity in the area. Move behind from the ditch there is ponded sedimentation.

The sheltered southern part is heavily visited by tourists, while the northern part, on the northern boundary of the settlement, where there is a beach.

The high bank has 3 parts topographically: the high bank level, the slope, and the coast level. The height of the coast level is around ~105-108 mBf (meters above Baltic Sea level), while the top of the high bank is at a level of ~147-148mBf. The height difference between the two is ~40 metres

The wall of the high bank and the rubble slope are heavily overgrown with bushes and trees. Many abandoned and ruined buildings were also found in this strip. The undergrowth has been removed from the plateaux created by the previous slope movements, but dense undergrowth remains around the debris slope, immediately at the foot of the wall of the high bank (Figure 25).



*Figure 25 vegetation on sloped debris [17]*

In the northern part of the site - study area - the shoreline is clearly visible in situ and on contour maps, moved off to a depth of 2-3 m from the underlying plateau in a 15-30 m thick band. This moving may have occurred along a previous slip. However, descriptions from the last ~100 years do not mention such a movement of the wall of the high bank, only small-scale collapses. It is likely that this moving is hundreds of years old. The downthrown mass of soil was displaced and presumably rotated, causing layers of the displaced soil mass to slide away from the one behind it. (Figure 26) [24]



*Figure 26 Deformation on the edge of the high bank (photo taken at the top of the high bank) [17]*



### 3.1.5 FORMATIONS OF THE AREA

#### 3.1.5.1 QUARTERNARY PERIOD FORMATIONS

According to the Geological Map of Hungary, the surface, and the immediate surroundings of the Balatonvilágos high bank section are covered by holocene lake sediment (**lh**), upper Pleistocene loess (**eQp<sub>3</sub><sup>l</sup>**), upper Pleistocene-Holocene clastic aleurite (**dQp<sub>3</sub>-h<sup>yal</sup>**), lake shore made ground (**aQh<sup>f</sup><sub>2</sub>**), upper Pannonian Tihany Formation (**<sup>t</sup>Pa<sub>2</sub>**), Nagyvárzsonyian limestone formation (**<sup>nv</sup>Pa<sub>2</sub>**) and Fluvial proluvial sediment (**fpQp<sub>1-2</sub>**) as Figure 27 shows. [25]

Holocene lake sediment (**lh**): Quaternary Lake sediment, is typically composed of clayey limestone silt, sand, peat, rock flour.

Upper Pleistocene loess (**eQp<sub>3</sub><sup>l</sup>**): eolian loess of upper Pleistocene age, found in the surface, behind the high bank.

Upper Pleistocene-Holocene age lithic aleurite (**dQp<sub>3</sub>-h<sup>yal</sup>**) is a deluvial sediment with a rock composition that can be highly variable, depending on the degradation. It is widespread throughout much of the country, accumulating at the bottom of slopes and being washed away areally.

Landfill (**aQh<sup>f</sup><sub>2</sub>**): backfill of greater thickness, anthropogenic formation near the shore of Lake Balaton

The Tihany Formation (**<sup>t</sup>Pa<sub>2</sub>**) is a basin-permeable grey mollusoid clayey marl of aleurite and fine-grained sand with huminitic and charcoal clay, with less common yellow, grey, and greenish tarry clays and thin layers of lignite and dolomite. It can be up to 350 m thick.

Nagyvárzsonyian limestone formation (**<sup>nv</sup>Pa<sub>2</sub>**) is mainly white or brownish yellow, with a wavy surface. 10-50 cm thick, freshwater calcareous limestone. More widespread in the Balaton uplands. Typically, 20-30m thick.

Fluvial proluvial sediment (**fpQp<sub>1-2</sub>**) is made up of gravel, sandy gravel. It is made up of gravel, sandy gravel. Sediment from the Transdanubian Central Mountains, mainly composed of gravel and debris, occurs on the higher slopes of the mountains and on the hilltops south of Lake Balaton and Lake Venice. [25]

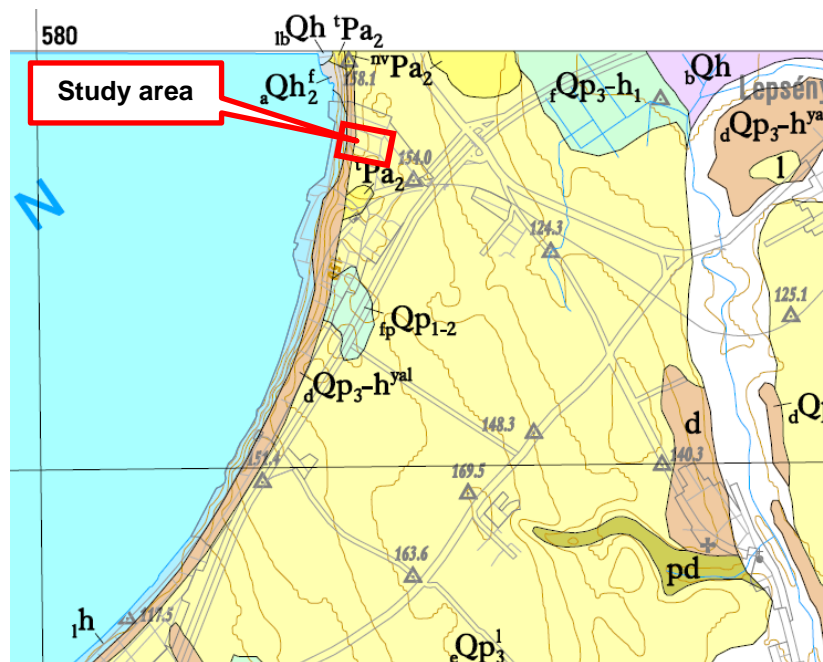


Figure 27 Quarter period formations at the study area (red rectangle) [25]

### 3.1.5.2 OLDER GEOLOGICAL FORMATIONS

#### 3.1.5.2.1 MIOCENE

Many of the formations in the area are of Miocene age, the most important being the Pannonian formations, which began 23 million years ago, after the Oligocene age, and ended about 5.3 million years ago, before the Pliocene age. The Earth gradually cooled during this period, heading towards what is known as the Ice Age. The boundaries of the Miocene cannot be tied to any one specific event, but rather only regional-scale changes define its beginning and end.

The fauna of the Carpathian Basin in the Pannonian Elevation is significantly different from that of the surrounding European areas, and the classification of the Hungarian Elements is used only in Hungary, as: lower Pannonian and upper Pannonian Elevation [26].

#### 3.1.5.2.2 PANNONIAN ELEVATION

During the nearly 10 million years of its evolution, the Pannonian Sea has formed the most massive sediment of all our geological eras, in some places 4-6 kilometres thick. In a broad sense, the Pannonian period is understood as the period from the Sarmatian to the Pleistocene (Ice Age), or the sediments deposited during this period. The Pannonian sediments cover a good three quarters of the country's territory. The lower Pannonian assemblages are still composed of fairly fine-grained calcareous and clayey marls, and less frequently of sandstones: these are either sediments of deeper waters or of the deltas of rivers emerging from the rising mountain ranges, deposited far inland [27] [26].

Then, after the Pannonian period, Hungary becomes dry, i.e. it gradually rises, and thick layers of clay and sand are formed in most parts of the country, at a depth of 10-100 m, where the Pannonian Sea used to be. In the Pleistocene Epoch (about 2 million years ago), the geology of Hungary was shaped by external forces such as water, wind, ground movements and swamps, which eroded the soil deposited on the Pannonian layer. In the Holocene period (about 10,000 years ago), the formation of gravel, sand, river deposits and river terraces shaped the present-day territory of Hungary [28] [26].

The lower Pannonian layer is assumed to be over-consolidated, given that it was formed after the Ice Age, where the effects of past tectonic movements, surface changes due to the erosive forces of wind, water, frost, and the layer deposited on top of it are remembered by the soil. Furthermore, laboratory results are consistent with this hypothesis [29] [27]

#### 3.1.5.3 DEEP GEOLOGICAL PROPERTIES

To get an idea of the deep geological conditions, I will examine the deep geological map and deep boreholes in the area around the study area. According to the deep geological map, the area is covered by quartzfillite formations (Figure 28). This is consistent with the deep drilling descriptions (Figure 29).

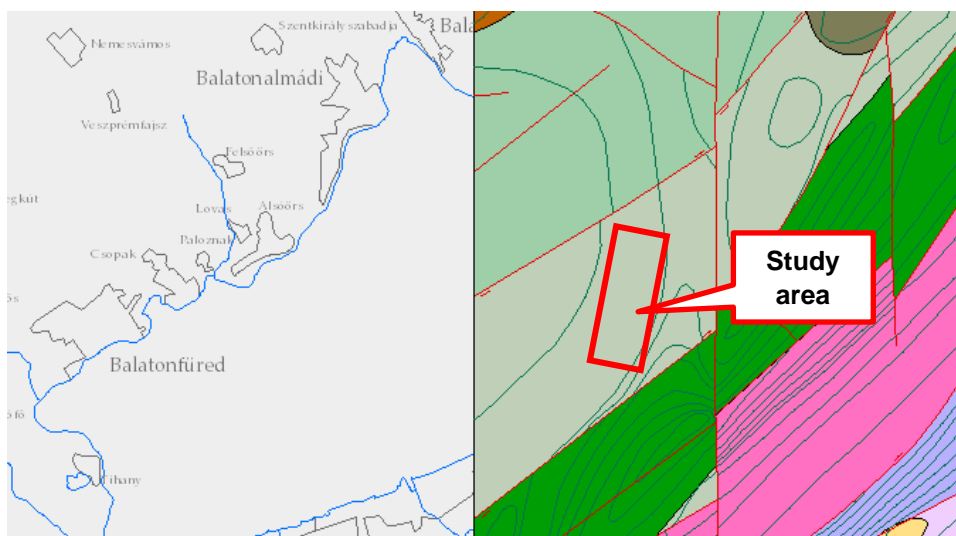


**Figure 28 Deep geological map of the north-eastern part of Lake Balaton [30]**



I have requested deep drilling descriptions near the study area from the MBFSZ (*Magyar Bányászati és Földtani szolgálat - Hungarian Mining and Geological Service*). The boreholes position can see in the Figure 29. The depth is between 7 and 254 meters below ground. The red box indicates the study area (Figure 29).

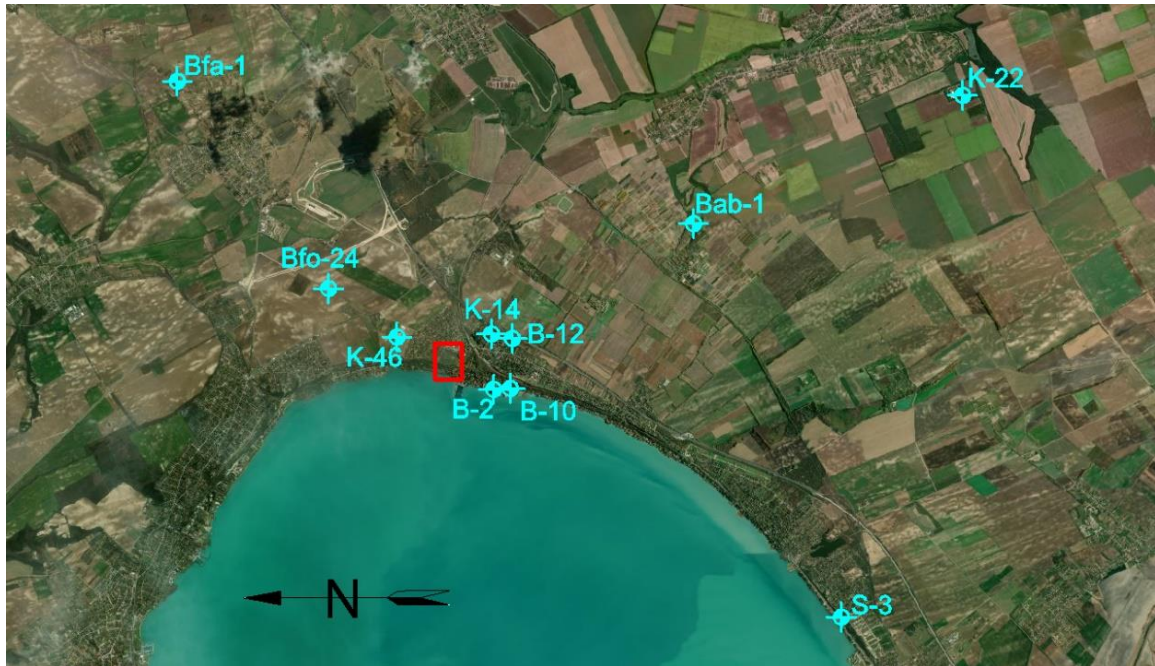


*Figure 29 Deep boreholes around the study area.*

The deep drilling descriptions gave me a good idea of the geology and deep geology of the environment. At the surface there is a 1-2 metres thick Holocene followed by a 2-20 metres thick Pleistocene layer. After that there is an upper Pannonian layer 80-150 metres thick, and then a lower Pannonian layer with 40-50 metres thickness at ~90-140 metres depth. This is followed by a Sarmatian layer ~140-195 metres deep and ~50 metres thickness. At a depth of ~200-250 m, the Ordovician age Balatonfőkajárian quartzfillite formation is present, which can be considered as the basement rock for earthquake purposes. In the Bfa-1 Balatonfőkajárian borehole, this rock appears at the surface, giving it its name, shows Figure 30



*Figure 30 Left: quartzfillite on the surface, righth: quartzfillite built cellar row in Balatonfőkajár (site phozo)*

### 3.1.5.4 QUARTZ PHILLITE

It is in the area between Balatonfő and the Lake Balaton line, in the so-called Balaton crystalline threshold. Its colour is typically grey to greenish-grey, consisting of quartzfillite, quartzite, chlorite schist, clayey, aleuritic rock types, acid volcanic debris interbeds and debris sediment types. 470-million-year-old, slightly metamorphosed, formed from sandstones. Thicknesses range from a few metres to several hundred metres based on excavations. It was found from the drilling that the direction of metamorphism increases in a W-SW direction [31] [32].

### 3.1.5.5. ORDOCIVIAN AGE

Geologically, it belongs to the Ordovician period, which can be assigned to the Palaeozoic era, following the Cambrian, and preceding the Silurian (Figure 31). It began 485 million years before this and lasted 41.6 million years. Its beginning is marked by the Cambrian - Ordovician extinction event, and at the end of the age there was an even more severe extinction period. Many fossils from this period have survived, which helps to determine the age. There are also large quantities of oil and natural gas. (Figure 31)

In this age the modern North America, Europe and much of Gondwana were covered by shallow seas. The shallow seas that formed on continental shelves were favourable for the development of calcareous organisms. Much of the northern hemisphere was covered by the Panthalassa Ocean and smaller oceans such as the Proto-Tethys Ocean, the Paleo-Tethys Ocean, the Iapetus Ocean, the Rheia Ocean, and the Khanty Ocean, which closed in the Late Ordovician.

The Ordovician rocks are largely sedimentary with a significant proportion of limestone. The area of land exposed to erosion was relatively small.

The Bfa-1 sign drill was made in Balatonfőkajár, where the rock is on the surface. The nearest drill is the K-14 drill which is ~400m, and Bfo-24 drill, which is ~2500m away from the study area. [33]

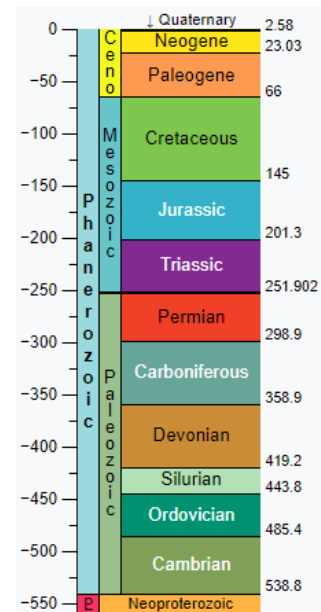


Figure 31 Eras and periods of the Phanerozoic [47]

### 3.1.6. THE TECTONIC CONDITIONS OF THE AREA

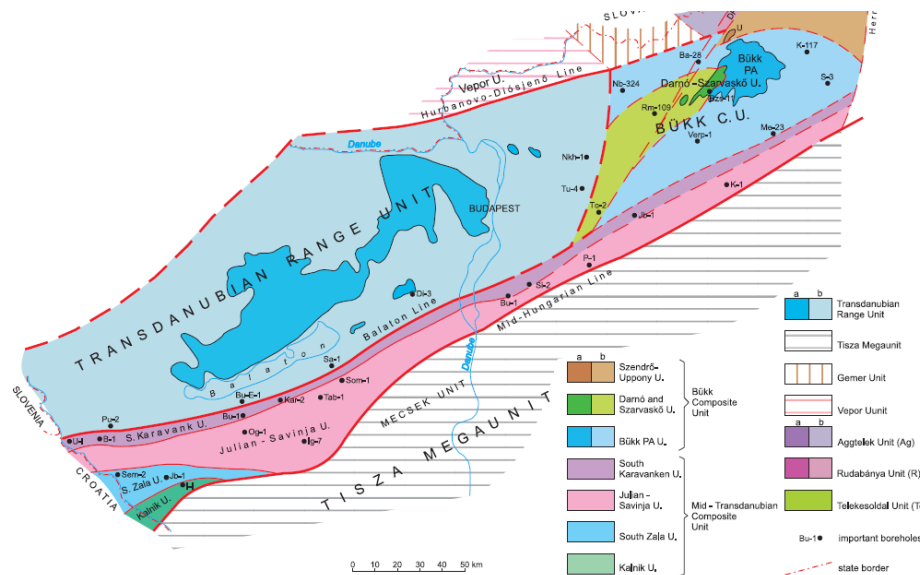


Figure 32 Component units and location of the Mid-Hungarian Zone [34]

Figure 32 shows the location of Lake Balaton in the surrounding geological units and the boundaries of the geological units. The study area is in the Transdanubian range unit. Another name for the area is



Pelso unit. This is because the unit north of the Balaton Line (Pelso Line) belongs to the African continental plate [34] [35].

In the eastern part of Lake Balaton, a high-resolution seismic data system has been mapping the most recent deformation events in the area over the last decade and a half, to provide a detailed neotectonic picture. These measurements will allow interpretation and compartmental mapping of neotectonic phenomena, the relationship between older (Miocene) and younger (post-Miocene, neotectonic in origin) structures and analysis of fault recurrence.

From the studies, a shearing belt parallel to the axis of Lake Balaton has been identified, which is built up by smaller faults. The more important faults are rooted in the pre-neogene drift, as is the Balatonfő line. Its function is supported in Miocene and post-Pannonian times. The earthquake activity at Berhida, northeast of Balaton, suggests that some of the faults may have been active in the Quaternary or even in the modern period [36].

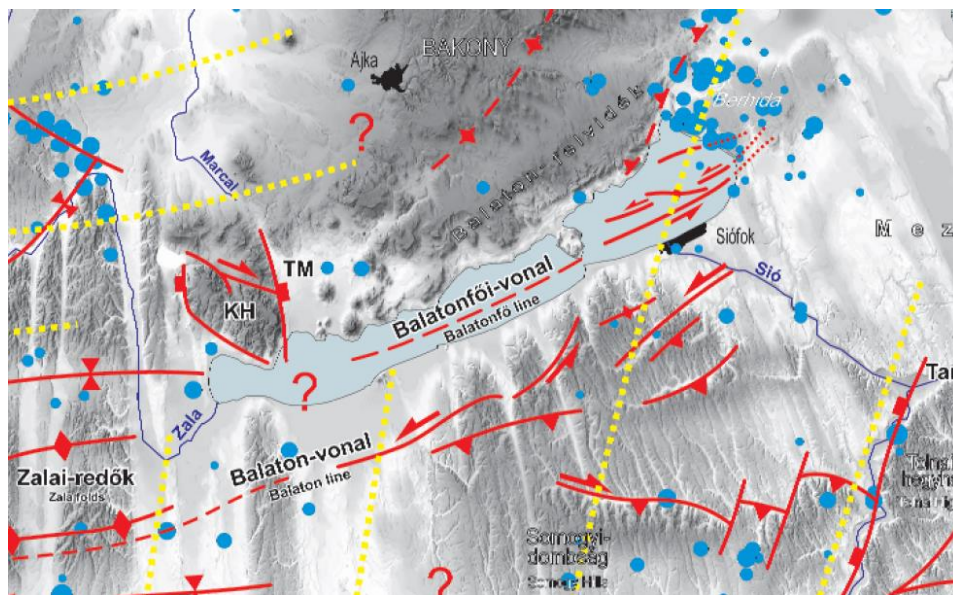


**Figure 33 Balatonfő and Balaton seismic lines, tectonic fault line, and earthquake epicentres [37] [36]**

Pannonian basin, which are mostly NE-SW trending in both the basement and the Neogene sediments. Therefore, the formation of the Balaton basin has traditionally been defined as a fault-driven, trench-driven collapse. Continuing along the axis of Lake Balaton towards the Velencei Mountains, the Balatonfői line runs through the basement, defining the Palaeozoic-Mesozoic formations of the Transdanubian-Middle and Central Transdanubian, with possible neotectonic activity. [36] [37]

As shown in Figure 33, the Balatonfő line is located 2-2.5 kilometres from the study high bank section, which means that a neotectonic activity would lead to the ongoing collapse of the coastal wall.

## 3.2 GEOTECHNICAL DATA AND ZONATION

### 3.2.1 BOREHOLES AND CPTS

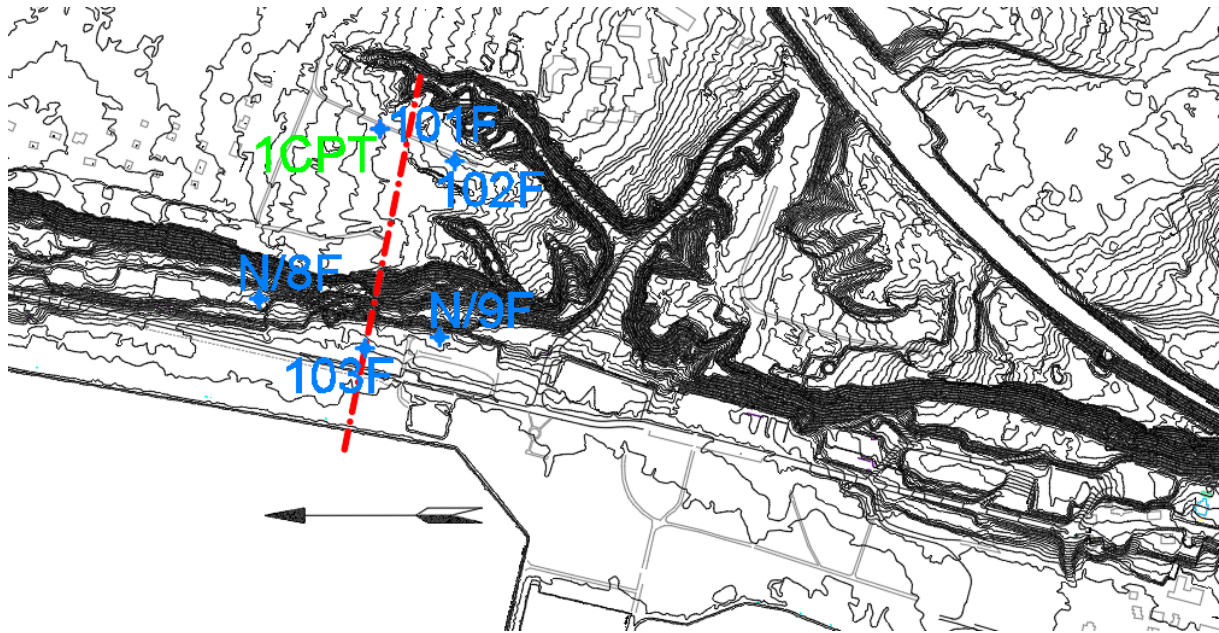


*Figure 34 Boreholes and CPT explorations on the study area*

Figure 34 shows the explorations on the topographic map of the study area. The blue ones are boreholes, and the green one is CPT exploration. Table 3 contains the information about the explorations. These data were provided by EFERTE Ltd as part of the ground investigation reports [38] [24].

The CPT sounding position can see on Figure 34. The depth of the sounding is 10m.

In situ soil testing was carried out using static sounding (CPTu), 1CPT. The drive unit of the probe is a PAGANI TG 73-200. The probe has a cross section of 10cm<sup>2</sup> and a tip angle of 60°.

*Table 3 Borehole and field tests at the study area*

Sign	Date of drilling	EOV Y	EOV X	Height [mBf]	Depth [m]
101F	2021.01.04-05	583302	183103	147.20	50
102F	2021.01.06-07	583270	183029	145.73	40
103F	2021.01.08	583085	183118	107.08	10
N/8F	2021.08.03	583134	183223	114.30	10
N/9F	2021.08.04	583096	183044	107.70	10
1CPT	2021.01.13	583302	183103	147.20	10

### 3.2.1.1 GROUND- AND STRATIFY WATERS

The boreholes identified stratified waters at various depths, which are summarised in Table 4

*Table 4 Ground and stratified waters*

Ground and stratified waters					
Borehole	Reached water level	Water level [mBf]	Stratified water layer 1 [mBf]	Stratified water layer 2 [mBf]	Stratified water layer 3 [mBf]
101F	-	-	122,2 - 124,2	112,4 - 113,6	-
102F	-	126,23	118,83 - 119,73	116,23 - 117,73	113,63 - 115,03

### 3.2.2 SOIL CLASSIFICATION

According to the laboratory tests the soils can be divide 5 categories:

1. Debris slope: A collapsed bank wall due to earlier slides. It contains a mixture of sand, silt, and clay.
2. Sand and silty sand, the Pannonian sediment upper stratum between -2,8-13,4 and -11,2-20,5m depth yellowish-brown, grey. The lower Pannonian sediment with 0,1-1,5m thickness, with rusty veins, cemented. Sieve analysis results: ~0-3% gravel, ~75-100% sand, ~0-23% silt, 0-3% clay. Steep sieve distribution curve.
3. Sandy silt, silt. Less knitted than the Stratum C and D. Thickness is between 0,1-2,3m. Sandy silt, silt, sandy clayey silt, kneadable low plasticity clay Sieve: ~0% gravel, ~9-62% sand, ~35-83% silt and ~3-10% clay
4. Medium plasticity clay, yellowish-brown, sandy, Stiff/hard, Lime concreting, kneadable/stiff/firm medium plasticity clay, sandy clayey silt, clayey silt, silt  
Sieve: ~0% gravel, ~18-28% sand, ~56-78% silt and ~4-16% clay
5. High and very high plasticity clay, light grey, grey, greyish, rusty-, sandy-, organic veins. Shell residual, organic veins in 10-50cms, a bit organic, dark grey, dark brown

Three geotechnical zones were established based on strength and stiffness:

Based on the laboratory tests, the high bank can be separated into 3 parts, based on the changes in the undrained shear strength parameters. This division is consistent with the geology.

1. GZ1: Top 28-29 metres of the high bank
2. GZ2: The lower part
3. GZ3: Includes the debris slope, part of the once sloping wall of the high bank.

The subdivision used in the cross section is shown in Figure 35

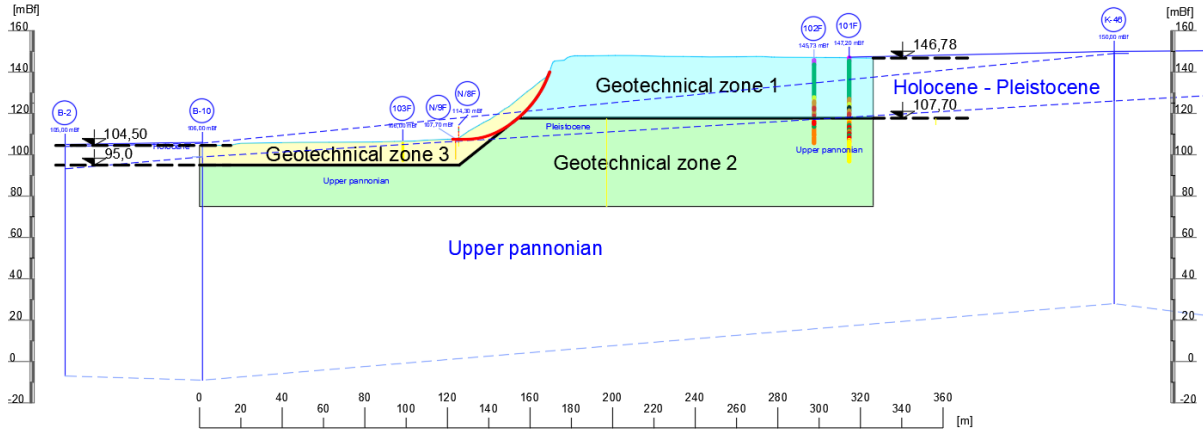


**Figure 35 Geological setting of the 101F, 102F, 103F, 1F and 2F boreholes and K-46, B-2 are deep boreholes**

In the study area, triaxial tests were carried out on samples taken from 3 boreholes (101F, 102F and 103F). After a depth of 28 meter below the surface, the two deep boreholes on the high banks (101F and 102F) showed a difference in E50 and su values based on the tests. This difference is consistent with the geological description.

Figure 35 shows the studied cross-section divided into geotechnical zones.

The light blue dashed line is the layer boundary, according to the deep boreholes, and the black line is based on the laboratory results. On the surface there is a thin Holocene layer, then Pleistocene, and after that according to deep borehole data, there is Pannonian Upper stratum. This layer is formed before the ice age and is over-consolidated due to the erosive effects of tectonic movements, water, wind, and frost. It is therefore necessary to divide the Pannonian layer into two parts, because it has a different consolidation, which has developed over millennia. [29, p. 35] [27]

### 3.2.3 LABORATORY TESTS

The geotechnical characterization included a sieve analysis test, plastic index determination, triaxial compression test - drained (CD) and undrained (UU), undrained direct shear test and material density analysis are performed. The test results are included in the ground investigation reports [24] [17]. The tests were carried out according to international standards.

#### 3.2.3.1. SIEVE ANALYSIS

In the laboratory, a sieve analysis was carried out on selected soil samples to classify the soils. The results were grouped by geotechnical zones:

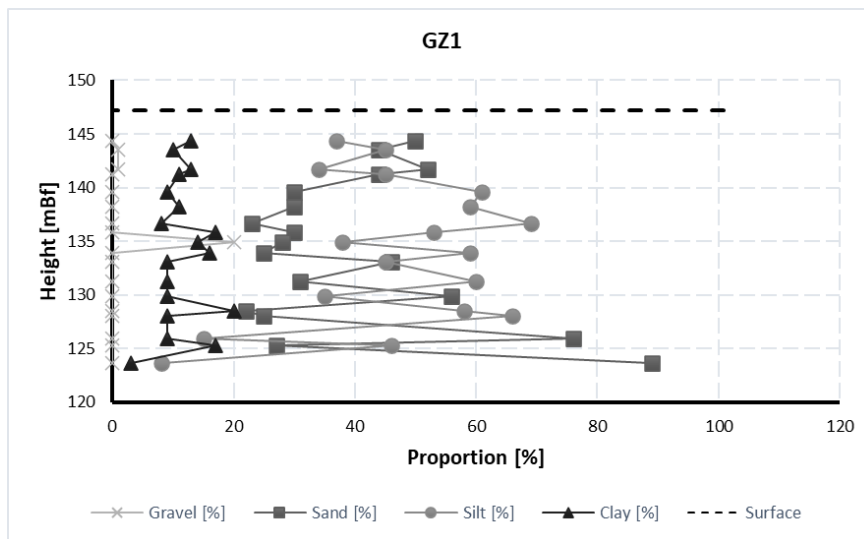


**Figure 36 Sieve analysis result regarding the Geotechnical Zone 1**

As the Figure 36 shows the GZ1 is a sandy silt or silty sand material with around 10% clay content. At the boundary of the geotechnical zone, the sand content increases.

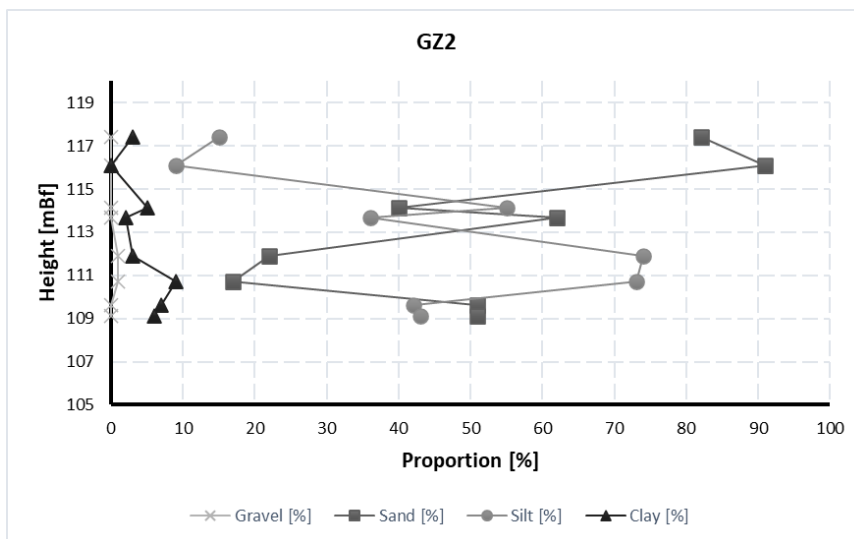


**Figure 37 Sieve analysis result regarding the Geotechnical Zone 2**

Figure 37 shows the sieve analysis of the GZ2. Its composition is very similar to GZ1 but with a lower clay content, ~5-9%

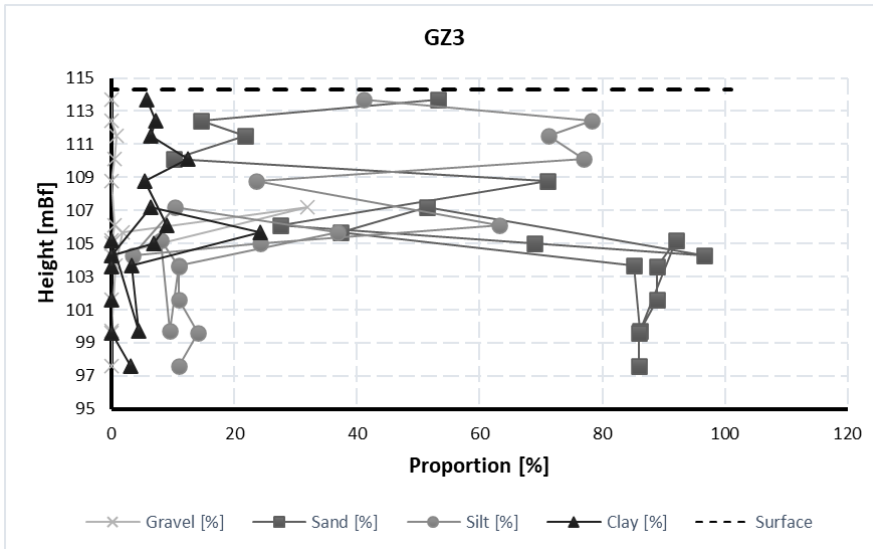


**Figure 38 Sieve analysis result regarding the Geotechnical Zone 3**

The composition of GZ3 is largely composed of slope debris that has been displaced by slides in recent years. The Figure 38 suggests a sand content of around 90%. The silt content has a scatter: between 105-115mBf changes between 10-80%, below that until 97,5 mBf is around 10%. The proportion of clay content varies roughly between 5-12%.

All 3 geotechnical zones have a negligible gravel content of around 0-2%.

### 3.2.3.2. ATTERBERG LIMITS

For the classification of the clays, the natural water content, the Atterberg limits and the consistency index were measured in the laboratory.

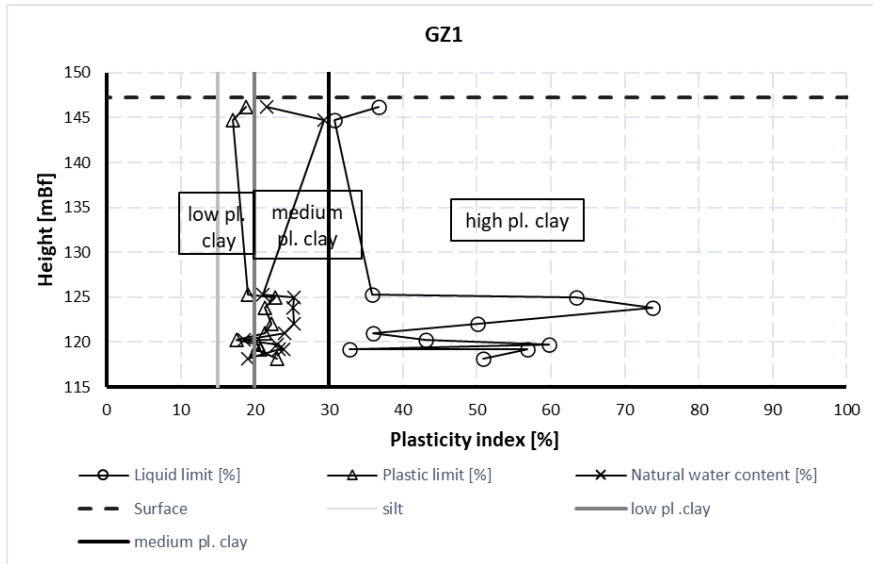


**Figure 39 Atterberg limit results regarding the Geotechnical Zone 1**

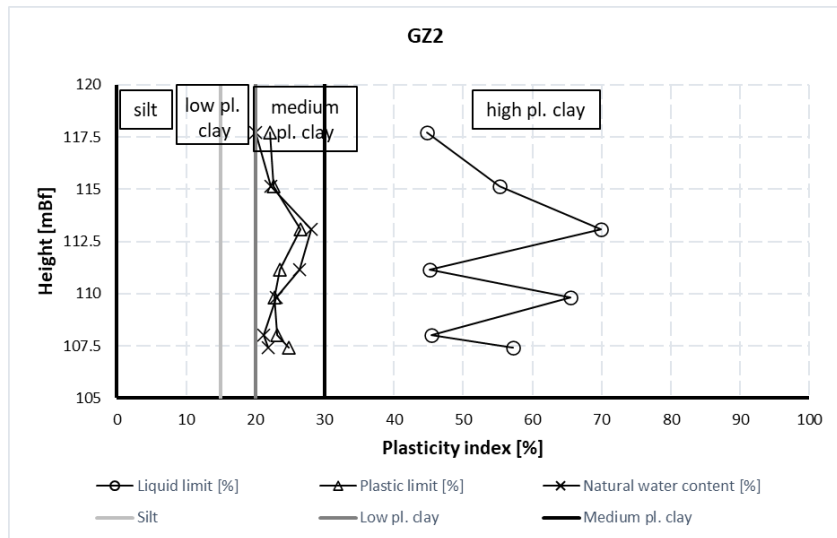


Figure 40 Atterberg limit results regarding the Geotechnical Zone 2

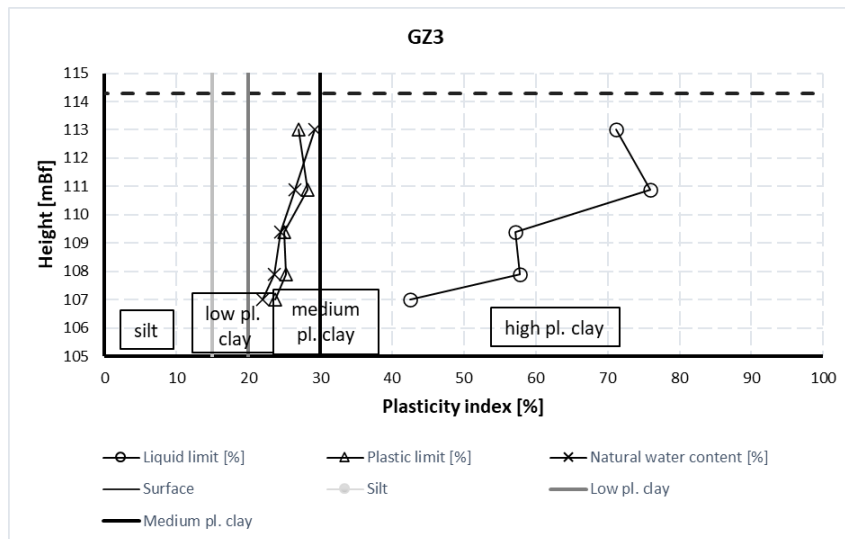


Figure 41 Atterberg limit results regarding the Geotechnical Zone 3

Figure 39, Figure 40 and Figure 41 shows the plastic index, liquid limit, and natural water content laboratory test results for each geotechnical zone. Tests were carried out on more clayey samples. There does not appear to be much variation between the values of the different geotechnical zones. Consistently, the natural water content falls around the plasticity limit.

### 3.2.3.3. TRIAXIAL ANALYSIS

In the triaxial compression test, unconsolidated - undrained (UU) and consolidated - drained (CD) tests were performed.

In the UU type (unconsolidated-undrained) triaxial test, the specimens were fractured while maintaining a hydrostatic stress condition, and the pore water was not drained.

In the CD-type (consolidated-drained) triaxial test, the samples were fractured while maintaining a hydrostatic stress state and waiting for complete consolidation at each load step, during which the pore water was drained.

The results of the CD tests are summarised in the following figures.

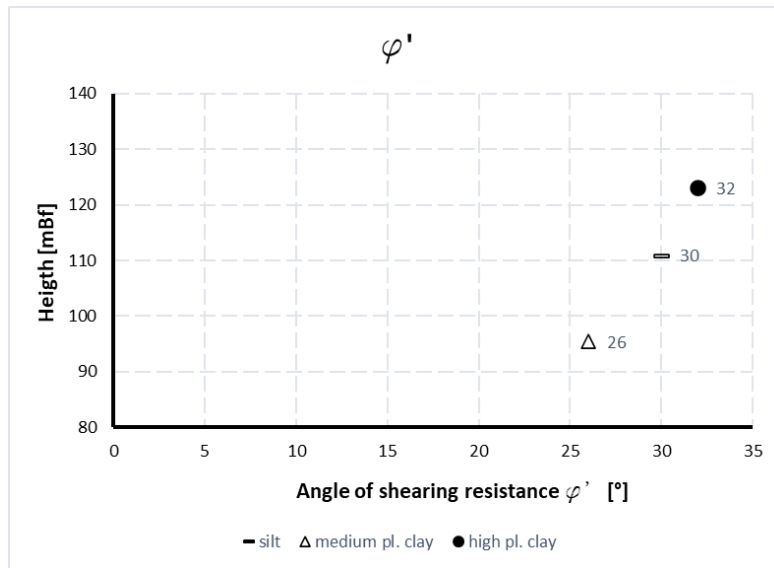


Figure 42 Angle of shearing resistance from drained triaxial analysis

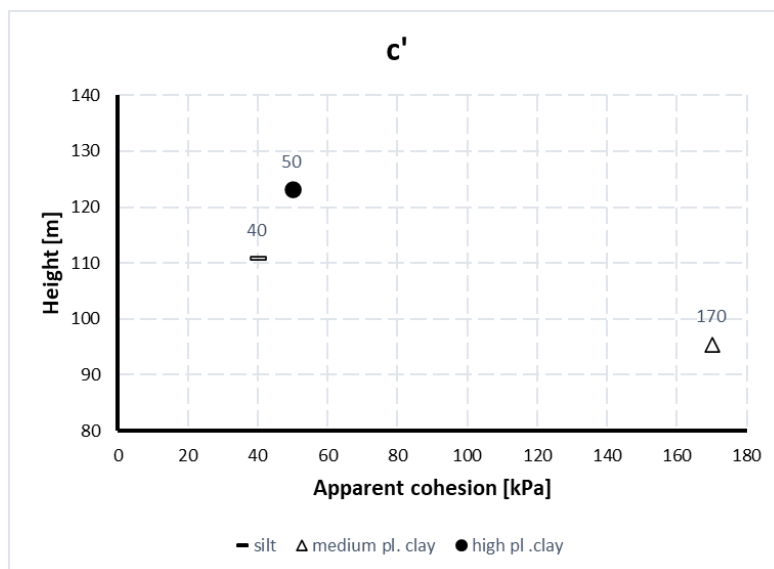


Figure 43 Apparent cohesion from drained triaxial analysis

Figure 42 shows the angle of shearing resistance results. The values go from 26 to 32 degree. The value decreases as the depth increases.



Figure 43 shows the cohesion values from the CD test. Values go from 40 to 170 kPa. But the scatter of the cohesion is high. The cementation in the wall of the high bank increases the cohesion of the high bank, as shown in the photos taken on site. In the case of the large blocks of detached from the wall of the high bank in Chapter 3.1.3.3. In addition, due to the aquifers mentioned in Chapter 3.1.3.2. apparent cohesion is created in parts of the high bank by the suction effect, mostly in the granular layers, and therefore the real cohesion of the high bank might be lower than this. Considering these effects, the coherence values measured in the 40 and 50 kPa laboratory seem realistic. The value of 170 kPa, however, is so different from the other two values that it has been excluded to approximate it for safety.

3.2.3.4. UNDRAINED DIRECT SHEAR TEST

The direct shear test was used to determine the shear strength parameters at a shear strain rate of  $v = 0.5 \text{ mm/min}$ . The results of the test are summarised in the Figure 44 and Figure 45.

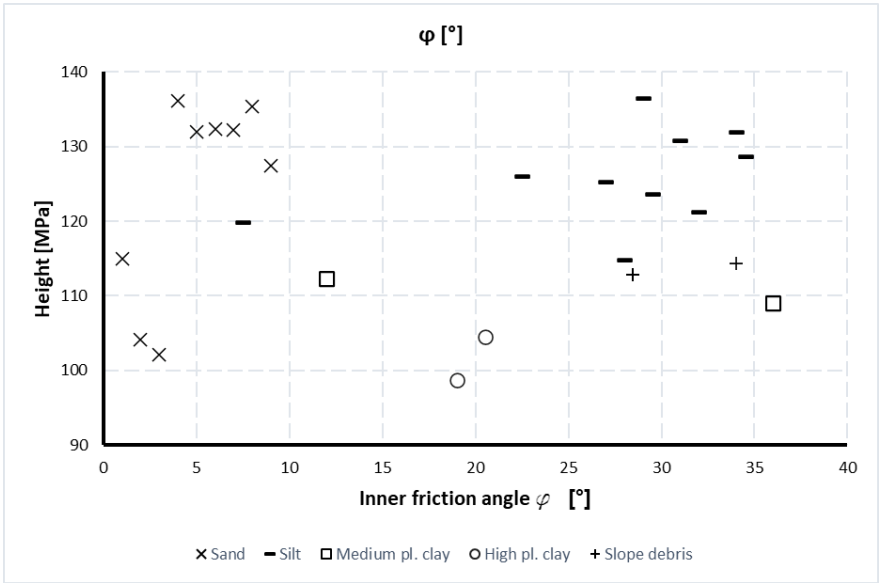


Figure 44 Angle of shearing resistance from undrained direct shear test

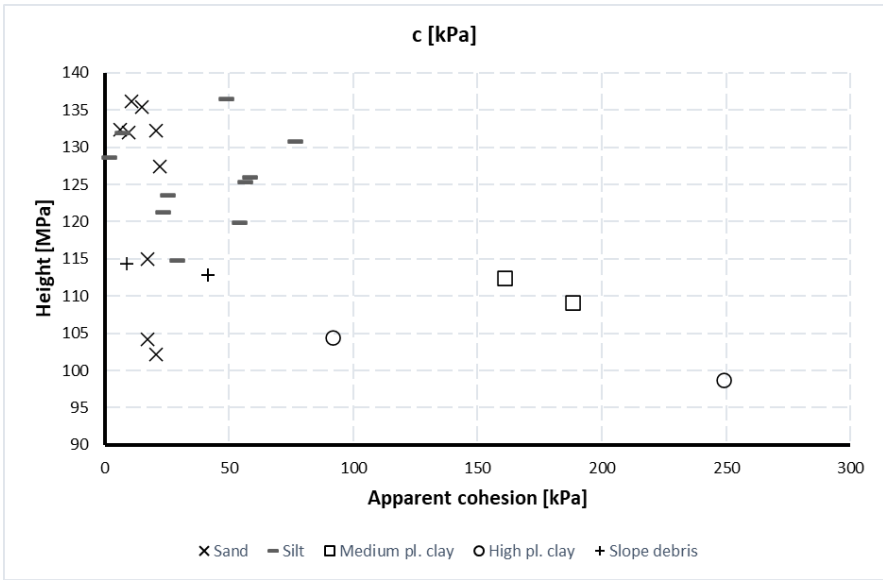


Figure 45 Undrained shear strength from undrained direct shear test

The inner friction angle result can see on Figure 44. There result is scattered but seems that the average is between  $30^\circ$  and  $35^\circ$ .

There is a high scatter in the cohesion values as well. It can be seen that from a depth of 25 metres, the strength of the soil increases (Figure 45).

3.2.3.5. MATERIAL DENSITY AND PHASE COMPOSITION STUDIES

A material density test was performed on undisturbed samples taken during drilling to determine the phase composition of the soil, which was used to calculate the wet and saturated bulk density of the soils.

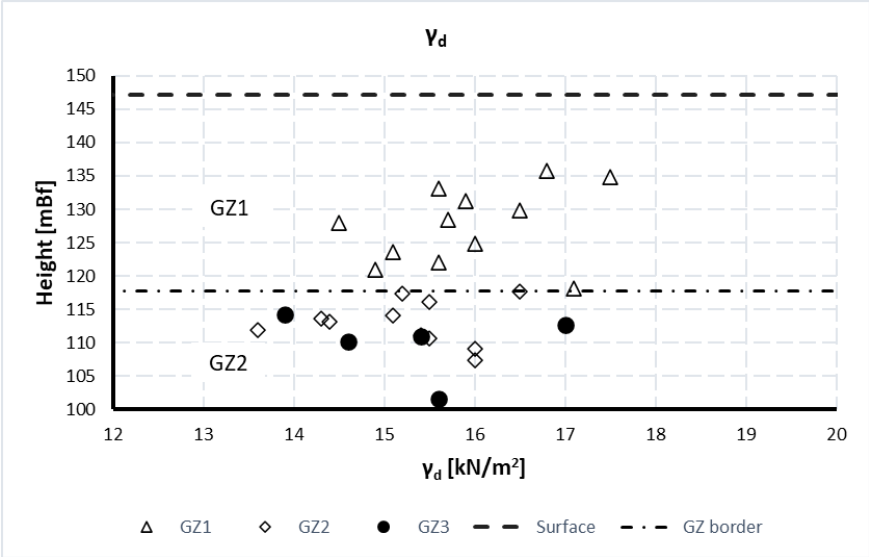


Figure 46 Dry unit weight from material density analysis

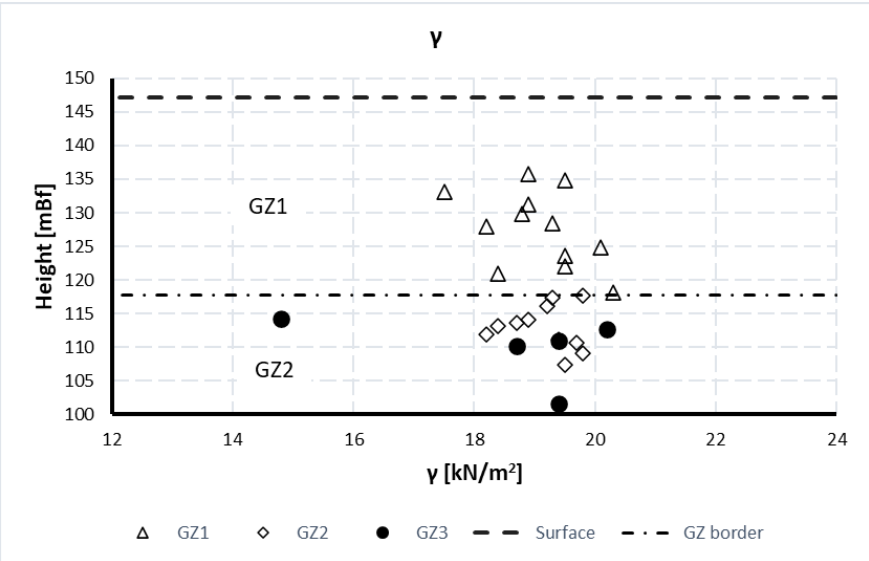
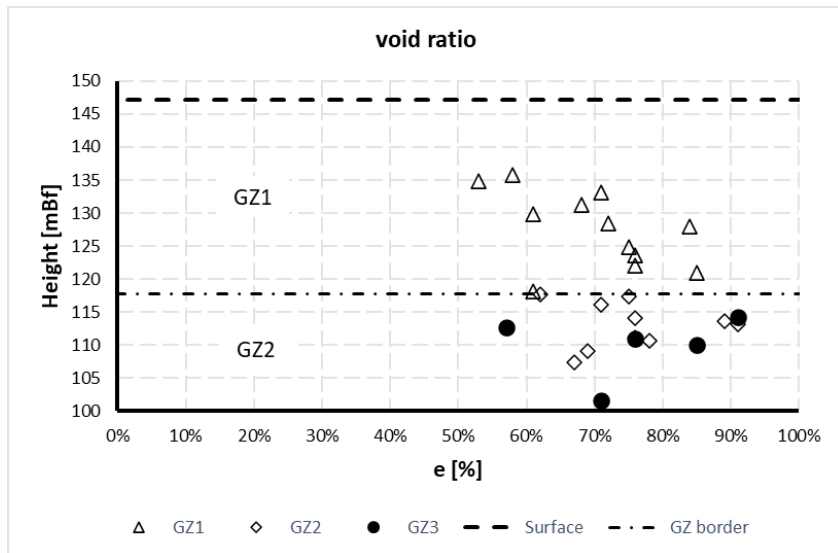


Figure 47 Unit weight from material density analysis

The dry and natural unit weights for the 3 geotechnical zones are similar. For the dry between 14 and 18, for the natural 18 and 20,5 (Figure 46, Figure 47).



**Figure 48 Void ratio from material density analysis**

Figure 48 shows the void ratio of the geotechnical zones. The values of GZ1 are seems bit lower, but there is no big difference in the data.

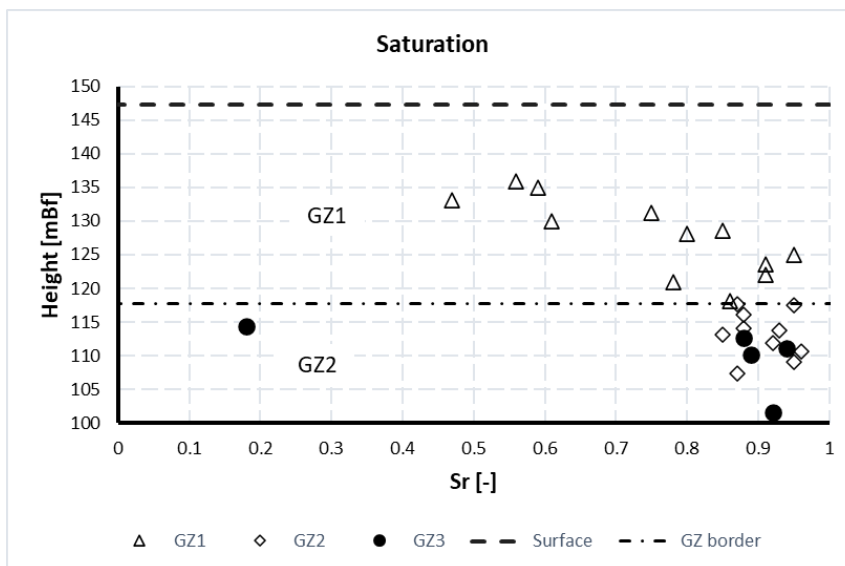


**Figure 49 Saturation ratio**

Regarding the saturation, the GZ1 values are significant lower, and scattered, than the others. It goes from 0,45 to 0,95. The GZ2 and GZ3 values are between 0,85 and 0,95 (Figure 49).

### 3.2.4 FIELD TESTS

#### 3.2.4.1 CPT SOUNDING

**Table 5 CPT test categorisation**

Static pressure soundings		
Name of layer	Stratum name	Average cone resistance values (MPa)
		1CPT
Organic soil	Made ground	0,31 (0,0-1,9)
Sandy silt / silty sand / sand	B	12,19 (3,7-10,0)

Table 5 shows the CPT test results from the Ground investigation Report [38]. To make sure the layering is correct, I plotted the layers on the Robertson diagram as Figure 50 shows.[39]

Redefined layer partitioning is shown in Table 6:

**Table 6 separating layers by CPT results**

	Average cone resistance (MPa)	Depth (m)	Soil classification
Organic soil	0,31	0,0 – 1,9	-
Silty layer	7,7	1,9 – 3,7	Medium dense
Silty layer	12,2	3,7 - 10	Dense, granular, hard clay

The result of the CPT test plotted to the Robertson  $q_t/F_r$  diagram, and then corrected the stratification according to these diagrams. (Figure 50)

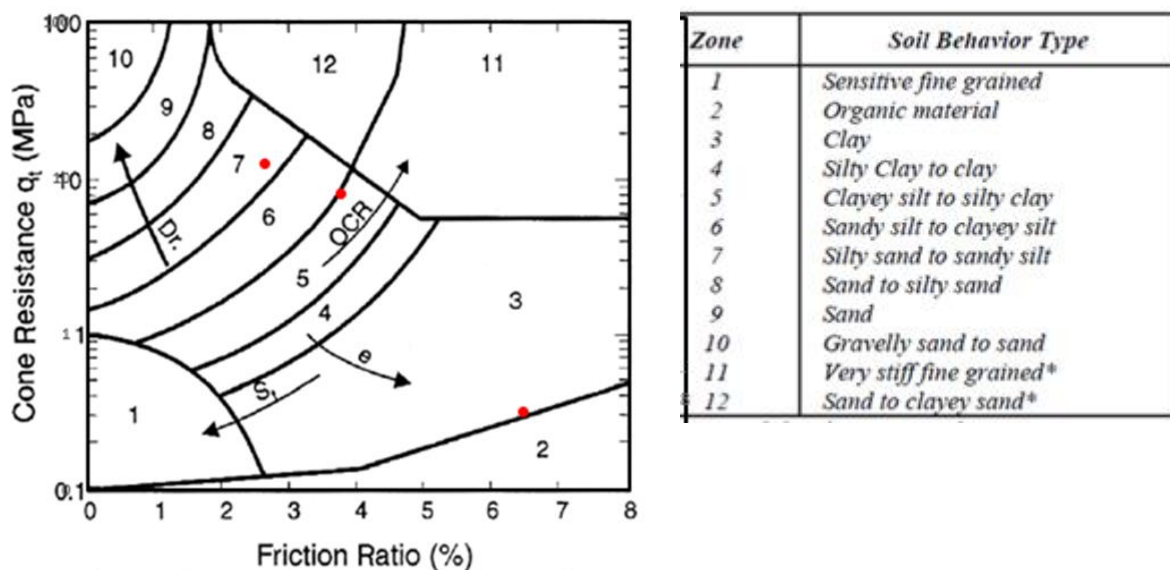


**Figure 50 Silty soil CPT data on Robertson diagram [39]**

### 3.2.5 SOIL PARAMETERS

The soil parameters were determined by a correlation procedure, which is described in detail for each parameter. There is a scatter in the values obtained, therefore a minimum, a median and maximum value limit has been set for each parameter, for each geotechnical zone, to make it easier to determine the real value in the iteration phase.

The outer limits of the test are set to cover 80% of the results, with the minimum limit ~10% larger than the smallest value and the maximum limit ~10% smaller than the largest value.

The field and laboratory tests used did not provide data on the cohesion, undrained shear strength and E50 parameters of GZ3 and will be determined during the iteration process.

#### 3.2.5.1 ESTIMATION OF ANGLE OF SHEARING STRENGTH

*From triaxial studies:*

The angle of shear strength parameter was determined from the plastic index using the Soronsen and Okkels iteration procedure. Starting from many data, a curve was defined that combines PI and  $\phi'$ . By fitting PI values to this curve,  $\phi'$  values were determined. [40, p. 3]

*From CPT studies:*

From the CPT, Kulhawy and Mayne defined a procedure to correlate the value of  $q_c$  with  $\phi$ . However, the calculated values differ significantly, by 30-35%, from the other results, so I have not taken them into account. [39, p. 11]

Estimating  $\phi'$  from correlation by PI test result with all triaxial and CD test in the study area. [41, p. 3]

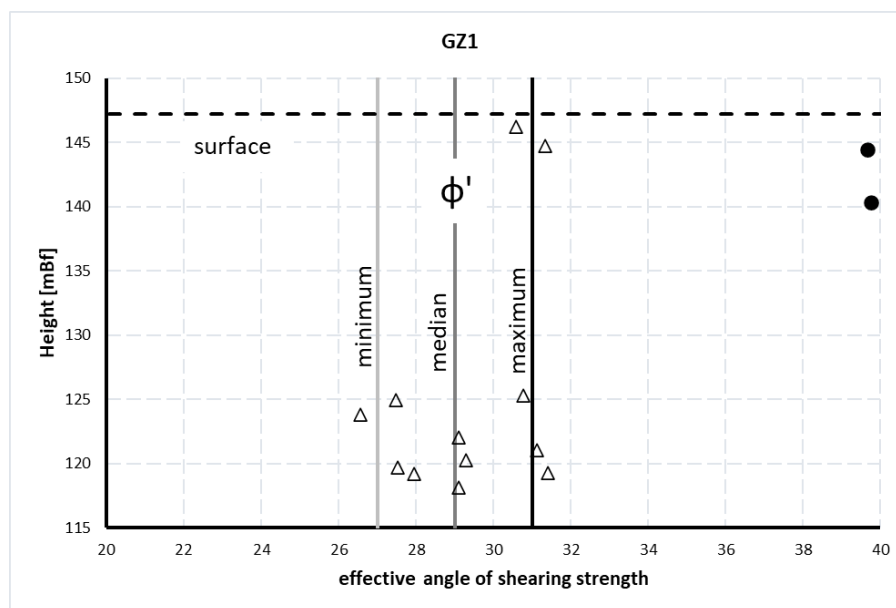
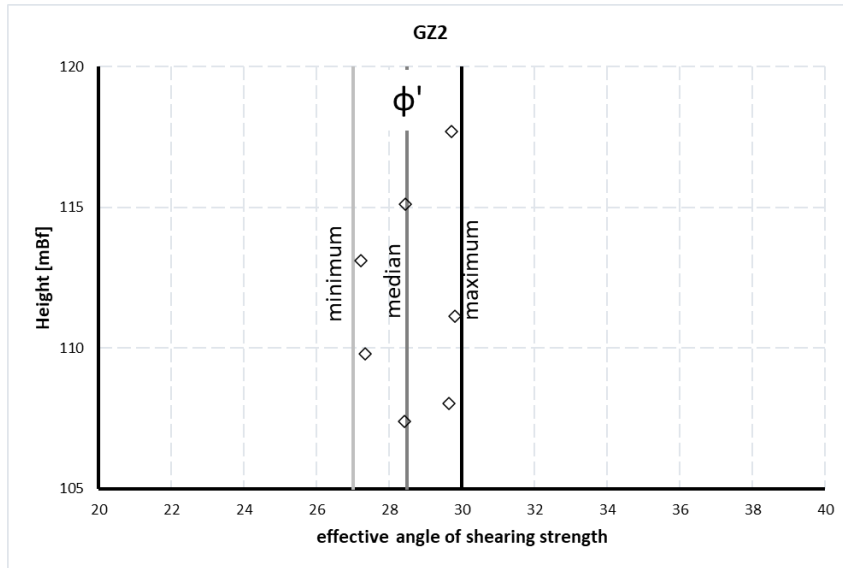
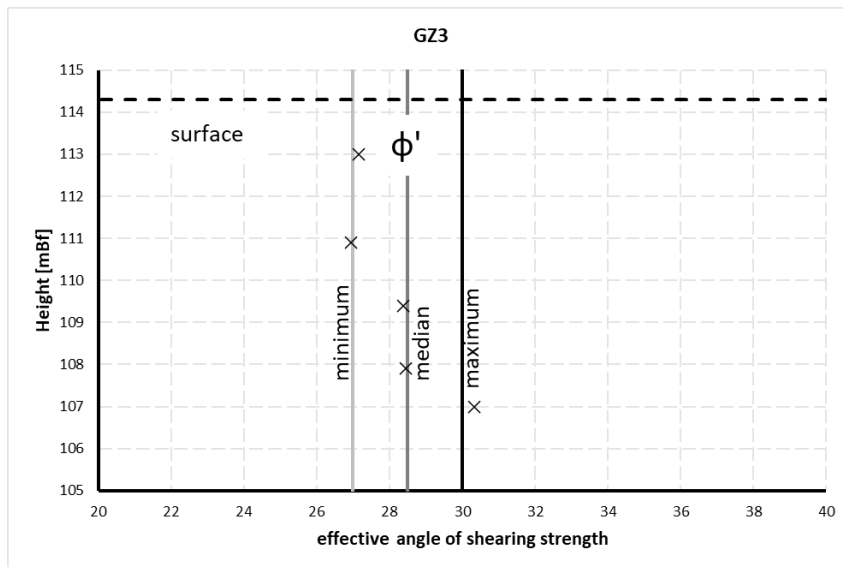


Figure 51 E50 values of GZ1



**Figure 52 E50 values of GZ2**



**Figure 53 E50 values of GZ3**

GZ1 had  $\phi'$  values between  $27^\circ$  and  $31^\circ$ , GZ2 and GZ3 between  $27^\circ$  and  $30^\circ$  (Figure 51, Figure 52 and Figure 53).

### 3.2.5.2 ESTIMATION OF E50 VALUES

From triaxial test

E50 values were determined from triaxial analysis. The sample for the test was obtained from core drilling in the field. As shown in the figure below, each sample is loaded with 3 load steps. In this case the first 200 kPa - red curve, then 400 kPa - blue curve, and 600 kPa - green curve. These values are the  $\sigma_3$  stresses that occur over the entire surface of the sample. The load in the vertical axis direction is  $\sigma_1$ . The difference between  $\sigma_1$  and  $\sigma_3$  is the deviator stress ( $q$ ). This is needed to determine E50. (Equation 2)

**Equation 2 Calculation of deviator stress**

$$q = \sigma_1 - \sigma_3$$

A line is then drawn to half of the maximum deviator stress from  $\sigma_1=0$ , as shown in Figure 54. The slope of this line is the E50 value, where  $\Delta\sigma$  is the stress difference and  $\Delta\varepsilon$  is the strain difference (Equation 3, Figure 54)

**Equation 3 Calculation of young modulus**

$$E = \frac{\Delta\sigma_a}{\Delta\varepsilon_a}$$

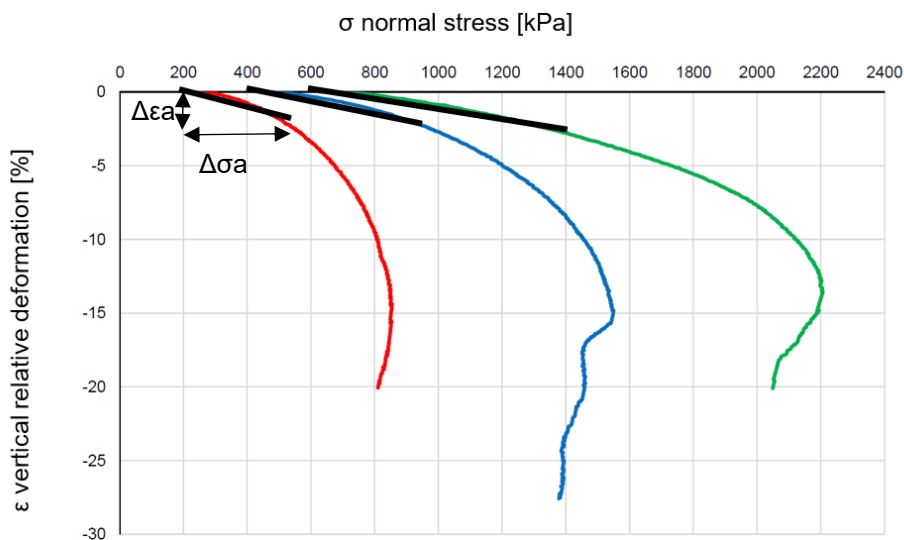


**Figure 54 Triaxial analysis of the 101F borehole sample at a depth of 31,2m**

From CPT test

To determine the E50 value from CPT data, I used Robertson's formula, which is shown below:

$$\alpha_M = 0,03 * (10^{0,55 * I_c + 1,68})$$

$\alpha_M$  is the constrained modulus cone factor, where  $I_c$  is the average consistency index value for the regarding layer.

Corrected cone resistance ( $q_t$ ) can calculate by the following way

$$q_t = q_c + (u_2 * (1 - a))$$

where  $q_c$  is the cone resistance,  $u_2$  is the pore water pressure, and  $a$  is the net area ratio of the cone, in this case: 0,75.

This equation is the correlation between constrained modulus ( $M$ ) and cone resistance ( $q_t$ ):

$$M = \alpha_M * (q_t - \sigma_{v0})$$

where  $\sigma_{v0}$  is the vertical stress in the initial point.

From constrained modulus the secant modulus can calculate by the following way:

$$E_{50} = (1 + \nu) * \frac{(1 - (2 * \nu)) * M}{1 - \nu}$$

where  $\nu$  is the Poisson ratio of the soil, I calculated with 0,3. [39]

The following figures show the E50 values for each Geotechnical Zone:

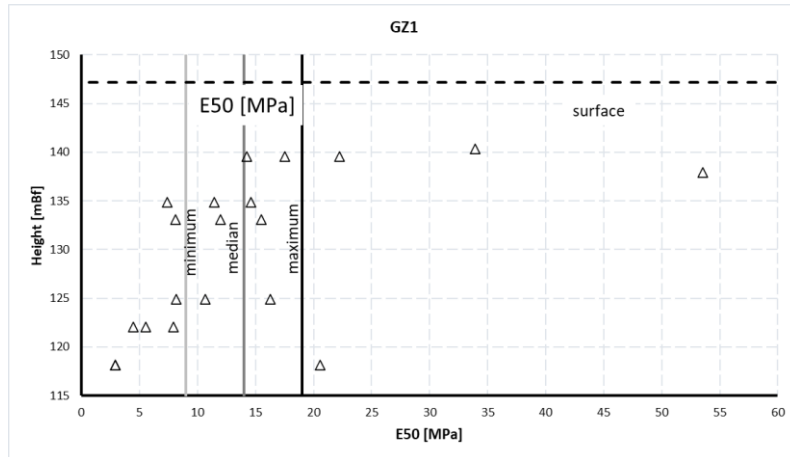


**Figure 55 E50 values regarding Geotechnical zone 1**

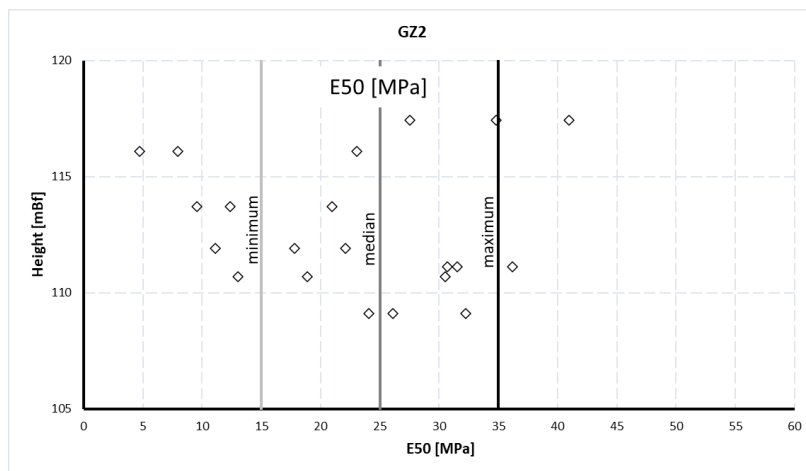


**Figure 56 E50 values regarding Geotechnical zone 2**

There is a visible difference between the values of GZ1 and GZ2. GZ1 values range from 9 to 19 MPa, GZ2 from 15 to 25 MPa. (Figure 55, Figure 56)

### 3.2.5.3 ESTIMATION OF UNDRAINED SHEAR STRENGTH

*From CPT test*

The following formula can be used to determine the value of the undrained shear strength from a CPT test: [42]

$$su = \frac{q_t - \sigma_{v0}}{N_{kt}}$$



Based on the  $q_c$  value from the CPT test, the soil classification was found to be silty soil and therefore the  $N_{kt}$  value can be taken as 23 [43, p. 4].

*From Triaxial test*

The undrained shear strength was determined as shown below:

$$q = \sigma_3 - \sigma_1$$

Where  $\sigma_3$  is the lateral pressure value,  $\sigma_1$  is the axial pressure parameter.  $q$  is the deviator stress. The  $\sigma$  values in the triaxial test report

$$s_u = \frac{q}{2}$$

The undrained shear strength is half the deviator stress.

The  $\sigma$  values were obtained from the triaxial test report [24] [17].

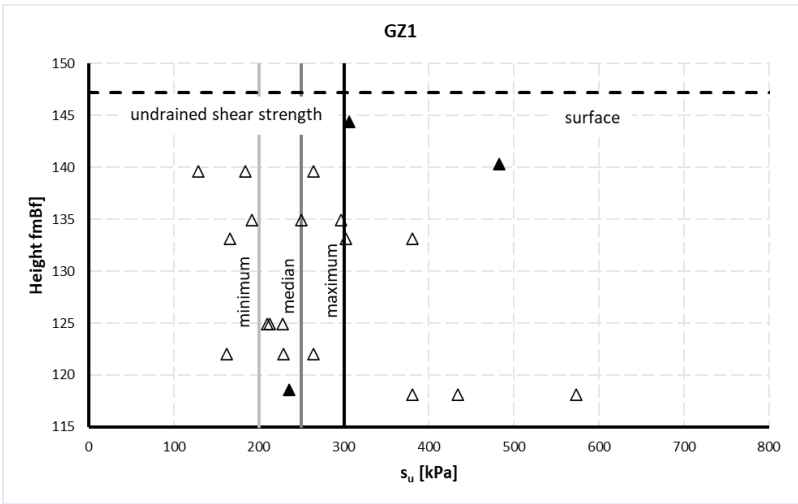


**Figure 57 Undrained shear strength of GZ1**

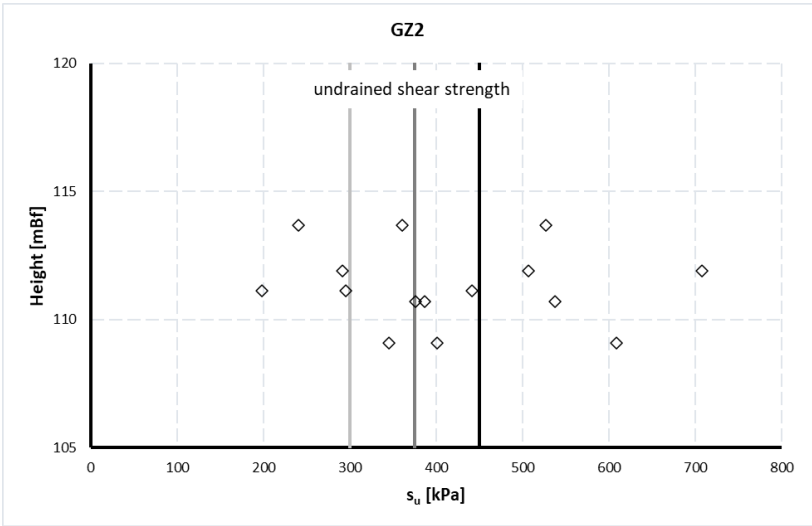


**Figure 58 Undrained shear strength of GZ2**

Figure 57 and Figure 58 shows the lower, median, and the higher limit undrained shear strength of each geotechnical zones.

### 3.2.6 DEFORMATION CURVES

The most common geotechnical application of deformation curves is in earthquake investigation. By cyclic shear testing, the hysteretic curve of a sample can be used to determine the behaviour of the soil under small displacements. This is useful in liquefaction studies. This is because then the pore water pressure increases so rapidly that even sand and granular layers exhibit undrained behaviour because there is no time for the pore water to flow.

The deformation curve generated from the triaxial test is not suitable for determining liquefaction because it does not provide information in the small displacement range -  $10^{-5}$  to  $10^{-8}$  meter/meter. Similarly, the more advanced soil model, the HSS (Hardening soil model with small- strain stiffness), does not provide information. However, it does provide information on soil behaviour over a larger displacement range ( $10^{-5}$  –  $10^{-1}$ ).

Results from CD and UU triaxial studies were used to generate the curves. The initial and residual Young's modulus were divided, this is the normalized Young's modulus. This value was then divided by the strain value. The horizontal axis of the deformation curves shows the value of the displacement on a logarithmic scale, the vertical axis is the normalized Young's modulus, the residual value of the Young's modulus divided by the initial value. [44, p. 4]

From the field samples, triaxial CD and UU tests were performed and the deformation curves were plotted by soil type, which are shown in the figures below:

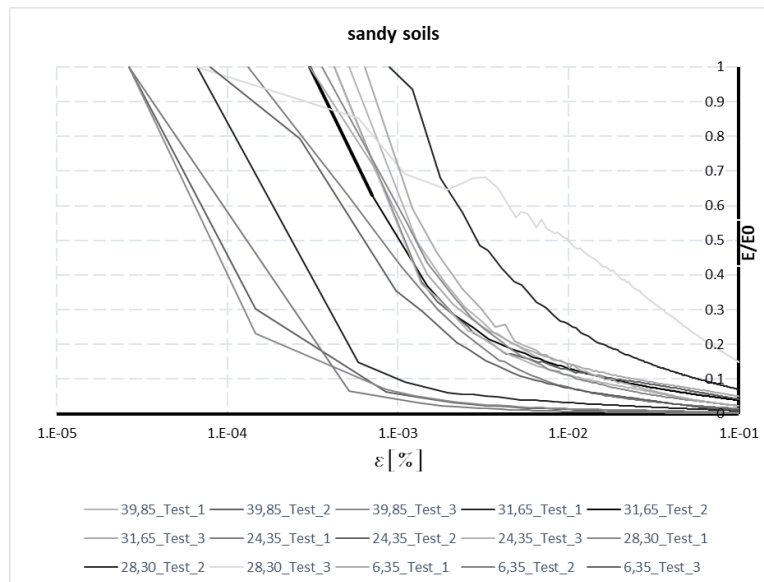


**Figure 59 Deformation curves regarding sandy soils**

Curves on the Figure 59 shows a bit high scatter. This can be because the difference between the curves. One type of the sand seems very compressible, (the lower) and the other seems a bit less compressible.

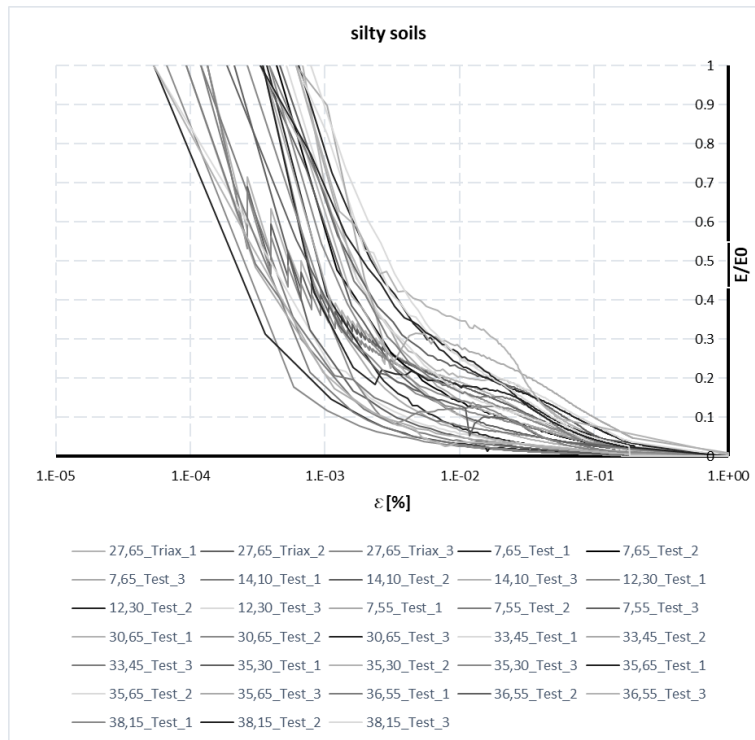


**Figure 60 Deformation curves regarding silty soils**

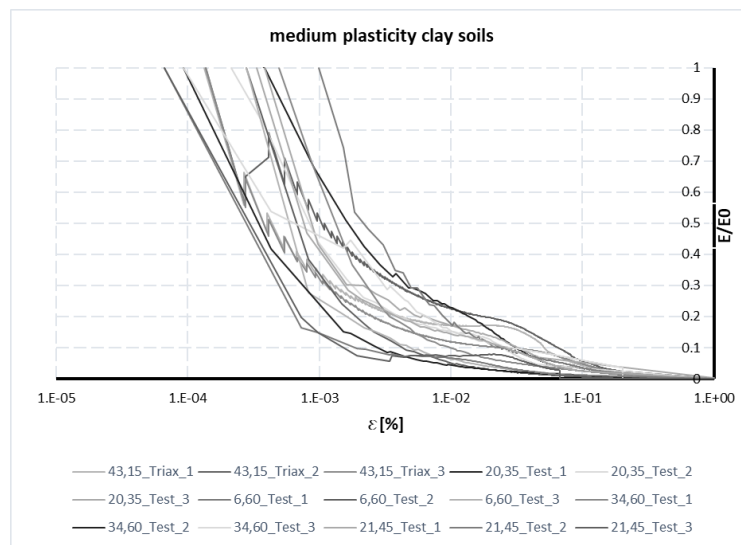


**Figure 61 Deformation curves regarding medium plasticity clay soils**

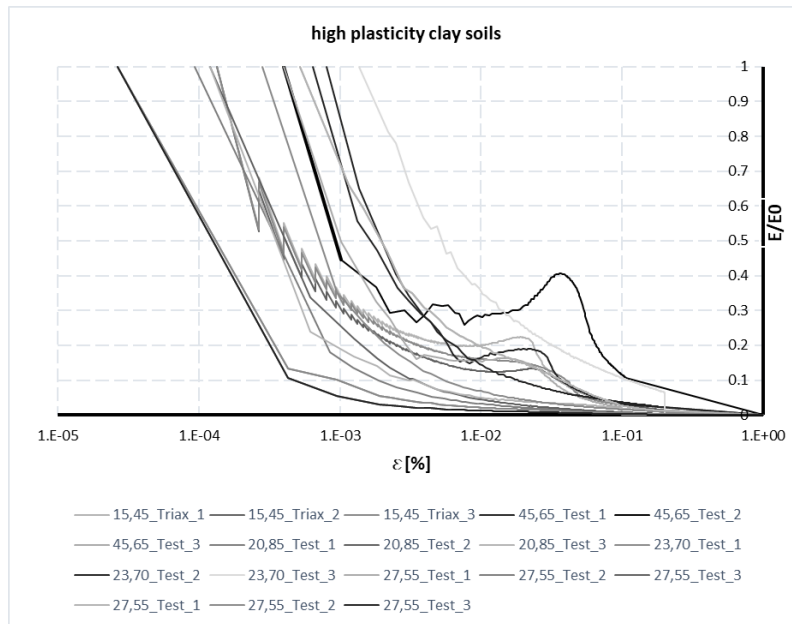


**Figure 62 Deformation curves regarding high plasticity clay soils**

The curves on the Figure 60 shows a greater consistency. The deformation values can be defined almost clearly from this.

The medium plasticity soils have also a more consistent deformation curves, can see on Figure 61.

The high plasticity clay curves also show scatter in the results, as the sandy soils. (Figure 62)

From the deformation curves, it can be concluded that all four soil types have similar values for volume change. Thus, it is possible to create geotechnical zones from the different soil types.

# CHAPTER 4 – BASIS FOR ANALYSIS AND STATIC STABILITY ANALYSIS

In this chapter the structure of the model that used in Plaxis in detail will be presenting. After that the applied phases during the calculation process. During the back analysis under static loading process the parameter bounds defined in the previous section are then adjusted, whereby Plaxis is used to obtain the values between the parameter bounds to determine which parameters will result in a safety factor value just above than one for GZ1 and GZ2. The parameters are modified one by one, so that their effect at the change in the safety factor can be seen directly. The parameters for GZ3 are then determined. However, no laboratory or field test results are available, so the aim is to approximate a safety factor value of 1.1 in this case for the GZ3.

The finite-element version of Plaxis is preferable compared with the limit equilibrium version for this task because the gravitational loading, which is the initial phase at each computational step, can be better modelled by the finite-element method.

## 4.1 MODEL STRUCTURE

### 4.1.1 GEOMETRY

Once the location of the cross-section was selected for modelling, the next step was to produce the cross-section. A contour model was produced from a geodetic survey of the site, provided by EFERTE Ltd [17]. The contour map model was converted into a 3D terrain model from which a cross section was created using the AutoCAD Civil 3D alignment generation tool. The cross-section is shown in Figure 63.

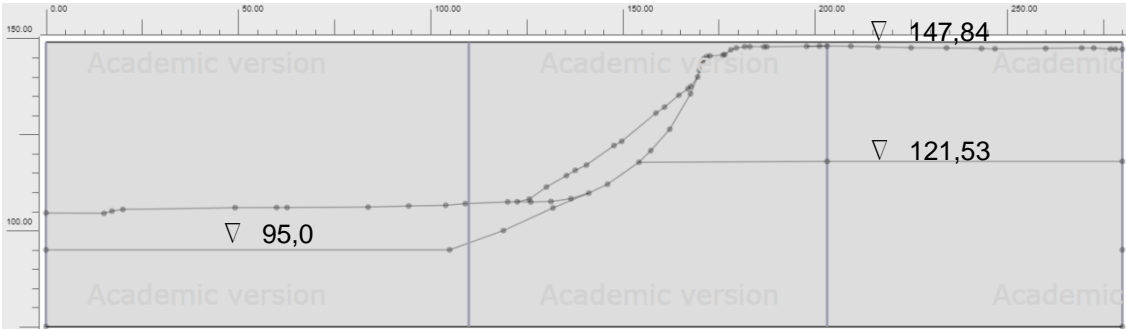


Figure 63 Model geometry



Figure 64 Model geometry of the slope debris

In Chapter 3.1.3.3. it was shown in on-site photos (Figure 26) that the upper edge of the high bank slide down with a width of 4-5 m, which is also shown on the geometry in Figure 64 with a red ellipse on.

The geometry of the debris slope is created according to the geometry. It starts at the point on the slope where there is a break point, near the upper edge, and it finishes at the breaking point, at the junction of flat ground and slope (marked by red arrows on Figure 64). A string was fitted to these two points. This string has been empirically taken from the surrounding debris slope borings not used in this thesis, made by EFERTE Ltd.

**4.1.2 MESH**

The finite element mesh was created using Plaxis tool adopting fine meshing option. A total of 12745 elements were created (Figure 65).

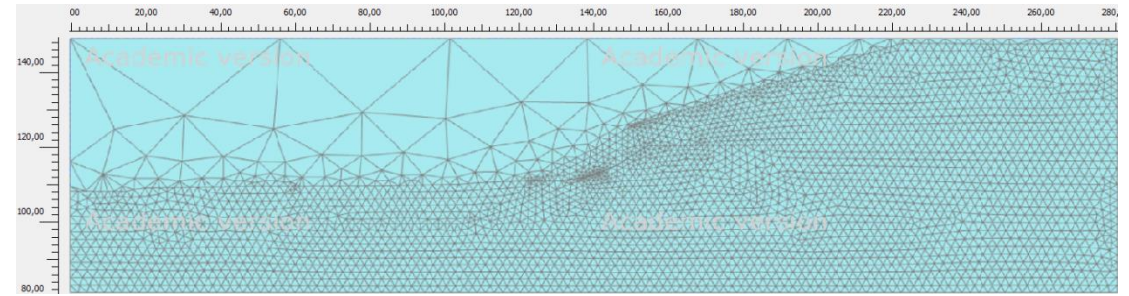


**Figure 65 Mesh of the cross-section**

**4.1.3 GROUNDWATER AND SEEPAGE CONDITIONS**

Generally, in the modelling, the average water level of Lake Balaton (105.3 mBf) was taken as the global water level. (Figure 66).

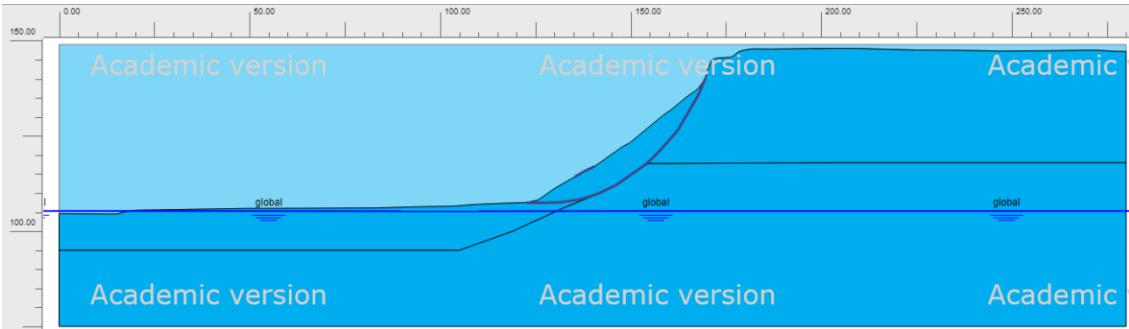


**Figure 66 Water flow conditions in the model**

Otherwise, as can be read in 3.1.3.2 and 3.2.1.1 subchapters, the high bank contains percolating stratified waters as indicated by the drilling and site visit.

Stratified water occurs in several bands of different elevation along the high bank, Figure 67 shows where stratified water has been identified and how it has been modelled in Plaxis. The aquifers appear in each band in the high bank, but it cannot be excluded that they also flow in other sections of the high bank, or that these aquifers may even vertically interconnect. The explorations on the high bank have shown that the aquifers flow in the granular layers and are surrounded by a layer of clay or clayey soil in which there is little or no water flow. Therefore, three aquifers were identified based on the excavated aquifer layers and modelled in Plaxis.

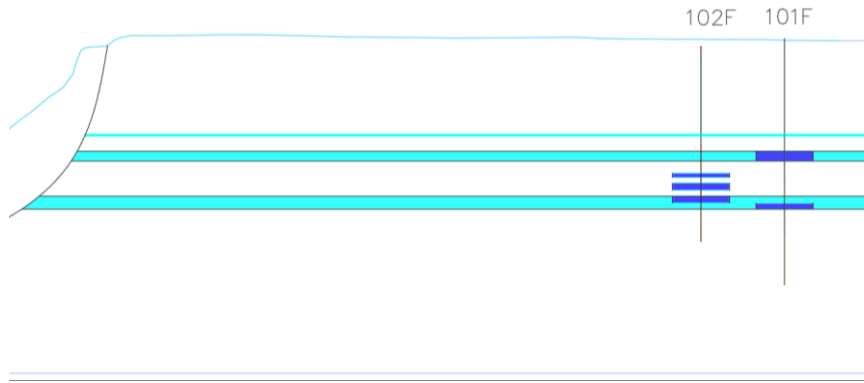


**Figure 67 Observed (dark blue) and applied (light blue) aquifers**

The "Flow Conditions" menu in Plaxis allows to set the stratified waters. In the sub-option "water conditions" it possible to select the option "Head" instead of "global water level". With this the hydraulic head water of the layer can be set. The height value of the top of the stratified layer should be entered into the program. This procedure has been applied to all three-layer waters and to all calculation steps. (Figure 68, Figure 69)

**Table 7 Properties of the modelled aquifers**

Aquifer	Top of layer [mBf]	Head level [mBf]
1	147.84	127.7
2	147.84	124.2
3	121.53	115.03

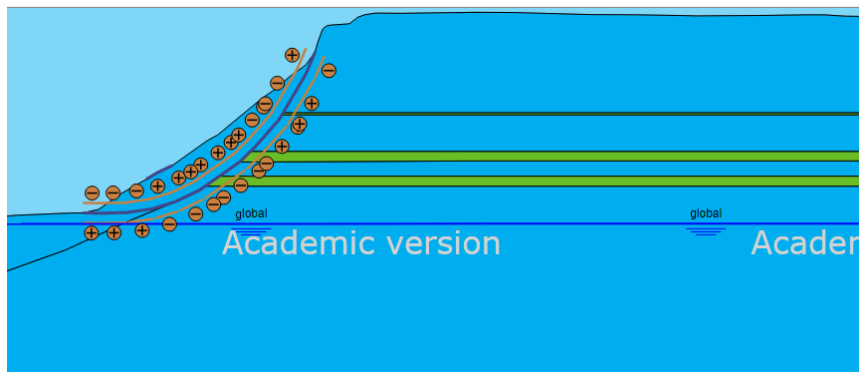


**Figure 68 Modelling of stratified waters in Plaxis**



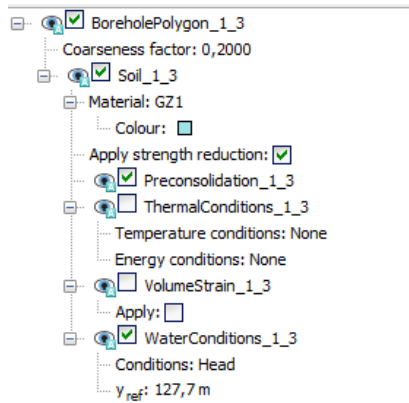


**Figure 69 Adjustment of layered water in Plaxis**

Generally, the calculations were done using the global water level in Plaxis. However, since the high bank is characterised by stratified waters and can significantly affect the stability, this procedure was used for the pseudo static calculations and at the reinforcement analysis.

#### 4.1.3 STAGED CONDITIONS

In Plaxis, after setting the flow condition, the next step is the “staged construction” menu, where it is possible to set the details for the phases. In Plaxis, it is necessary to fill in the entire model area specified in Geometry. However, individual layers can be turned off, such as the part above the high bank geometry, has been turned off in this phase. (Figure 70)

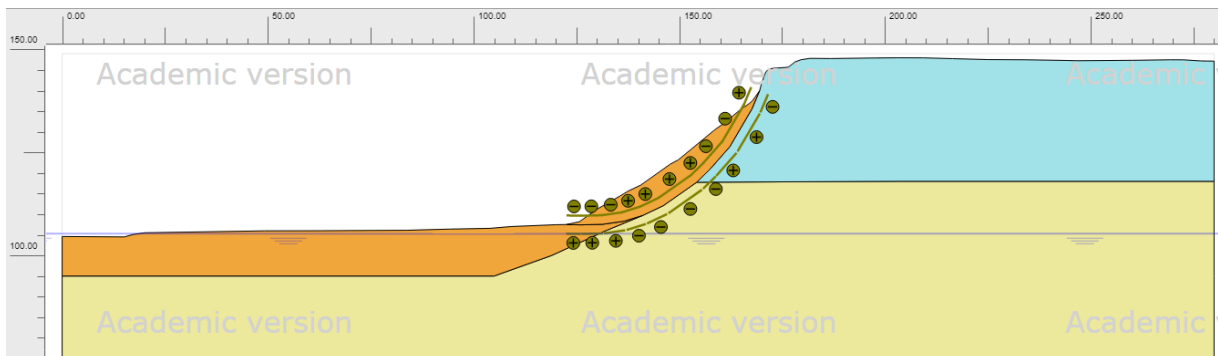


**Figure 70 Staged construction menu of the model without aquifers**

## 4.2 MODELLING

### 4.2.1 PHASES

For the iteration Mohr-Coulomb soil model was use.

The calculation of the safety factor requires 3 phases, which are shown in Figure 71.

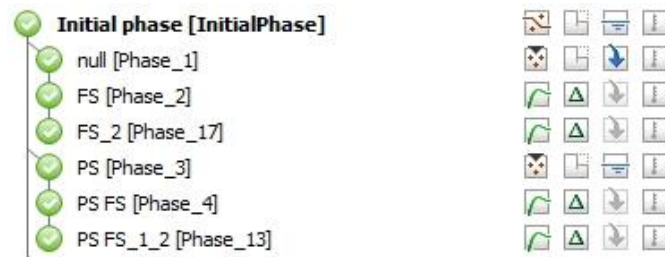


Figure 71 Calculation phases in Plaxis

#### Initial phase

The Initial phase in this case is a calculation considering the gravity loading. In the gravity load calculation, the program generates initial stresses based on the soil volume weight. This calculation is a plastic test. Figure 72 [45, p. 314]

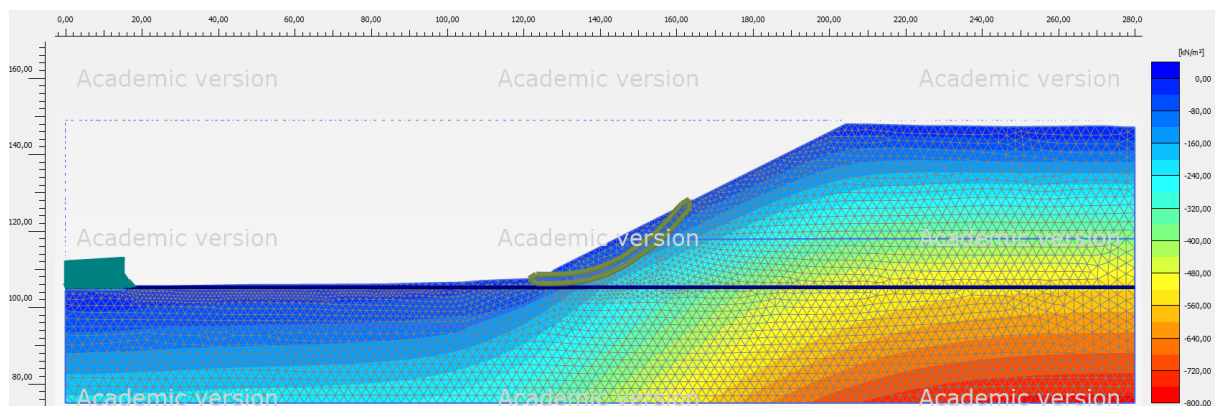


Figure 72 Initial stress field of the model at gravitational loading

#### Null phase

According to the Plaxis 2D reference manual, if an initial stress field is created by the Gravity load that is not in equilibrium, or where Mohr-Coulomb plastic points occur, a Plastic "nil phase" should be applied. The nil or null phase is a plastic calculation without additional loading applied. There may be a case where the model crashes at this stage, but the factor of safety analysis runs. However, it may show a false result. It is therefore also important to calculate this phase to see if the model is not sufficiently stable. [45, p. 316]

#### Factor of safety

The safety factor calculation follows the 'null phase'. It is a safety type of calculation. It calculates the resistance of the slope to failure due to the gravitational load of that phase.

In more detail: it is a  $\phi$ , cohesion reduction. So, the program reduced the shear strength parameters until model failure occurs, which means in this case, The calculation of the factor of safety value can see at Equation 4.

**Equation 4 Calculation of factor of safety**

$$\Sigma M_{sf} = \frac{\tan\phi_{input}}{\tan\phi_{reduced}} = \frac{c_{input}}{c_{reduced}} = \frac{su_{input}}{su_{reduced}} = \frac{\text{Tensile strength}_{input}}{\text{Tensile strength}_{reduced}}$$

At the beginning of the calculation the  $M_{sf}$  value is 1,0. The calculation of the factor of safety is due by the *load advancement number of steps* procedure. The program using the incremental multiplier as default: 0.1, which is used to determine the increment of the strength reduction. As default setting, the number of iteration is set by 100. [45, p. 319]

In the back analysis, the target value of  $M_{sf}$  in the iterations for GZ1 and GZ2 is 1.0, because just before the slip occurs, the safety factor of the slope is 1.0. In that case the objective is to determine the pre-slip parameters of the slope without debris drop (GZ3).

Factor of safety values can be plotted using the Plaxis 2D output sub-program. The value is the real safety factor parameter where convergence has been achieved, as shown in Figure 73.

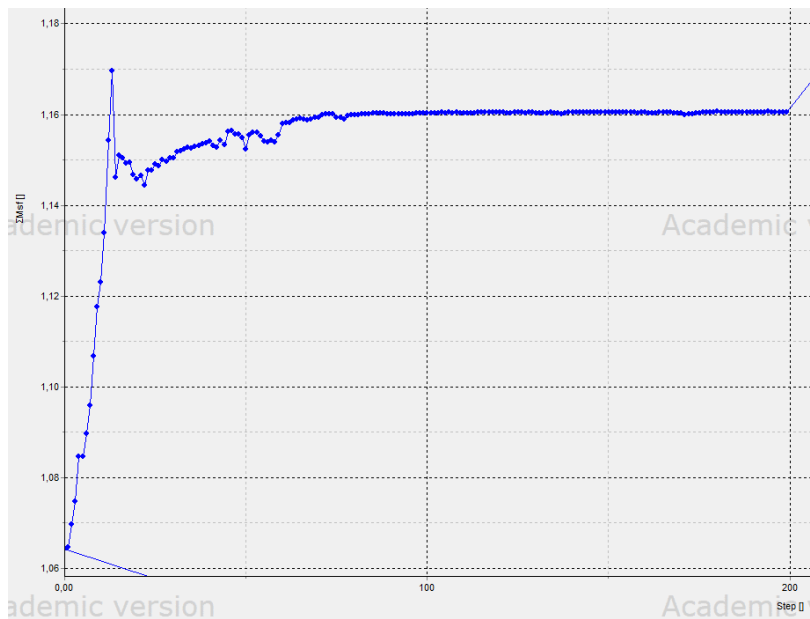


**Figure 73 Steps over Factor of safety curve of an iteration analysis**

There were several cases where this did not occur, out of the 100 steps used as default setting. For these cases, additional sub-steps had to be added to the test. After reaching a sufficient number of iteration steps, the convergence of the FS curve was also achieved for the problematic cases.

In Figure 74 you can see the factor of safety result plotted, where you can see the possible slip surface.

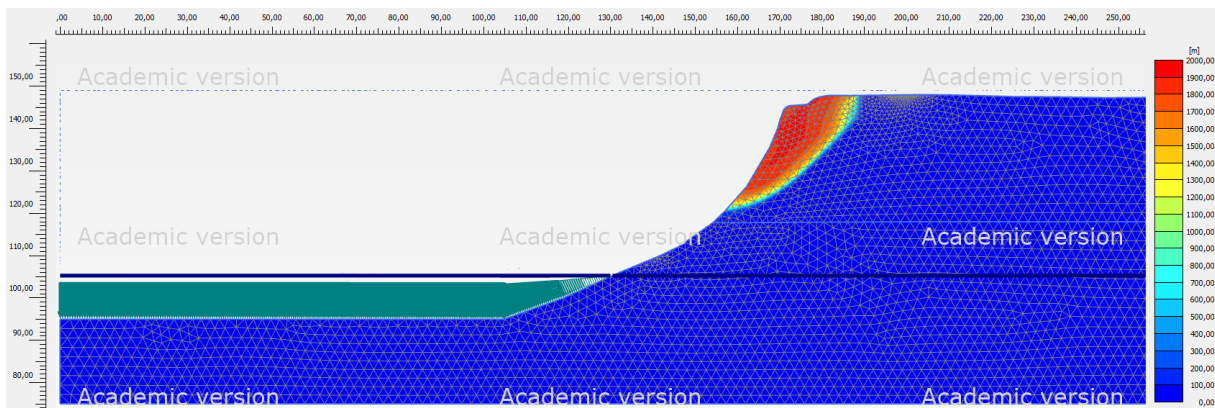


**Figure 74 Shape of moving slip surface in Factor of Safety analysis, Drained case**

### Pseudo static phase

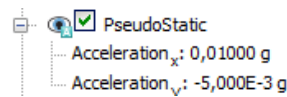


Figure 75 Setting pseudo static parameters in Plaxis

As shown in Figure 75, the pseudo static values can be set in Plaxis. For the pseudo static test, there is a vertical and a horizontal component that can be calculated from the horizontal value. According to the Hungarian national annex of EUROCODE 8, the vertical value is half of the horizontal value. The vertical value can have both a positive and a negative sign, so both cases should be analysed in the calculation.

### Pseudo static factor of safety

The purpose of this test is also to determine the value of FS, with the difference that the previous test is preceded by a pseudo static calculation. The result can be obtained in the same way from the Plaxis Output sub-program.

### 4.2.2. INTERFACE ELEMENTS

According to the Plaxis 2D reference manual, interface elements should be placed where a reduced shear surface can be developed. This highly possible at the surface of the potential slip surface, and therefore interface elements have been placed at the border of GZ3 and other two geotechnical zones as shown in Figure 76. [45, p. 114]

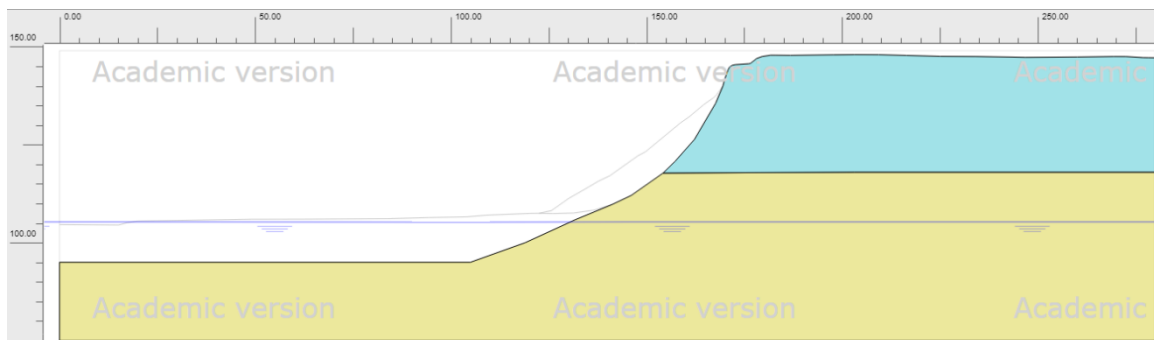


Figure 76 The model with interface elements and the GZ3 turned off

The Plaxis default setting of the interface elements placed can consider the lower shear resistance of the potential slip surface by the difference in  $R_{inter}$  value between the two layers. The Plaxis Manual recommends that in cases where there is not enough data available - such as shear strength - a value of 2/3 should be used as the  $R_{inter}$  value, as shown in Figure 77. In the case of GZ3, no value is available, so in this instance a value of 0.67 has been used. For layers GZ1 and GZ2, the default  $R_{inter}$  value of 1.0 was used. [45] Table 8

General Parameters Groundwater Thermal Interfaces Initial			
Property	Unit	Value	
<b>Stiffness</b>			
Stiffness		Standard	
<b>Strength</b>			
Strength		Manual	
$R_{inter}$			0,6700
Consider gap closure			<input checked="" type="checkbox"/>

Figure 77 Setting of interface elements

**Table 8  $R_{inter}$  parameters for Geotechnical zones**

$R_{inter}$	
GZ1	1.00
GZ2	1.00
GZ3	0.67

Of course, the potential slip can also occur back from the upper edge of the high bank. The use of interface elements does not mean that a slip surface can only form there, but it does allow modelling of the lower shear stress along the geometry of the slope debris.

#### 4.2.3 BOUNDARY CONDITIONS

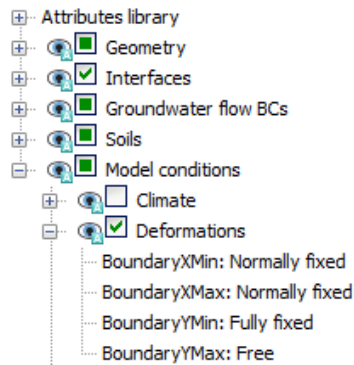


**Figure 78 Boundary conditions**

Figure 78 shows the applied boundary conditions. These settings are the default settings. These values means that the model is supported by rollers for X-directional displacement. In the Y-direction, the model is without support at the top and a fixed support at the bottom

### 4.3 BACK ANALYSIS UNDER STATIC LOADING

In this subsection, the sensitivity analysis is described in detail after the model structure. Using the parameter ranges defined in Chapter 3. The objective is to recover the state of the high bank before the slides, when the failure has not yet occurred. Then the value of the safety factor is just greater than one. To do this, the values of each parameter are calculated within the parameter range. Initially, the average value of the parameter range will be set. The parameter tests were done one parameter at a time.

The following cases were examined in the strength analysis calculation. At this phase drained and undrained type of calculations were done. The drained and undrained settings were applied simultaneously for GZ2 and GZ3. This meant in practice that E50,  $\phi'$  and cohesion were iterated in the drained case; E50 and undrained shear strength in the undrained case (Table 9).

**Table 9 Combinations studied**

	Case 1	Case2
GZ1	Drained	Drained
GZ2	Drained	Undrained
GZ3	Drained	Undrained

In this case the Initial phase, the null phase and the FS phase were used for the calculation.

#### 4.3.1 SENSITIVITY STUDY ON GZ1 AND GZ2 PARAMETERS

To assess the quality of the model parameters derived from laboratory and field test results, test runs were performed. In the previous chapter, the possible range of soil parameter values were defined for each geotechnical zone, which are summarised in Table 10.

**Table 10 The possible range of the parameters for GZ1 and GZ2**

	GZ1			GZ2		
	min	mean	max	min	mean	max
E' [kPa]	9	14	19	15	25	35
Cref [kPa]	40	45	50	40	45	50
$\phi'$ [°]	27	29	31	27	28.5	30
Su [kPa]	200	250	300	300	375	450
Poisson ratio [v]	0.3	0.4	0.5	0.3	0.4	0.5

The numerical analysis was primarily done without GZ3 to determine the set of minimum value of the model parameters for which the slope has a factor of safety close to 1. The interface elements have also been disabled in this phase (Figure 76).

During the iteration process, the mean values of the parameters were initially set for the calculations. The parameter values were changed one by one, in the following order: E50, angle of shear resistance, cohesion, undrained shear strength. GZ1 first, then GZ2 parameters were changed. Once a parameter value was set, it was not changed later, the next one was set. Thus, the parameters of GZ1 and GZ2 were determined. The following figures show the results of the iterations generated. The parameter boundaries mentioned earlier are marked with a grey vertical line: pale grey - minimum, grey - mean, black – maximum values. Most of the figures show the values of two parameters.

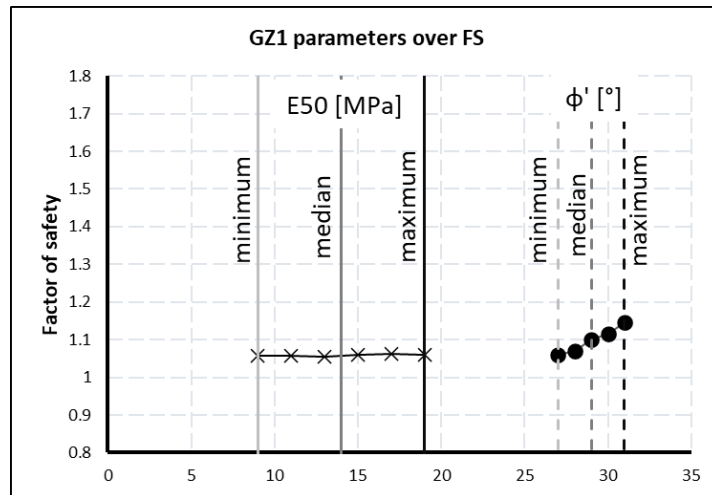


**Figure 79 E50 and  $\phi'$  values of GZ1 over FS**

Figure 79 shows that the change of the E50 values has no effect on the FS value. This is because the E50 value affects the beginning or middle of the  $\sigma$ - $\epsilon$  graph, while the FS value calculated from the result, that depends on the residual values of the graph. So even if the E50 value changes, it only slightly influences the result.

The effective angle of shearing resistance is a strength parameter that is related to the displacement and deformation of the high bank. As shown in the Figure 79, there is a linear relationship between  $\phi'$  and the value of FS.

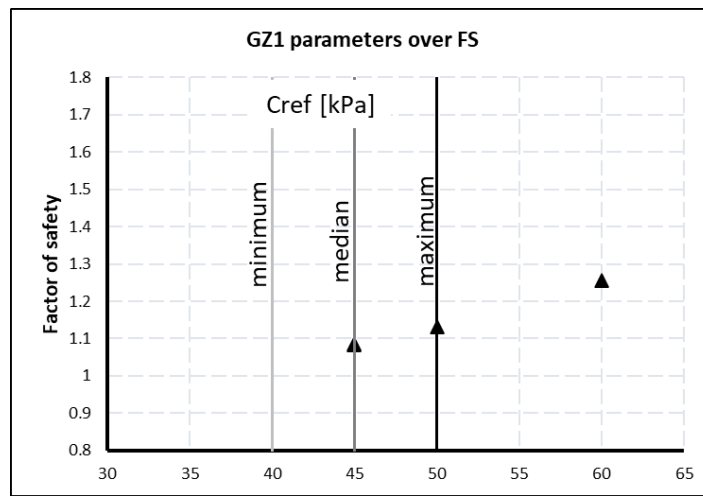


**Figure 80 Cohesion values of GZ1 over FS**

As Figure 80 shows the higher the cohesion, the higher the FS value for the GZ1. The connection between them is almost linear. There was an outlier in the cohesiveness values found in the laboratory test, which were not considered. The figure confirms this, as you can see, for a value recorded higher than the upper limit, there are no longer values related to 1, so the real value is likely to be between the two lower measured values, which are the limits.



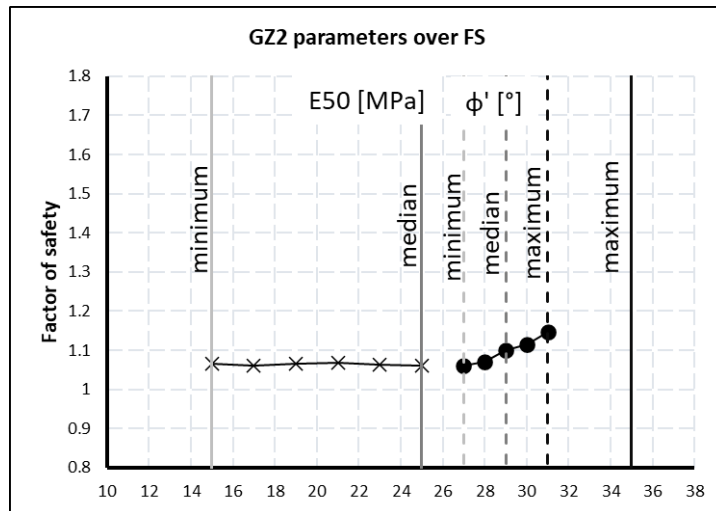


**Figure 81 E50 and  $\phi'$  values of GZ2 over FS**

On Figure 81 can see that the behaviour of E50 values for GZ2 is shows similar behaviour as for GZ1. As the value of  $\Phi'$  increases, the value of the safety factor also increases, although to a lesser degree than for cohesion.

As shown in Figure 82, the change in cohesion in GZ2 does not have as large an effect on the FS value, but below 50 kPa it does not correlate to lower  $\phi'$  or E50, i. e. the minimum value of cohesion is higher here than in GZ1. The change of the undrained shear strength parameter also does not make much effect on the factor of safety.

After the analysis of GZ1 and GZ2 parameters, GZ3 was the next to be studied. The GZ3 soil is made up of falling debris, predominantly by the material of the GZ1 layer, but in a displaced and loosened state. The aim of this study was to find the lowest cohesion and angle of shearing resistance in the iteration drained case and in the undrained case, the lowest undrained shear strength. This was verified by checking that the "null" phase that follows the Initial Phase is stable if it has run, and not if it has collapsed. Then, as before, the safety factor = 1.0 was approximated from above.

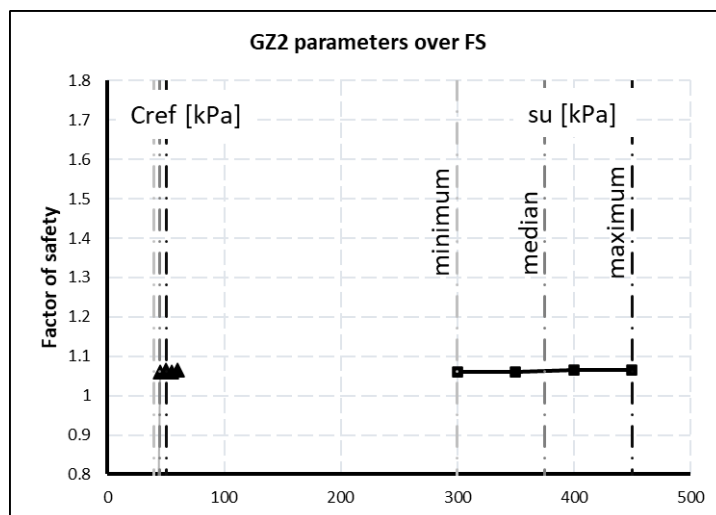


**Figure 82 Cohesion and undrained shear strength values of GZ2 over FS**

As the relationship between E50 and FS was explained in the previous case, increasing the value of E50 does not result in a clear increase in FS, that is, the relationship between the two is not linear. (Figure 82)

A summary of the selected parameters is shown in Table 11. The iteration calculations show that for E50, increasing or decreasing the parameter has only a small effect on the value of FS. Therefore, for both GZ1 and GZ2, the median value or close to it was selected. No linear relationship is observed for su either, and therefore the lower value of the values measured in the laboratory has been used. For  $\Phi'$  and cohesion, the lower values were selected from those that were found to be appropriate in the calculation.

**Table 11 Iterated parameters for GZ1 and GZ2**

	GZ1	GZ2
E50 [kPa]	15000	25000
phi' [°]	27	28
cohesion [kPa]	45	45
su [kPa]	-	300

### 4.3.2 SENSITIVITY STUDY ON GZ3 PARAMETERS

This iteration process is identical to the previous one, but the GZ3 have been activated, as Figure 83 shows. In this case, both the drained and undrained cases have been considered, in coordination with GZ2 and GZ3.

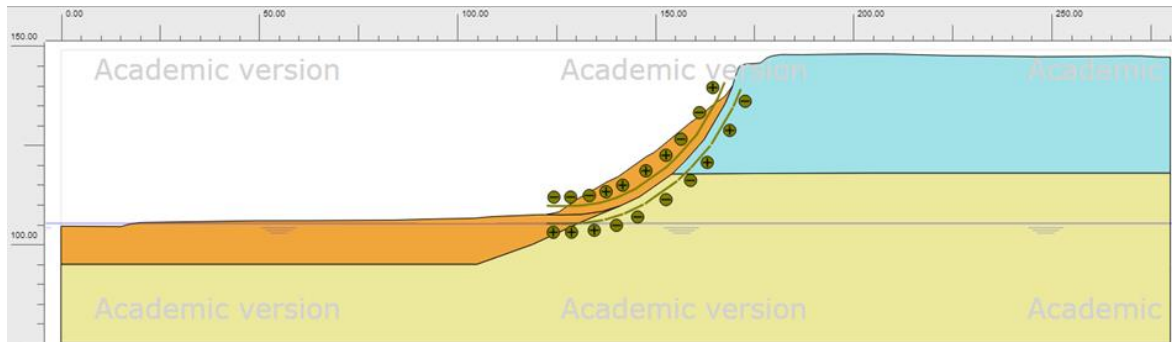


Figure 83 The model with the activated GZ3

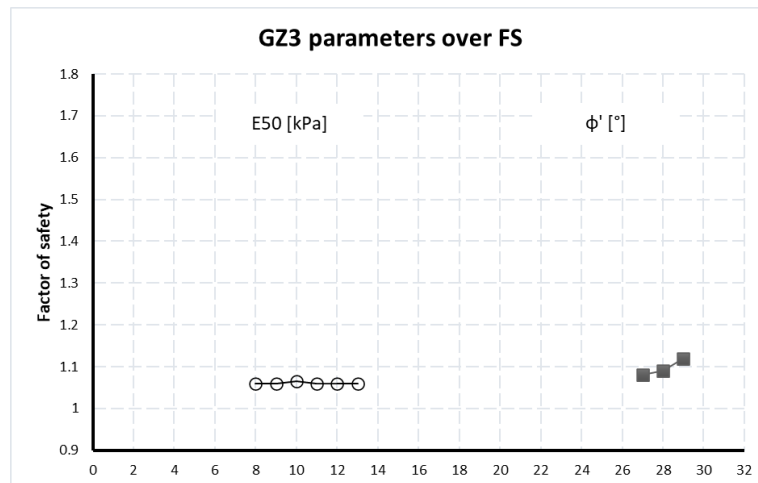


Figure 84 E50 and phi' iteration values of GZ3

As in the previous studies, changing the E50 value had a minor effect on the FS value. The relationship between the angle of shearing resistance and FS is linear in this case as well (Figure 84).

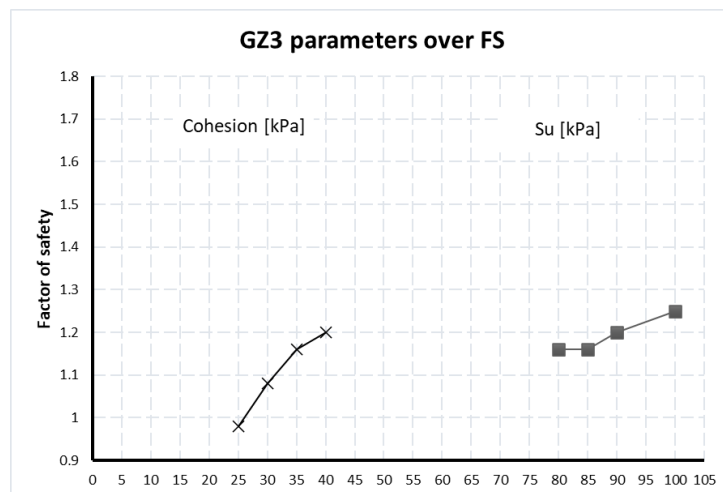


Figure 85 Cohesion and Su iteration value of GZ3

There is also a nearly linear relationship between cohesion and undrained shear strength values. Higher cohesion is associated with higher  $F_s$  values. (Figure 85)

#### 4.3.4 SUMMARY OF THE SOIL PARAMETERS

Table 12 shows the determined parameters for GZ1, GZ2 and GZ3. The parameters used in the tests came out close to the lower half of the parameter range. This confirms that the values calculated from laboratory and field tests are a good approximation to the real situation.

The initial assumption was that the strength parameters of GZ3 are low, namely cohesion and undrained shear strength values. The results show that they are not 0, but significantly lower than for the values of GZ1 or GZ2.

*Table 12 Applied soil parameters*

	GZ1	GZ2	GZ3
E50 [kPa]	15000	25000	12000
$\phi_i'$ [°]	27	28	27
cohesion [kPa]	45	45	15
$s_u$ [kPa]	-	300	75
Interface	1	1	0,67

## CHAPTER 5 – SLOPE SEISMIC STABILITY ANALYSIS

### 5.1 SENSITIVITY ANALYSIS

Once the parameters of all three geotechnical zones have been established, the next step is to investigate the soil acceleration value that the high bank can withstand.

For this purpose, different pseudo static values were calculated on the model. First at low values, then at progressively higher values, and finally the value that defined in the Hungarian national annex to Eurocode 8.

In this phase of the calculation, both the pseudo static and the pseudo static factor of safety phases were activated.

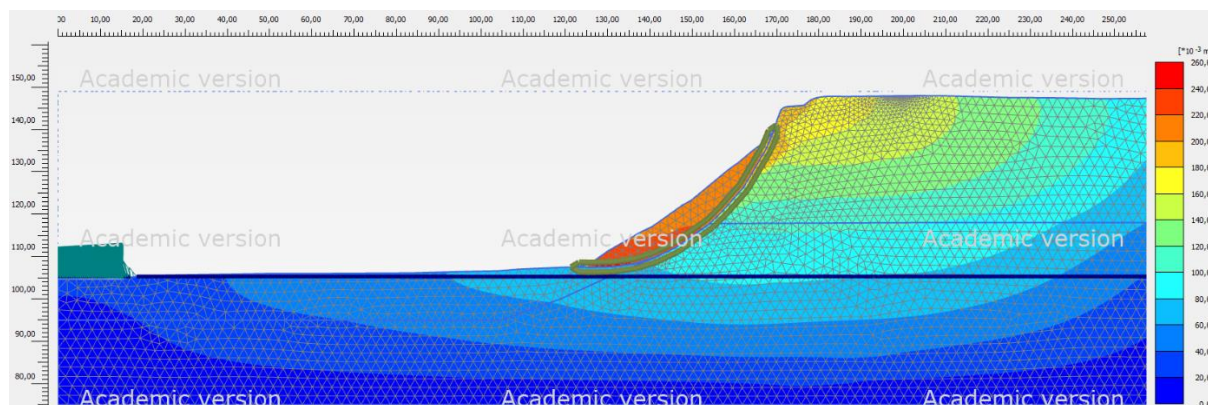


**Figure 86 Formation of a slip surface under 0,05\*g horizontal ground acceleration**

Figure 86 shows the shape of a slip surface formed by a pseudo static force. As shown, the highest displacement values are observed in the slope debris.

In the pseudo static analysis, the vertical acceleration value can be considered in both positive (up) and negative (down) directions, so there are now 4 different cases in total. (Table 13)

**Table 13 calculated variations**

	Case 1	Case 2	Case 3	Case 4
GZ1	Drained	Drained	Drained	Drained
GZ2	Drained	Undrained	Drained	Undrained
GZ3	Drained	Undrained	Drained	Undrained
Kh [g]	0.0135	0.0135	0.0135	0.0135
Kv [g]	0.00675	0.00675	-0.00675	-0.00675

The horizontal ground acceleration value for the area has been defined in 2.4.3 seismic design action subchapter, based on the EUROCODE Hungarian National Annex. The result is 0.135\*g or 1,324 m/s<sup>2</sup>.

$$a_g = 0,5 * a_{gR} * \gamma_I * S * S_T = 0,5 * 0,15g * 1 * 1,5 * 1,2 = 0,135 * g = 1,324m/s^2$$

**Table 14 Applied horizontal and vertical ground acceleration**

Kh	0,0135*g	0,1324 m/s <sup>2</sup>
Kv	±0,00675*g	0,0662 m/s <sup>2</sup>

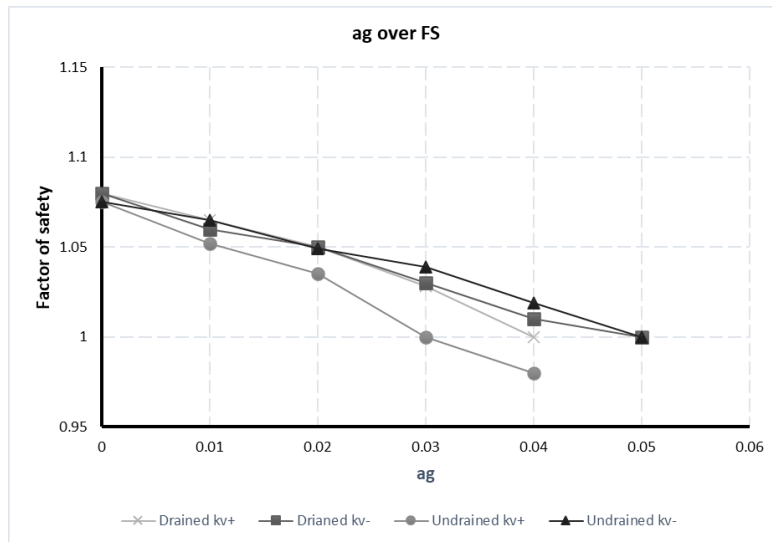


**Figure 87 Effect of horizontal and vertical ground accelerations on factor of safety**

Figure 87 shows in its current state, the high bank can withstand a soil acceleration of 0.03-0,04\*g. As can be seen in the figure, for a value higher than this, the safety factor goes below 1, which means that it fails. Therefore, the design soil acceleration value for the area 0.135\*g, which is significantly higher.

In this study, the use of aquifers was also tested to see how much they affect the stability. (Figure 88)

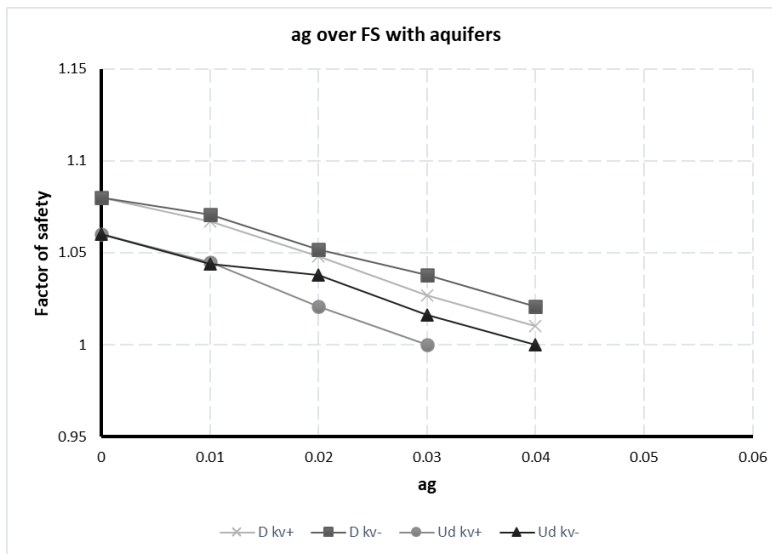


**Figure 88 Effect of horizontal and vertical ground accelerations over factor of safety with aquifers**

The stability limit with water aquifers is almost the same: 0.03-0.04\*g in the previous case and 0.03-0.04\*g in this case. In other words, the application of aquifers does not significantly affect stability according to the results. (Figure 87, Figure 88)

## 5.2 RECOMMENDATIONS FOR SLOPE STABILITY IMPROVEMENT

The previous study showed that the high bank has a FS lower than 1 for the seismic design loading of the area in the present situation. For this reason, reinforcement measures are needed to ensure that slope stability for the design earthquake.

In the following two types of stabilization measures are presented, one by reducing the slope inclination and the other by nailing.

### 5.2.1 CUTTING

#### 5.2.1.1. 1:2 SLOPE RATIO CUTTING

One possible reinforcement is the use of cutting. Figure 89 and Figure 93 shows the sub-modelled cut, where the value of the factor of safety approached 1.0 from above.

In the first case the slope ratio: 1:2, the other case: 1:3.

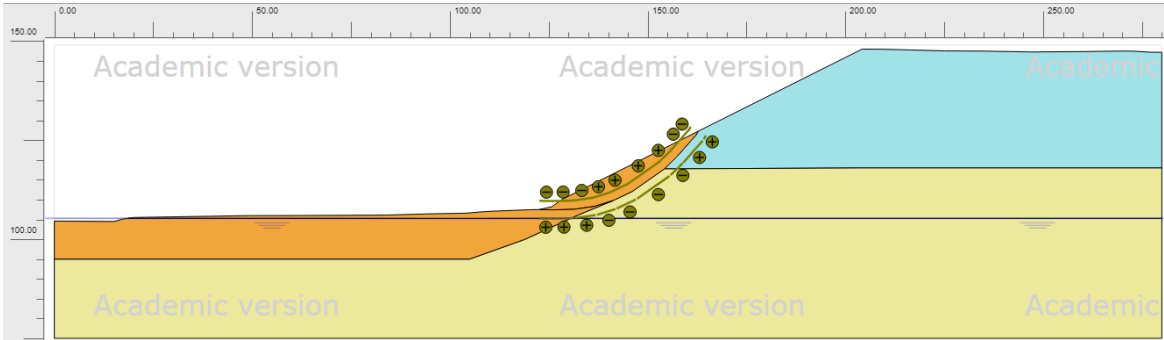


Figure 89 Cutting with 1:2 slope ratio

Through multiple iterations, the cut-off was determined as a reinforcement where the high bank can withstand the soil acceleration value for the area. The application requires the cutting of 341 m<sup>2</sup> of land mass (Figure 89)

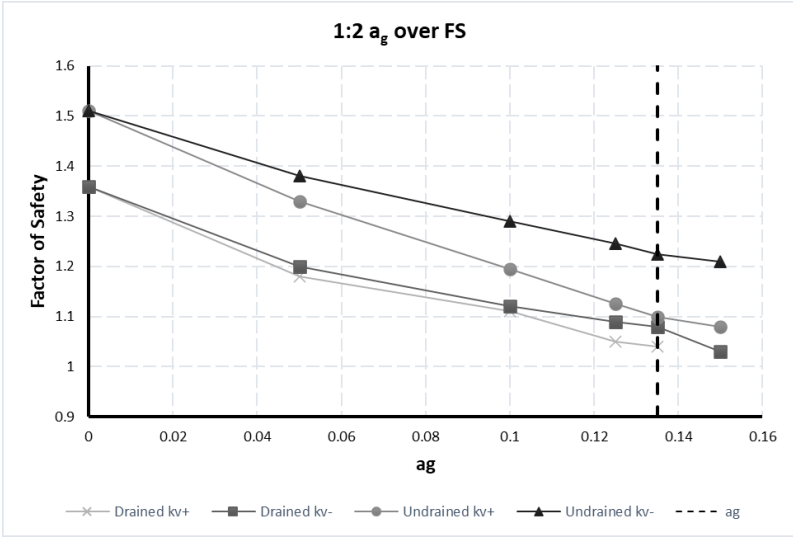
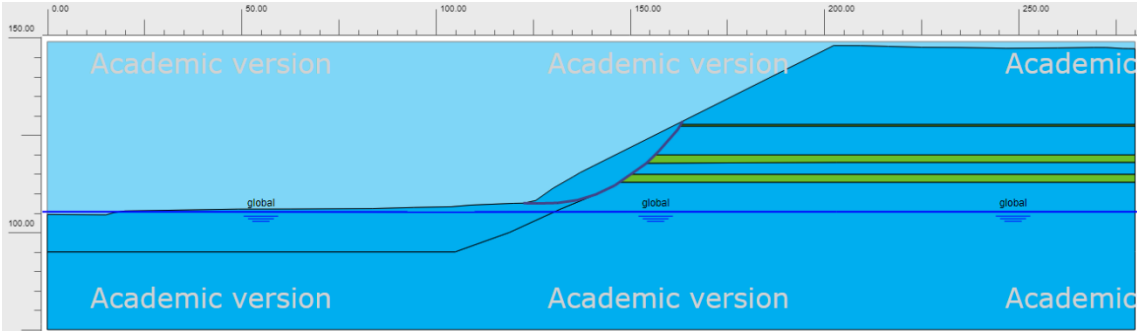


Figure 90 Horizontal acceleration values over factor of safety regarding 1:2 cut

Figure 90 shows the horizontal acceleration over factor of safety values at the 1:2 slope ratio cut. The soil acceleration values were taken in 5 steps, each with a separate safety factor. These steps are 0,05\*g, 0,10\*g, 0,125\*g, 0,135\*g and 0,15\*g. This was necessary because the determination of the cut-off rate was taken in an iterative manner and was supported by these steps.

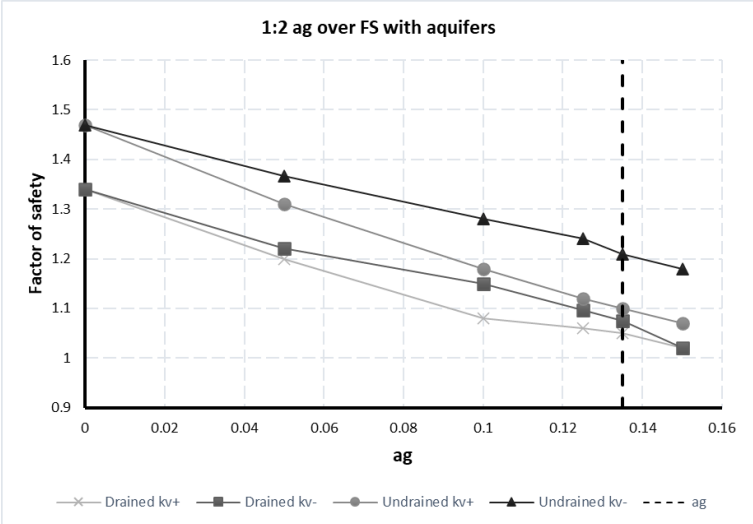
As can be seen, the values obtained in the drained case were lower and the values obtained in the case of the + sign (up) for the vertical soil acceleration were also lower.

Figure 91 shows that this procedure has also been tried with activated aquifers.



**Figure 91 Cutting with 1:2 slope ratio with aquifers**

In this case, 341 m<sup>2</sup> of earthworks are required, which is the same as the cut-off rate used in the case without aquifers. The fact that these two values are the same may be because the failure is likely to occur in the falling debris.



**Figure 92 Horizontal acceleration values over factor of safety regarding 1:2 cut with aquifers**

Figure 92 shows the shows the horizontal acceleration over factor of safety values at the 1:2 slope ratio cut with aquifer. In this case there were 5 iteration steps as well, to find the appropriate cut. The modelling of undrained behaviour is more important, because when an earthquake occurs, water does not flow out of the pervious soils like sand, and so they exhibit undrained behaviour.



5.2.1.2. 1:3 SLOPE RATIO CUTTING

Another alternative is the slope ratio of 1:3, often used in construction practice. In this case, 670 m<sup>2</sup> of soil mass has to be cut off. (Figure 93).

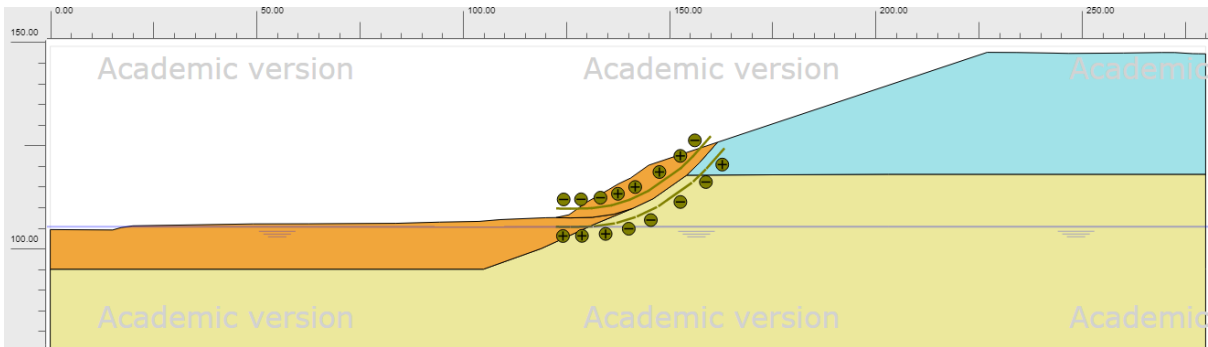


Figure 93 Cutting with 1:3 slope ratio

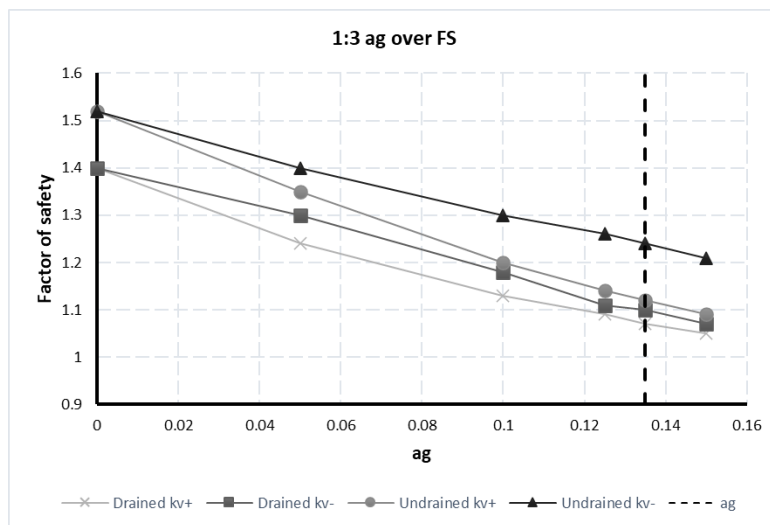


Figure 94 Horizontal acceleration values over factor of safety regarding 1:3 cut

Figure 94 shows the horizontal soil acceleration values in relation to the safety factor. In this case, the drained and the + vertical acceleration direction (drained kv+) is the lowest.

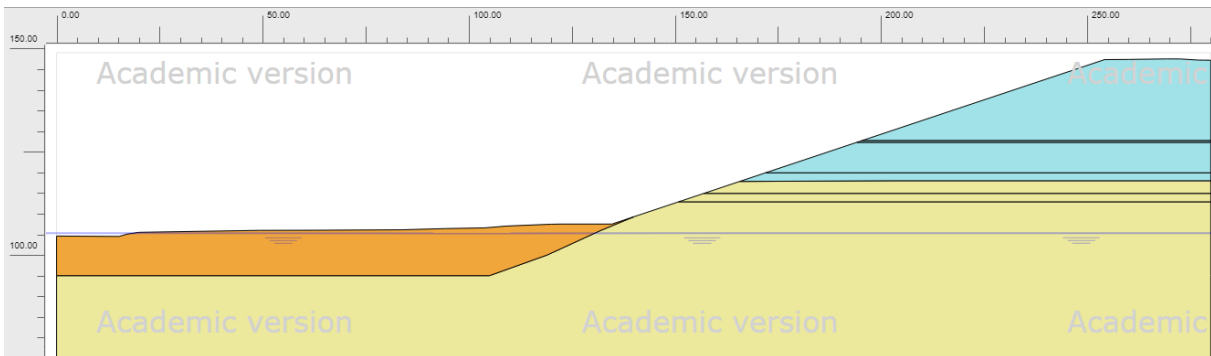
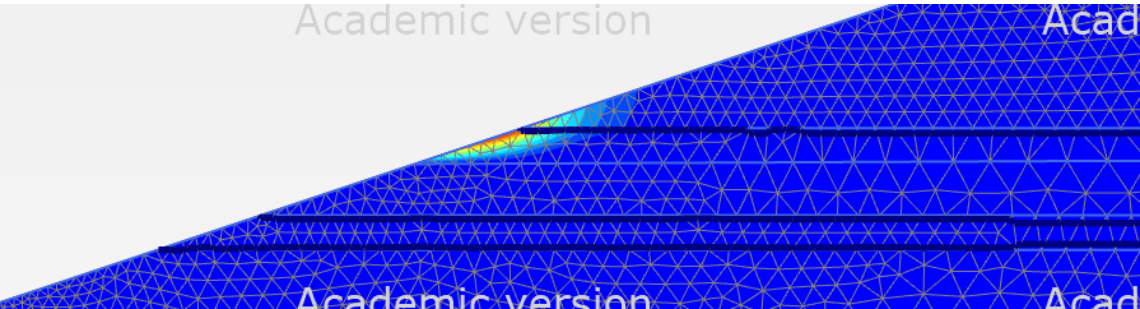


Figure 95 Cutting of slope debris at a ratio of 1:3

With the use of aquifers, the calculation of the gravity loading failed in Plaxis using a 1:3 slope ratio. Even in the case where all the slope debris was cut off, as can be seen in Figure 95

In Figure 96 it can be seen that a tension crack has formed in the copper. It usually because that the angle of shearing resistance is higher than the slope angle. Which is similar to the infinite slope failure. For this reason, a 1:3 slope ratio was found to be inappropriate. Plaxis is therefore unable to perform the calculation.



**Figure 96 Tension crack at the level of an aquifer**

**5.2.2 NAILS**

Another possible solution to increase stability is soil nailing. By inserting and fixing soil nails into the soil, the nails are extended beyond the slip surface that may occur, thus holding the nails in the soil that would not slip without this reinforcement. This increases the volume of soil that slides off, but should result in a larger surface area for the slip to occur, which requires a greater force to displace, i.e. in this case, a greater ground acceleration.

This reinforcement was modelled in preliminary with the Geo 5 slope stability program, which uses the Limit equilibrium method (LEM). This gave an approximate value of how many and what parameters of soil nails are needed to increase the stability by enough. The reinforcement was then modelled in the Plaxis 2D program, which uses a finite element method. These procedures allow a comparison between LEM and FEM modelling.

**5.2.2.1 GEO5 PRE-ITARATION**

For the modelling, the terrain of the slope was loaded into Geo5, and then the parameters of the three geotechnical zones and layer boundaries were set.

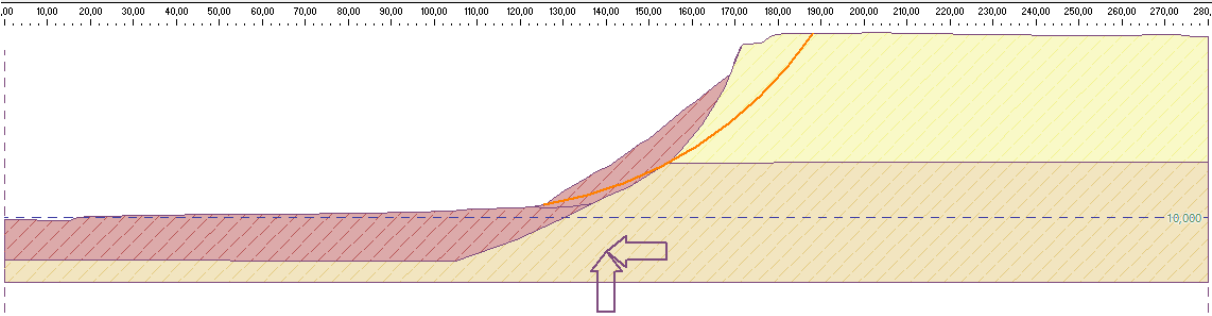


**Figure 97 Optimised slip surface without nails**

Figure 97 show the optimised slip surface without nails. It can be seen that, in contrast to Figure 86, the potential slip surface does not form along the falling debris, instead it forms ~18 meters back from the edge of the high bank.

— Nail location

Start pt. : x = 167,16 [m]  
z = 62,02 [m]

Length : l = 20,00 [m]

Inclination :  $\alpha$  = 40,00 [°]

Nail spacing : b = 1,00 [m]

— Tension strength

calculate

Nail diameter :  $d_s$  = 32,0 [mm]

Tensile strength :  $f_y$  = 750,00 [MPa]

— Pull out resistance

calculate from effective stress

Hole diameter : d = 125,0 [mm]

— Nail head strength

input  $R_f$  = 50,00 [kN]

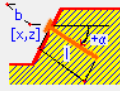


**Figure 98 Soil nail properties**

The number of soil nails to be used in the cross-section was then determined by iteration. The following parameters were applied: length: 20m, inclination: 20°, horizontal spacing: 1m, vertical spacing: 0,85m, nail diameter: 32mm, tensile strength: 750MPa, hole diameter: 125mm, nail head strength: 50kN. (Figure 98)

The location of the soil nails used in the slope is shown in Figure 99.

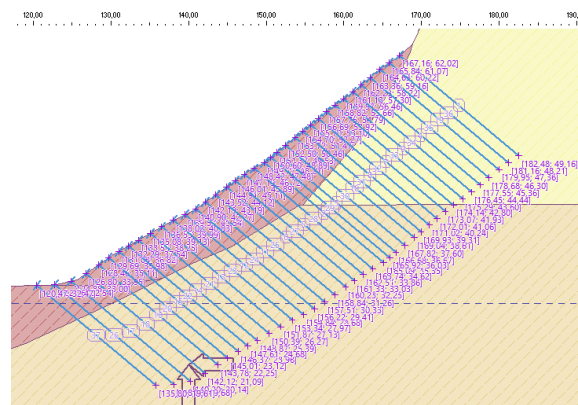


**Figure 99 Location of soil nails used in Geo5**

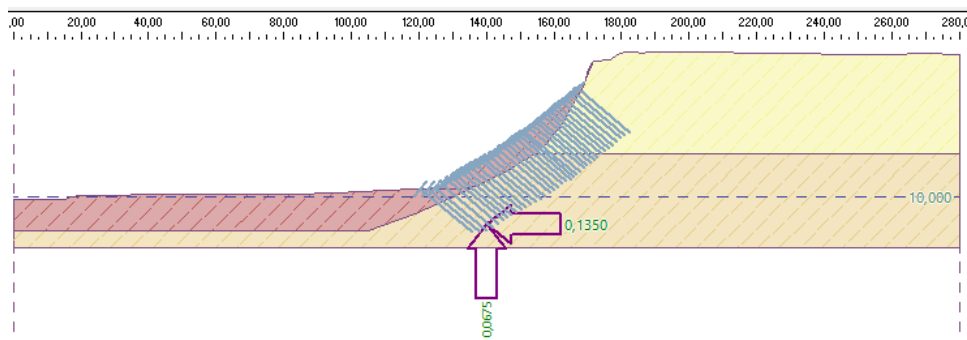


**Figure 100 The applied horizontal and vertical soil acceleration values on the slope**

The groundwater level was set to the level of Lake Balaton in Geo5.

The Geo 5 program uses the partial factors of the Hungarian national annex EUROCODE 7 for the slope stability test, as shown in Figure 101 and Figure 102. For the earthquake test, the general settings of EUROCODE 8 are used. Figure 100)

Partial factors on actions (A)		State STR				State GEO			
		Unfavourable		Favourable		Unfavourable		Favourable	
Permanent actions :	$\gamma_G =$	1,35	[-]	1,00	[-]	1,00	[-]	1,00	[-]
Variable actions :	$\gamma_Q =$	1,50	[-]	0,00	[-]	1,30	[-]	0,00	[-]
Water load :	$\gamma_w =$					1,00	[-]		
Partial factors for soil parameters (M)									
Partial factor on internal friction :	$\gamma_\phi =$	1,35	[-]						
Partial factor on effective cohesion :	$\gamma_c =$	1,35	[-]						
Partial factor on undrained shear strength :	$\gamma_{cu} =$	1,50	[-]						

Figure 101 Partial factors used for permanent design situation in Geo 5

Partial factors on actions (A)		State STR				State GEO			
		Unfavourable		Favourable		Unfavourable		Favourable	
Permanent actions :	$\gamma_G =$	1,00	[-]	1,00	[-]	1,00	[-]	1,00	[-]
Variable actions :	$\gamma_Q =$	1,00	[-]	0,00	[-]	1,00	[-]	0,00	[-]
Water load :	$\gamma_w =$					1,00	[-]		
Partial factors for soil parameters (M)									
Partial factor on internal friction :	$\gamma_\phi =$	1,30	[-]						
Partial factor on effective cohesion :	$\gamma_c =$	1,30	[-]						
Partial factor on undrained shear strength :	$\gamma_{cu} =$	1,45	[-]						

Figure 102 Partial factors used for seismic design situation in Geo 5

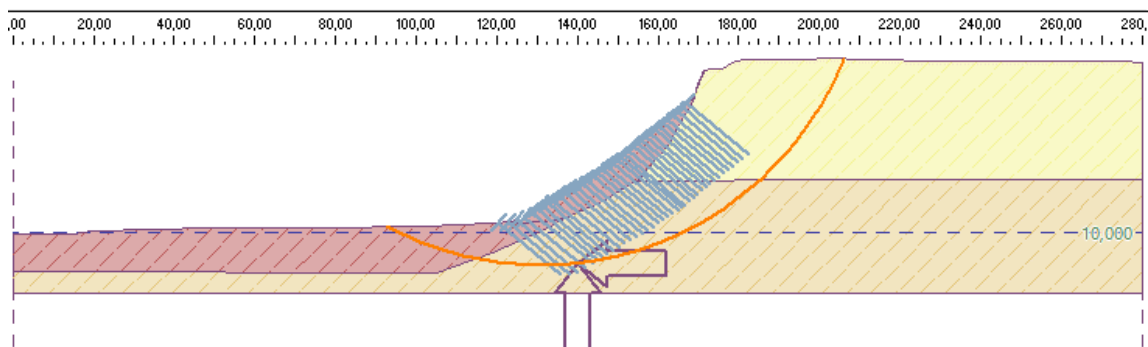


Figure 103 The optimised slip surface in Geo 5 model

The Geo 5 slope stability program is able to optimise the possible slope surface during the analysis, i.e. it iteratively selects the riskiest slope and shows its utilisation. (Figure 103)

#### Slope stability verification (Bishop)

Sum of active forces :  $F_a = 18729,06$  kN/m

Sum of passive forces :  $F_p = 18907,93$  kN/m

Sliding moment :  $M_a = 1494766,04$  kNm/m

Resisting moment :  $M_p = 1509041,71$  kNm/m

Utilization : 99,1 %

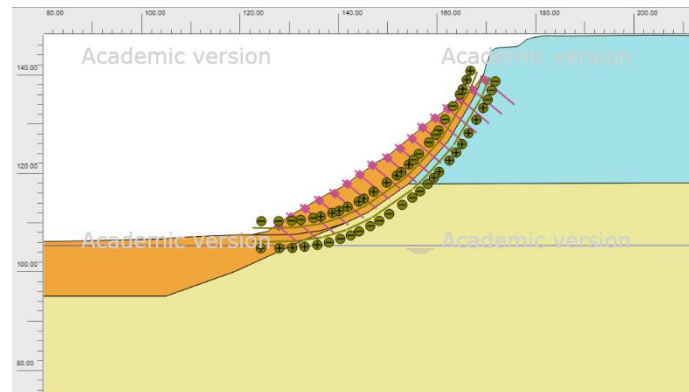
Slope stability ACCEPTABLE

Figure 104 Bishop method

Figure 104 show the result on the slope with Bishop method, 99,1% utilization.

### 5.2.2.2 MODELING IN PLAXIS 2D

The soil nailing reinforcement was also modelled in Plaxis, the location of the nails is shown in Figure 105



**Figure 105 Reinforcement with nails**

The parameters of the soil layers modelled in Plaxis were taken from one of the example solutions presented by Plaxis, the applied parameters are shown in Figure 106. [46]

As can be seen in Figure 86, the potential slip surface possibly formed at the slope debris, so it is worth placing the soil nails there as shown in Figure 105.

Properties		
E	kN/m <sup>2</sup>	210,0E3
γ	kN/m <sup>3</sup>	60,00
Beam type		Predefined
Predefined beam type		Massive circular beam
Diameter	m	0,3200
A	m <sup>2</sup>	0,08042
I	m <sup>4</sup>	0,5147E-3
L <sub>spacing</sub>	m	1,000
Rayleigh α		0,000
Rayleigh β		0,000
Axial skin resistance		
Axial skin resistance		Linear
T <sub>skin, start, max</sub>	kN/m	1000
T <sub>skin, end, max</sub>	kN/m	1000
Lateral resistance		
Lateral resistance		Unlimited
Base resistance		
F <sub>max</sub>	kN	0,000
Interface stiffness factor		
Default values		<input checked="" type="checkbox"/>

**Figure 106 Applied parameters for soil nails in Plaxis**

The result was that the following parameters could be used to keep the high bank stable during earthquakes: 17pcs, 9m long soil nail. With a horizontal spacing of 1m and a vertical spacing of 1,9m. Diameter of nails 32mm, angle with horizontal: 40°, and have E= 210kPa, γ= 60kPa. (Figure 105)

Also, for the soil nails, iteration steps were used to determine the appropriate number and strength of soil nails. Therefore, the safety factor was also calculated for 4 horizontal soil acceleration values in this case.

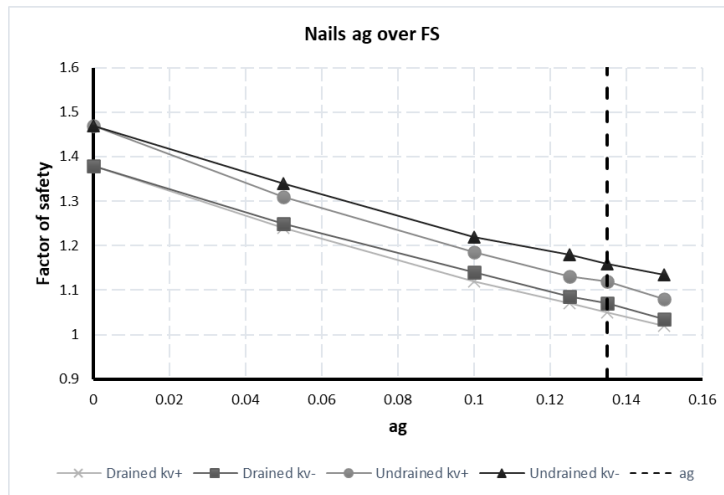


**Figure 107 Horizontal acceleration values over factor of safety regarding nailing**

The initial FS value is high for soil reinforcement. The soil acceleration value for the area in the undrained case is just right, taking FS=1. (Figure 107)

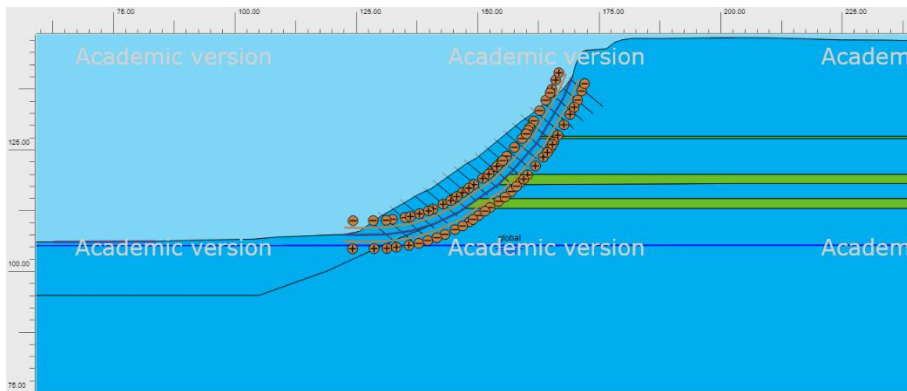


**Figure 108 Nail reinforcement with aquifers (green bands - aquifers)**

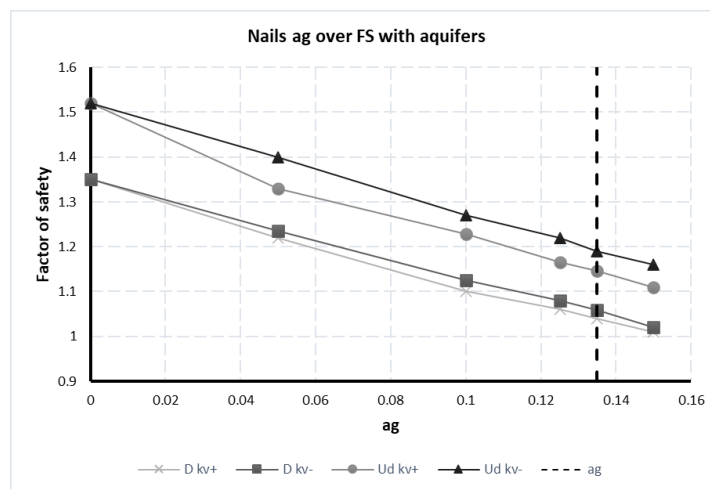


**Figure 109 Horizontal acceleration values over factor of safety regarding nailing with aquifers**

In the case of soil nailing, the iterations to keep the high bank stable for aquifers also showed that it is necessary to densify the soil nails and to increase the length of the nail. Applied nail parameters: 21pcs, - meters long, horizontal spacing: 1m, vertical spacing: 1,5 meters. Diameter of nails 32mm, angle with horizontal: 40°, and have  $E=210\text{kPa}$ ,  $\gamma=60\text{kPa}$ . (Figure 108, Figure 109)

## **CHAPTER 6 - CONCLUSIONS AND FURTHER DEVELOPMENT**

### **6.1 CONCLUSIONS**

In Chapter 2, there is a description of earthquake formation, wave types, the world's earthquake hazard, and then a description of earthquake events that have occurred near the study area. After that, the typical horizontal ground acceleration at the site is determined according to the Hungarian national annex of Eurocode 8.

In Chapter 3 the study area is geologically described, topographically, geologically, hydrographically. Description of the formation of the high bank. The boreholes revealed that there are percolating aquifers in the high bank, which contributed greatly to the earlier high bank slides. A comparison of the geological and deep boreholes revealed that the high bank is built up from the upper and lower formations of the Pannonian geological strata. Finally, seismic data analysis over the last decade has shown that the study area is related to a fault line that is currently considered active.

This was followed by a presentation of the drillings and the laboratory tests carried out on the samples taken. In addition, the results of the CPT excavation in the field will be presented. Based on the results, 3 geotechnical zones were established in the cross section. For each of these parameters, a minimum, median, and maximum range was constructed based on the results.

In Chapter 4, the values of the parameter range table from the laboratory and field tests were refined. That is, sensitivity testing was performed. The aim was to search for the parameter before the high bank slides, when the slide has not yet occurred, but is almost there. This is represented by the approximation of  $FS=1$  from above. Thus, the parameters GZ1 and GZ2 were fitted. In the next step, the previously calibrated parameters were used to calibrate GZ3. Here the aim was to approximate a value around  $FS \sim 1.1$ .

In Chapter 5, the calibrated parameters were used to model the current state of the high bank with the defined geotechnical zones, the calibrated parameters, and the geometry to determine the horizontal soil acceleration value that the high bank can withstand. The results showed that it is significantly less than required and therefore a wall of the high bank reinforcement is needed. The results were almost identical for the aquifers that were turned on. There are 3 different recommendations for reinforcement: 1:2 and 1:3 slope ratio cutting and soil nailing.

For a 1:2 cutting with the aquifers turned on, the same slope cut-off is found to be appropriate. In the case of the 1:3 slope ratio, with the activated aquifers, the Plaxis calculation did not run, as a tension crack formed at the top aquifer layer boundary, even if all the slope debris were cut off.

The soil nailing was first modelled with Geo5, using the Limit Equilibrium Method, with length: 20m, inclination:  $40^\circ$ . In Plaxis, the 17pcs, 9 meters, with  $40^\circ$  inclination nails was needed, in the case of aquifers 21 nails.

In Geo5 and Plaxis modelling, there is a significant difference in the length of the nails. This may be because in Plaxis, interface elements were activated at the falling debris with a multiplication factor of 0.67, so that, in Plaxis, the failure occurs there without reinforcement, as shown in Figure 86. At Geo 5, however, it has a different shape, as shown in Figure 97. This is due to the shorter nails being able to hold the soil mass stably. This example illustrates the difference between LEM and FEA modelling.

The 1:2 and 1:3 slope cuts shown, the 1:2 ratio cut, or the soil nailing seems the appropriate solution. A The 1:3 cut is not good because it would mean too much excavation. Soil nailing also seems to be an applicable method, as it does not require very long nails, nor too many. However, trees and bushes on slope of the high bank and a terrain slope of  $30-32^\circ$  make it difficult to implement. Therefore, a cut-off ratio of 1:2 seems appropriate.

## 6.2 FURTHER DEVELOPMENT

1. The high bank pseudo static earthquake load was tested, it would be worth running a real earthquake record with earthquake parameters like those of the study area to see what the results show. This would be beneficial because a real earthquake may give different results, as the pseudo static method may not give accurate results. It could also be used to generate a vulnerability curve.
2. Time constraints did not allow, but it may be worth to investigate additional cross sections in the area, examine their soil parameter characteristics, and then build a model from that to see what results can be obtained from this in comparison.
3. More detailed modelling of aquifers can also provide more realistic results. A more detailed modelling of the aquifers would be beneficial to obtain more realistic results because the aquifers, as the results show, have a significant impact on the stability. More detailed modelling could be done by picking up exactly where it has been explored in the field, rather than simplifying.
4. By modelling the area under study in 3 dimensions, which in fact means looking at several cross-sections together. That is, using several excavations, the boundaries of the geotechnical zones and the soil parameters would be defined. In this way, a wider range of parameters would be valid. The surface would be formed by connecting the surfaces of the cross sections.



## **BIBLIOGRAPHY**

- [1] "Földrengés.hu - Earthquake." <http://www.foldrenges.hu/>
- [2] "1755 Lisbon earthquake - Wikipedia." [https://en.wikipedia.org/wiki/1755\\_Lisbon\\_earthquake](https://en.wikipedia.org/wiki/1755_Lisbon_earthquake) (accessed May 13, 2022).
- [3] "Epicenter - Wikipedia." <https://en.wikipedia.org/wiki/Epicenter> (accessed May 13, 2022).
- [4] "Seismic Waves: Definition, Types & Diagram | StudySmarter." <https://www.studysmarter.co.uk/explanations/physics/waves-physics/seismic-waves/> (accessed Jul. 17, 2022).
- [5] R. M. Allen, "Earthquake Hazard Mitigation: New Directions and Opportunities," *Treatise Geophys. Second Ed.*, vol. 4, pp. 593–625, 2015, doi: 10.1016/B978-0-444-53802-4.00090-7.
- [6] F. Visnovitz *et al.*, "High resolution architecture of neotectonic fault zones and post-8-Ma deformations in western Hungary: Observations and neotectonic characteristics of the fault zone at the Eastern Lake Balaton," *Glob. Planet. Change*, vol. 203, p. 103540, Aug. 2021, doi: 10.1016/J.GLOPLACHA.2021.103540.
- [7] "Földrengések Magyarországon – Earthquakes in Hungary Wikipédia." [https://hu.wikipedia.org/wiki/Földrengések\\_Magyarországon](https://hu.wikipedia.org/wiki/Földrengések_Magyarországon) (accessed May 17, 2022).
- [8] "1985-ös berhidai földrengés – 1985 Berhida earthquake Wikipédia." [https://hu.wikipedia.org/wiki/1985-ös\\_berhidai\\_földrengés](https://hu.wikipedia.org/wiki/1985-ös_berhidai_földrengés) (accessed May 17, 2022).
- [9] E. C. for Standardisation, "Eurocode 8: Design of structures for earthquake resistance," no. The European Standard EN 1998-1., 2004.
- [10] "MSZ EN 1998\_1\_2008\_EC8\_földrengés - Hungarian national annex."
- [11] Z. T. Tóth L, Győri E, Mónus P, "MSZ EN 1998-1 ( EUROCODE 8 ) Nemzeti melléklet Szeizmikus zónatérkép - National Annex Seismic zone map," vol. 1, no. Eurocode 8, p. 2006, 2006.
- [12] "Google Earth." [www.earth.google.com](http://www.earth.google.com)
- [13] D. Zoltán, *Magyarország kistájainak katasztere - Cadastre of small areas in Hungary*. MTA Földrajztudományi Kutatóintézet - MTA Research Institute of Geography, 2010.
- [14] Z. Horváth, "Balatoni magaspártok összehasonlító értékelése - Comparative assessment of Balaton high banks," 1946.
- [15] "The Map of the Pannonian Sea - Reconstruction • viborc." <https://viborc.com/map-of-the-pannonian-sea-reconstruction/> (accessed May 22, 2022).
- [16] FTV Zrt., "Talajmechanikai és hidrogeológiai szakvélemény a mozgásveszélyes partfalak stabilizációs programjával - Soil mechanics and hydrogeological expertise with the stabilisation programme for embankments at risk of movement," 2009.
- [17] Hübner Balázs and Dr. Szendefy János, "Geotechnikai Tervezési Beszámoló a Balatonvilágos Club Aliga területén tervezett szálloda alatti magaspárt előzetes állékonyságvizsgálatához - Geotechnical Design Report for the preliminary stability study of the high bank," 2020.
- [18] Lóczy Lajos, *A Balaton tudományos tanulmányozásának eredményei I. - The results of the scientific study of Lake Balaton*. A Magyar földrajzi társaság Balaton-bizottsága - The Balaton Committee of the Hungarian Geographical Society, 1921.
- [19] F. Síkhegyi, G. Tímár, K. Brezsnaynszky, C. Galambos, and A. Zlinszky, "A Balaton ábrázolása térképeken - Maps of Lake Balaton," *A Balat. Kut. - Lóczy Lajos nyomdokán*, pp. 311–399, 2020.
- [20] A. Térképek, "Történelmi Térképek Online - Historical Maps Online." <https://maps.arcanum.com/hu/> (accessed May 22, 2022).
- [21] "Magyarország mozgásveszélyes területei - Movement sensitive areas in Hungary." [https://map.mbfisz.gov.hu/FDT\\_veszely\\_oroszag/](https://map.mbfisz.gov.hu/FDT_veszely_oroszag/) (accessed Jun. 06, 2022).
- [22] S. J. B. Zoltán, C. Aliga, and Z. Dr. Szendefy, János; Bán, "Talajvizsgáló jelentés a Balatonvilágos Club Aliga üdülőterület beépítési koncepciójának tervezéséhez - Ground investigation report for the planning of the development concept of the Club Aliga recreation area in Balatonvilágos," pp. 1–33, 2021.
- [23] "fentrol.hu." <https://www.fentrol.hu/hu/> (accessed May 17, 2022).
- [24] J. H. B. Dr. Szendefy, "Talajvizsgáló Jelentés a H-8171 Balatonvilágos Club Aliga északi részén tervezett mélyszivárgó tervezéséhez - Ground Investigation Report for the design of a deep seepage at Balatonvilágos Club Aliga North." 2021.
- [25] L. Gyalog and F. Síkhegyi, "Magyarország földtani térképe - Geological map of Hungary," *Magy. Állami Földtani Intézet*, <https://map.mfgi.hu/fdt100/>, p. 2005, 2005.
- [26] "Miocén - Miocene – Wikipédia." <https://hu.wikipedia.org/wiki/Miocén> (accessed May 12, 2022).
- [27] P. E. Kézikönyvtár, "Vastag pannon üledékek a medencében - Thick Pannonian deposits in the basin." <https://www.arcanum.com/hu/online-kiadvanyok/pannon-pannon-enciklopedia-1/a-magyarsag-kezikonyve-2/magyarorszag-foldje-1A/a-pannon-belto-a-jegkor-es-a-jelenkor->

- osfoldrajza-68/vastag-pannon-uledekek-a-medenceben-6C/ (accessed Jun. 18, 2022).
- [28] N. Rozgonyi-Boissinot, "Magyarország műszaki földtana - Technical geography of Hungary," 2020.
- [29] P. Oláh, "The preconsolidation of the Pannonian layer of Central-Hungary," 2020.
- [30] "Service, Magyar bányászati és földtani szolgálat - Hungarian mining and geological - Map server." [www.map.mbfisz.gov.hu](http://www.map.mbfisz.gov.hu).
- [31] J. Fülöp, *Magyarország geológiája - Geology of Hungary*. Magyar Állami Földtani Intézet - Hungarian Geological Survey.
- [32] K. L. és M. G. Budai Tamás, Császár Géza, Csillag Gábor, Dudko Antonyina, "A Balaton-Felvidék Földtana - the Geology of the Balaton Highlands," *Angew. Chemie Int. Ed.* 6(11), 951–952., 1999.
- [33] "Ordovícium – Wikipédia." <https://hu.wikipedia.org/wiki/Ordovícium> (accessed May 12, 2022).
- [34] J. Haas, *Geology of Hungary*. Springer, 2011. doi: 10.1016/b978-0-12-387667-6.00013-0.
- [35] "Pelso Plate - Wikipedia." [https://en.wikipedia.org/wiki/Pelso\\_Plate](https://en.wikipedia.org/wiki/Pelso_Plate) (accessed Jun. 17, 2022).
- [36] G. Bada *et al.*, "Neotektonikai viszonyok a balaton keleti medencéjében és tágabb környezetében nagyfelbontású szeizmikus mérések alapján - Neotectonic conditions in the eastern basin of Lake Balaton and its wider surroundings based on high-resolution seismic measurements," *Földt. Kozlony*, vol. 140, no. 4, pp. 367–389, 2010.
- [37] L. Tóth, P. Mónus, T. Zsíros, and M. Kiszely, "Seismicity in the Pannonian Region &#8211; earthquake data," *Stephan Mueller Spec. Publ. Ser.*, vol. 3, pp. 9–28, 2002, doi: 10.5194/smsps-3-9-2002.
- [38] Z. Dr. Szendefy, János ; Bán, "Talajvizsgálati jelentés a Balatonvilágos Club Aliga üdülőterület beépítési koncepciójának tervezéséhez - Ground investigation report for the planning of the development concept of the Balatonvilágos Club Aliga recreation area." 2021.
- [39] P. K. Robertson, "Interpretation of cone penetration tests - A unified approach," *Can. Geotech. J.*, vol. 46, no. 11, pp. 1337–1355, 2009, doi: 10.1139/T09-065.
- [40] K. K. Sorensen, K. K. Sorensen, and N. Okkels, "Correlation between drained shear strength and plasticity index of undisturbed overconsolidated clays Correlation between drained shear strength and plasticity index of undisturbed overconsolidated clays Corrélation entre la résistance au cisaillement des," no. December, pp. 423–428, 2013, [Online]. Available: <https://www.researchgate.net/publication/285583666>
- [41] S. M. Ahmed, "Assessment of clay stiffness and strength parameters using index properties," *J. Rock Mech. Geotech. Eng.*, vol. 10, no. 3, pp. 579–593, 2018, doi: 10.1016/j.jrmge.2017.10.006.
- [42] P. K. Robertson and K.L. Cabal, *CPT Guide 6th edition*. Gregg Drilling, 2015.
- [43] Z. Rémai, "Correlation of undrained shear strength and CPT resistance," *Period. Polytech. Civ. Eng.*, vol. 57, no. 1, pp. 39–44, 2013, doi: 10.3311/PPci.2140.
- [44] O. L. Ertugrul and A. C. Trandafir, "Seismic earth pressures on flexible cantilever retaining walls with deformable inclusions," *J. Rock Mech. Geotech. Eng.*, vol. 6, no. 5, pp. 417–427, 2014, doi: 10.1016/j.jrmge.2014.07.004.
- [45] Plaxis, "CONNECT Edition V21.00 PLAXIS 2D-Reference Manual," pp. 1–576, 2020.
- [46] Plaxis, "Slope Stability for a Road," pp. 1–13, 2021.
- [47] "Phanerozoic - Wikipedia." <https://en.wikipedia.org/wiki/Phanerozoic> (accessed May 17, 2022).